DISSERTATION

SPATIAL AND TEMPORAL VARIABILITY OF SNOW COVER IN THE ANDES MOUNTAINS AND ITS INFLUENCE ON STREAMFLOW IN SNOW DOMINANT RIVERS

Submitted by

Freddy Alejandro Saavedra Pimentel

Department of Geosciences

In partial fulfillment of the requirements

For the Degree of Doctor of Philosophy

Colorado State University

Fort Collins, Colorado

Summer 2016

Doctoral Committee:

Advisor: Stephanie Kampf
Co-Advisor: Jason Sibold

Steven Fassnacht
Jaffrey Nieman

ABSTRACT

SPATIAL AND TEMPORAL VARIABILITY OF SNOW COVER IN THE ANDES MOUNTAINS AND ITS INFLUENCE ON STREAMFLOW IN SNOW DOMINANT RIVERS

The climate is changing, and snowmelt-dominated river basins are particularly sensitive to climate warming. In the Andes Mountains in South America climate measurements are sparse and unevenly distributed in snow-covered areas. Thus, remote sensing offers opportunities to improve understanding of the spatial and temporal snow patterns in this region and explore how these patterns relate to climate and hydrologic response. This study uses snow cover data from the Moderate Resolution Imaging Spectroradiometer (MODIS) sensor to (1) identify snow climate regions across the Andes, (2) document trends in snow persistence and their relation to precipitation and temperature, and (3) develop statistical streamflow prediction models.

The second chapter of the study identified five snow climate regions: two tropical and three mid-latitude regions. In the tropical regions, snow cover was present only over 5000m on both sides of the Andes. In the mid-latitude regions the elevation of the snow line varied with latitude, dropping from 4000m to 1000m from 23 to 36°S. In the mid-latitudes, particularly where mountain peaks are highest, snow cover accumulates at lower elevations on the west side than on the east side of the Andes. The third chapter quantifies trends in annual snow persistence (SP) from 2000-2014. In the northern part of the study region, limited snow cover is present, and few trends in snow persistence were detected. A large area (70,515 km^2) south of 29°S is affected by a significant loss of snow cover (2-5 day less day of snow per year). In this latitude range, most of the land surface area with snow loss (62%) is on the east side of the Andes. The

trends of snow persistence relate to both precipitation and temperature, but the relative importance of each parameter changes across elevation and latitude. Precipitation has greater relative importance at lower elevations, whereas temperature has greater relative importance at higher elevations.

The final chapter explores the relationship between snow cover patterns and streamflow in snow-dominated rivers in the Chilean Andes (29-36° S). Snow covered area is correlated with water yield in snowmelt-dominated watersheds, but it is not as useful for water yield forecasts in watersheds with more limited snowmelt contributions. The snow cover information was combined with climatic variables (temperature and precipitation), and physiographic variables to develop statistical models of water yield (WY) and peak flow (PF). The final statistical model developed can forecast water year WY and PF in August using precipitation, snow cover, and area of watershed as predictors, with r^2 values of 0.8 and 0.7 respectively.

The approaches developed for applying snow cover information from remote sensing have led to important new findings about snow patterns in a large latitude range across the Andes Mountains. New tools developed for incorporating snow cover information into water yield and peak flow forecasts can aid water management under changing climate conditions.

ACKNOWLEDGEMENTS

As always, my first debt is to my wife, Claudia. Her support has been fundamental in my study but more important in my life. My research has been supported by the Chilean government through the Fulbright-CONICYT scholarship, which allowed my family and me to enjoy great years in my degree program. Thanks to my committee for being there when I needed you and for being always available and give me great advice. Thanks Jason and Steven. Specially thank to Jeffrey for the last minute incorporation into the committee due to the sad passing away of Robin. I particularly enjoy the lab group for their constructive and well thought out advice and parties together. Thanks Adam, Codie, Gabriel, and John. Last but least, I am very grateful for my advisor, Stephanie Kampf. She provided me the balance between freedom and guidance to explore and define my research. Thanks to all my friends to help to be far away from my family.

TABLE OF CONTENTS

CHAPTER 1: INTRODUCTION

The spatial and seasonal distribution of snow plays an important role in earth systems and human activities. More than one-sixth of the Earth's population depends on glaciers and winter seasonal snow packs for their water supply (Barnett et al., 2005; Knowles et al., 2006). At global scale, most of the winter seasonal snow is located in the North Hemisphere because of the larger land masses at high latitudes relative to the Southern Hemisphere (Foster et al., 2001). However in the Southern Hemisphere, snow still has an important role in some regions even though the land areas with snow are small compared to those in the Northern Hemisphere at the same latitudes.

The Andes Mountains has the largest snow reservoir outside of Antarctica in the Southern Hemisphere (Foster et al., 2009). This mountain range crosses the full length of South America across a broad latitude range in the southern hemisphere (Garreaud, 2009), with the northernmost extent of the Andes extending into the northern hemisphere. Most of the extratropical areas on the west slope of the Andes depend on water reserved as snowpack in headwater basins (Bradley et al., 2006; Peduzzi et al., 2010). In the central Andes of Chile (30°–37°S), snowpack is the primary source for streamflow (Cornwell et al., 2015; Masiokas et al., 2006). In a warmer world, less precipitation falls as rain rather than snow, and melting snow shifts earlier in the spring (Barnett et al., 2005; Knowles et al., 2006; Stewart, 2009). The Andes broadly reflect the global signal of warming: glacier retreatment in tropical (Rabatel et al., 2013) and extratropical areas (Barry and Seimon, 2000; Borsdorf and Stadel, 2015; Casassa, 2014), decreased precipitation across all latitudes (Barry and Seimon, 2000), and increased temperature

(Barry and Seimon, 2000). All changes have a strong elevation dependence and high spatial variability (Favier et al., 2009).

Changes in snow have consequences for streamflow production in snowmelt-dominated basins (Scherer et al., 2005; Stewart et al., 2005; Vicuña et al., 2010), and losses of snow will potentially have negative consequences for Andean water supply (Barry and Seimon, 2000). In the central Andes of Chile (30-37°S), river discharges are significantly correlated with the regional snowpack records (Masiokas et al., 2006), yet few studies on snowpack and streamflow changes have been made in this area compared with other mountain areas (Masiokas et al., 2006). Additionally, a very sparse network of snow courses and automated snow measuring stations (snow pillows) is present in the Andes Mountains (Aravena and Luckman, 2009; Cornwell et al., 2015; Masiokas et al., 2006). Even in regions with much more extensive snow monitoring, estimation of variability of snowpack characteristics from point measurements is difficult in mountainous environments due to high spatial variability (Molotch and Margulis, 2008). In this context, remote sensing data has great potential for supplying relevant spatial data for characterizing spatial and temporal patterns in snow.

Methods for using satellite remote sensing to map snow cover were developed in the 1960s, with the spatial and temporal resolution of available data improving over time (Dietz et al., 2012). Various remote sensing products have been used to map snow in all continents: Asia (Dedieu et al., 2014; Immerzeel et al., 2009) North America (Rango, 2009), South America (Foster et al., 2009), and Europe (Dedieu et al., 2014). Remote sensing has been applied to identify spatial-temporal trends in snow cover across large areas with inaccessible terrain (Immerzeel et al., 2009; Kwon et al., 2009) but in the Andes Mountain this study has not been conducted. A comprehensive understanding of the distribution of seasonal snow cover in the

Andes Mountains is essential to define a framework for studying snow in the region. The large latitudinal and elevation ranges in the Andes Mountains offer the opportunity to study how these two variables modulate the snow seasonal distribution. Mountains have complex topography and remote sensing can help to understanding how this topographic variability combines with precipitation and temperature to affect snow patterns in space and time.

Finally, snow remote sensing data can also aid in forecasting streamflow and improve hydrologic model performance (Parajka and Blöschl, 2008; Steele et al., 2010; Tekeli et al., 2005). Changes of streamflow in snow-dominated rivers have been attributed to increased temperatures and less precipitation (Knowles et al., 2006). However, local runoff varies due to the combination of geographic location, latitude, elevation, and meteorological condition. The Andes lack the detailed streamflow forecasting models that are available in other snow-dominated regions such as the western United States and Europe.

This dissertation develops methods for using remotely sensed snow covered area data to link spatial and temporal patterns of snow in the Andes to streamflow. The first part of the study (chapter 2) develops a new remote sensing methodology to characterize snow climatology across the Andes using snow cover data. This method identifies and maps snow regions across the Andes. The second portion of the study (chapter 3) uses the same remotely sensed snow cover data to quantify changes in snow cover and their spatial patterns with latitude and elevation and to explore how these changes have been affected by climate variables. Finally, the final portion of the study (chapter 4) examines how snow cover patterns relate to streamflow and develops a statistical model to predict water yield and peak flow in the central Chilean Andes (29-36°S) using snow cover data combined with other physiographic and climate variables.

CHAPTER 2: A SNOW CLIMATOLOGY OF THE ANDES MOUNTAINS FROM MODIS SNOW COVER DATA

2.1. INTRODUCTION

Snowpack provides a large reservoir of water in snow-dominated river basins. More than 80% of the population in semi-arid tropical and subtropical regions depends on mountains for fresh water (Liniger and Weingartner, 1998). In South America, Peru, Bolivia, Chile, and Argentina all depend on snow and/or glacier melt for water supply because rainy seasons are short, lasting only a few months (Bradley et al., 2006; Masiokas et al., 2013; Peduzzi et al., 2010; Rabatel et al., 2013). The location and duration of snow cover are driven by both precipitation and temperature (Barnett et al., 2005), and snow cover in turn affects both the water cycle and energy balance (Stewart, 2009). In the Southern Hemisphere, seasonal snow cover is mainly confined to southern South America, where extensive winter snow cover may occur (Foster et al., 2009). Unfortunately, in this region climate data are sparse and unevenly distributed (Aravena and Luckman, 2009). This poor availability of data is particularly true in mountain areas (Cortés et al., 2011; Masiokas et al., 2006). Additionally, estimation of variability of snowpack characteristic from point measurements is difficult in mountainous environments due to high spatial variability and scarce observations (Molotch and Margulis, 2008). Thus, remote sensing offers opportunities to improve understanding of snow cover seasonality and how it varies through the Andes region.

Snow water equivalent (SWE) is the key hydrological variable for water supply estimation, but remote sensing products used to derive SWE typically have coarse spatial resolution, and interpolation of SWE between point monitoring locations can be inaccurate (Fassnacht et al.,

2012; Molotch and Margulis, 2008). Optical sensors such as Moderate Resolution Imaging Spectroradiometer (MODIS) can be useful in providing finer spatio-temporal resolution snow covered area (SCA) information. Snow cover patterns and their seasonal variability are useful for both forcing and evaluating hydrologic models (Fassnacht et al., 2012; Martinec et al., 2008; Sturm, 2013), and patterns of snow cover can help identify climate signals (Barnett et al., 2005; Brown and Mote, 2009). The goal of this chapter is to develop a method for characterizing snow climatology across the Andes using MODIS snow cover data. There are two specific objectives: (1) to identify regions of the Andes where snow accumulates at similar elevations and times of year, and (2) to identify snow persistence zones within these regions.

2.2. STUDY SITE

The Andes Mountains span more than 8,000 km from 10º N to 57º S and through seven countries (Venezuela, Colombia, Ecuador, Peru, Bolivia, Chile, and Argentina) (Barry, 2008). They have an average height of about 4,000 m with several peaks over 6,000 m (Figure 2.1). The Andes have a strong effect on atmospheric circulation and contain a wide variety of climates defined by Köppen-Geiger classification (Kottek et al., 2006), with sharp contrasts between East and West sides. In the upper-level large-scale circulation, there are moderate easterly winds in tropical latitudes (±15º) and westerly winds at subtropical/extratropical latitudes (Garreaud, 2009). In tropical latitudes, austral summer months (DJF) are the wet season because easterly winds bring in moist air, and solar heating over the altiplano induces convection (Garreaud, 2009). In these latitudes, the easterly source of moisture leads to higher precipitation on the eastern side of the Andes. In the Equatorial and Tropical Andes (10°N to 17°S) (Barry, 2008),

the glacier equilibrium-line altitude (ELA) is above 5,000 m, but the glacier ablation zone extends close to 4,600 m (Rabatel et al., 2013). Further south (17°S to 31°S) in the dry Desert Andes (Williams and Ferringo, 1998), hyper-arid conditions prevail on the west side primarily due to a semi-permanent high pressure cell over the South East Pacific. This in conjunction with the inversion layer at about 1,000 m and the coastal topography prevent the inland penetration of moist air from the Pacific Ocean (Garreaud and Aceituno, 2007). The east side of the desert area (*Altiplano* region) is dry most of the year except during austral summer (DJF) when an increase in the intensity of Bolivian High enhances easterly flow from the lowlands of Amazonia (Garreaud et al., 2003).

In the extratropical Andes, precipitation increases as compared to the Desert Andes, particularly during the winter due to westerly air flow from the Pacific. Here the snow line elevation decreases strongly with latitude, and there are large glaciers (Barry and Seimon, 2000; Vuille and Ammann, 1997; Williams and Ferringo, 1998). South of 40°S precipitation is high as a result of strong prevailing westerlies. Prior climate descriptions have divided this area into two sub regions separated at 46°S: the northern Lakes Region, with a Mediterranean climate regime, and the Patagonian Andes, which has a large concentration of low-elevation glaciers (Barry, 2008) (Figure 2.1). Snowfall patterns have not yet been mapped in detail for this region, but they are indicators of the combined effects of latitude, elevation, and circulation patterns on climate. This study uses snow cover information to expand the understanding of spatial and seasonal snow patterns across the wide latitudinal range of the Andes.

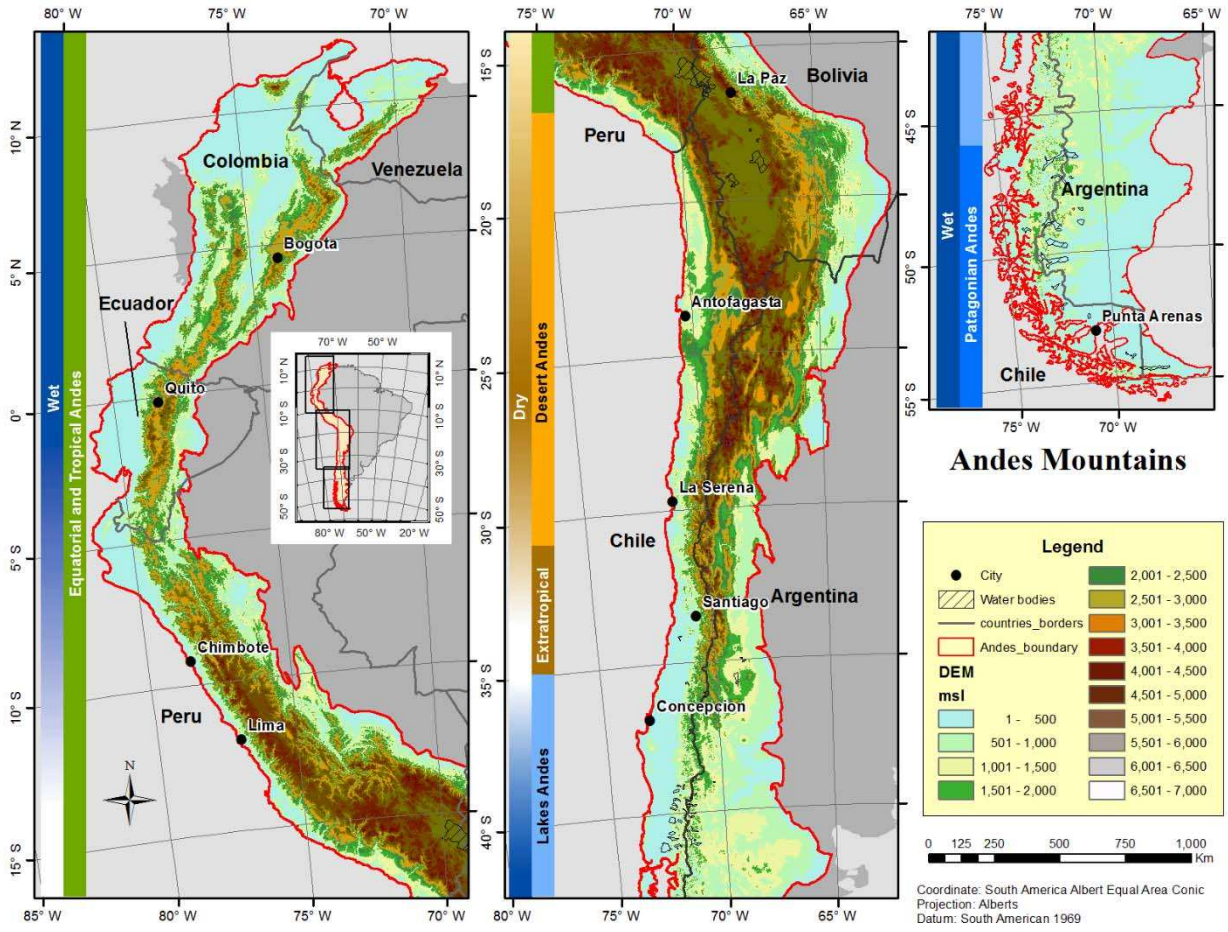

Figure 2.1. Digital Elevation Model (DEM) of the Andes Mountains with external side bars showing precipitation patterns and internal side bars showing Andes regions.

2.3. METHODS

2.3.1. Data

All snow cover analyses used data from the MODIS sensor, which is a passive imaging spectroradiometer that provides daily imagery of the Earth's surface and clouds in 36 spectral bands by two satellites (Terra and Aqua) (Hall et al., 2002). We used the MODIS - Terra eight-day 500m binary snow cover products Collection 5 (MOD10A2). The MOD10A2 represents the

maximum snow cover and minimum cloud cover during that eight-day period from the daily time step product (MOD10A1)(Riggs et al., 2006). The study area is covered by 19 MODIS images (tiles). For these tiles, the snow cover was determined every 8 days using the maximum MODIS binary snow cover products from 2000 to 2014 (MOD10A2) (http://reverb.echo.nasa.gov), giving a total of 12,860 tiles of MOD10A2.

To address the effect of elevation on snow patterns, a DEM was developed using two sources: (1) 600 tiles of Shuttle Radar Topography Mission (SRTM) 90 m spatial resolution (http://srtm.csi.cgiar.org), and (2) 579 tiles of Advanced Spaceborne Thermal Emission and Reflection Radiometer (ASTER) 30 m spatial resolution (http://reverb.echo.nasa.gov). The SRTM DEM was the primary source of elevation information; however this source had data gaps and other errors. Errors were identified and masked by looking for abnormal slope (over 300%) in the SRTM DEM. ASTER DEMs were used to fill in the gaps and errors in the SRTM data. In cases where both the SRTM and ASTER DEMs had data gaps, a Kernel filter of 10x10 windows was run to interpolate values in the gaps. The composite DEM was masked with the boundary of the Andes study area (Andes DEM). To examine snow cover patterns by elevation and latitude, the Andes DEM was divided into 100 m elevation bands and into latitude bands of 50 km from North to South. The continental divide along the Andes was defined using the Watershed Tool from ArcGIS to delineate the side (East or West) of drainage, and the study area was further divided into West and East Andes.

MODIS and DEM data were mosaicked and projected into the South American Alber's equal area azimuthal projection. This projection is often used in large scale analysis and shows minimal shape distortion to less than 2 percent within 15 degrees from the focal point (Kennedy

and Kopp, 1994). The focal point of this projection was set to 70ºW, 25ºS to cover most of the study area with low distortion.

2.3.2. Snow climatology analysis

Richer et al. (2013) developed spatiotemporal indices of snow and cloud cover using MODIS SCA for a mountain area in the Colorado Front Range, U.S. to define dominant tendencies in the location and timing of snow cover. They defined the snow cover index (SCI) and cloud cover index (CCI) by the follow equations:

$$SCI = \frac{S}{n-C} * 100 \quad \text{Eq. 1}$$

$$CCI = \frac{C}{n} * 100 \quad \text{Eq. 2}$$

Where S = number of years which a pixel was classified as snow, n = total number of years, and C = number of years in which a pixel was classified as cloud.

Both indices range from zero (no snow or cloud during all years) to one (presence of snow or cloud in all years). This study used SCI time series to identify snow climate regions by elevation and timing of snow accumulation. The first step was a pixel-by-pixel analysis to calculate the SCI and CCI for each eight-day interval over all years of data (2000-2014) following Richer et al. (2013). When the CCI was greater than 30%, the SCI was not calculated, and the pixel was masked as "cloud" (Moore et al., 2015). To examine variability in SCI patterns by region, the study area was divided into 50 km latitude bands, 100 m elevation bands, and side

(west and east) of the Andes Mountains for each 8-day time window. The average SCI and CCI were then calculated for each latitude-elevation-side subdivision. These subdivision average SCI values were reclassified in 10 equal parts from 0 to 100 (decile categories). As an additional step to mask cloud-impaired data, when the average CCI for an elevation interval was more than 30%, the SCI was not calculated, and this time window/elevation band was masked from the analysis (Figure 2.2a). To evaluate annual snow patterns, the snow persistence (SP) was also calculated as the average %SCI over the year for each latitude-elevation band (Figure 2.2b). Within each latitude band, a snow persistence curve (SPC) was developed as a plot of the change in SP with elevation. To determine the rate of change of SP with elevation, we fit a line to the curve between 5% and 90% SP. SP values lower than 5% were not used due the asymptotic behavior of curve that affected strongly the r^2 of linear regression. Higher values than 90% were also excluded because they were present in just a few bands and usually represented few pixels at high elevation. From these linear fits, we saved the inverse slope value, which indicates how sharply the annual average snow persistence changes with increasing elevation.

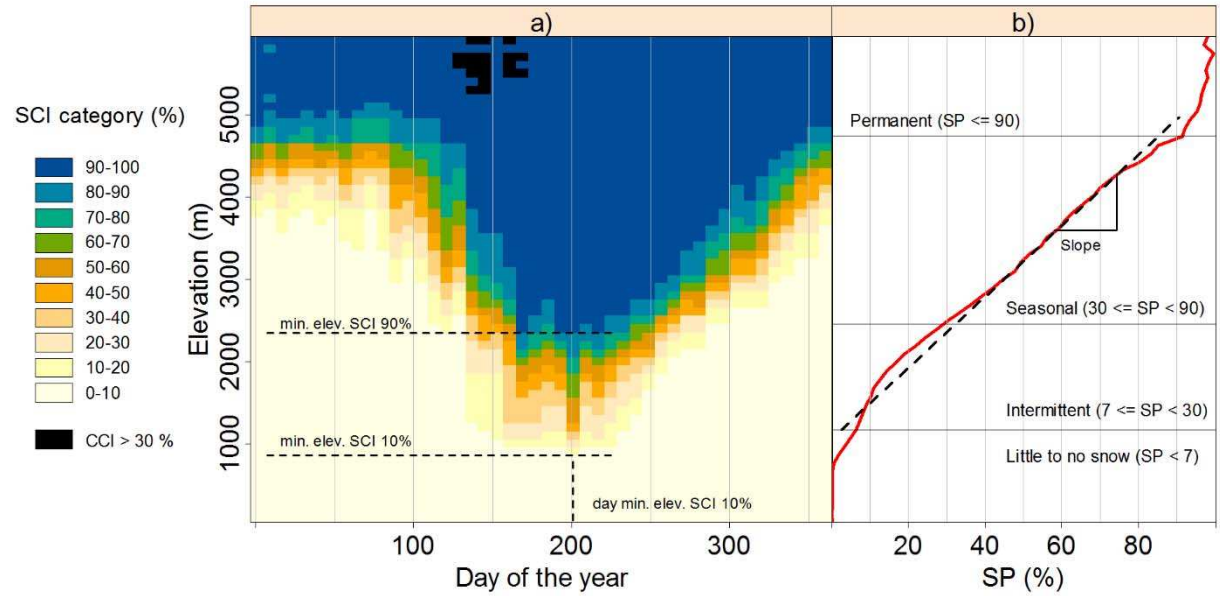

Figure 2.2. Example calculation of (a) 2000-2014 SCI with cloud-impaired areas masked using CCI>30%, and (b) 2000-2014 snow persistence curve (SPC) showing linear fit to the curve between SP 5-90%.

To address objective 1 and identify regions where snow accumulates at similar elevations and times of year, three parameters were extracted from SCI and SP data analysis for each 50 km latitude band (east and west): (1) minimum elevation for each SCI decile category (Figure 2.2a), (2) slope of the SPC (Figure 2.2b), and (3) day of year of minimum elevation for each SCI decile category (Figure 2.2a).

Using these three spatio-temporal snow cover indices, cluster analysis was used to identify regions with similar snow climatology. Spatial patterns were characterized using the minimum elevation of SCI=20% and the slope of the SPC. The seasonal patterns were defined by the day of minimum elevation for SCI=20%. SCI=20% represents an approximate elevation of the snow line in each latitude band, where snow line is defined as the lowest elevation that regularly experiences snow cover (>20% of years). SCI 20% was selected for snow line definition and cluster analysis due the lower noise than SCI 10% and fewer data gaps relative to higher SCI categories. Before running the cluster analysis, all three indices were standardized by subtracting

of the mean and dividing by the standard deviation. The standardization of data is required so that each variable contributes equally in the cluster analysis (Norusis, 2012). The K-means clustering analysis was used due the moderate number of data, and different numbers of clusters were tested (from 2 to 6) to find the best solution that could be easily interpreted (Abonyi and Feil, 2007). The Partitioning Around Medoids (*pam*) function in the "Cluster" package for R software was used due the robust version of K-means (Maechler et al., 2015). Finally, the combination of the three cluster analysis outputs (minimum elevation, slope of SPC, and day of year of minimum elevation) was used to map regions with similar spatial and seasonal patterns of snow cover.

For objective 2, to identify snow persistence zones, thresholds of SP were used as boundaries of snow zones. SP captures the dominant tendency of an area to be snow covered or snow-free. Based on Jan 1th through July 3th values of SP, Moore et al. (2015) defined four snow zones: little or no snow (<25%), intermittent (25-50%), transitional (50-75%), and persistent snow zone (>75%). By their definition, intermittent snow does not persist throughout the winter and is not present every winter; transitional snow persists throughout the winter, but the timing of spring snow loss is earlier in the spring at lower elevations, and persistent snow lasts throughout the winter and spring and exhibits synchronous loss of snow with elevation in the late spring. Compared to the western U.S. study area of Moore et al. (2015), the timing of snow accumulation in the Andes is different due to the large latitude range and position of most of the mountain range in the Southern Hemisphere. Therefore, the current study re-defines the thresholds for snow zones based on annual SP rather than partial year and the patterns present in the Andes (Figure 2.2): (1) little or no snow (<7%), (2) intermittent snow zone (7-30%), (3) seasonal snow zone (30-90%), and (4) permanent snow zone (≥90%). Definitions for zones 1 and

2 in this study are the same as in Moore et al. (2015). Zone 3 (seasonal snow zone) encompasses the transitional and persistent snow zones defined in Moore et al. (2015), and Zone 4 (permanent snow zone) represents areas where snow lasts year-round during most years.

2.4. RESULTS

2.4.1. Cloud masking

Cloud cover had a substantial impact on SCI calculations. Cloud cover was more prevalent in the winter and spring in the central part of the study area (from 10°S to 38°S), and homogeneously distributed over time in the northern and southern parts of the study area. The highest proportion of cloud cover for an individual pixel was more than 95% in wide areas of the tropics north of 8°S and in Patagonia south of 39°S. Using the threshold of CCI > 30% to mask areas of high cloud cover impairment led to reducing the study area to the area between 8°S and 39°S (Figure 2.3). Additionally, the area around large salt flats, *salares*, (20°S), was also masked from this study because the high reflectance on the surfaces of some of the *salares* causes them to be misclassified as snow (Riggs et al., 2006). The remaining study area covers around 1.45 million square kilometers.

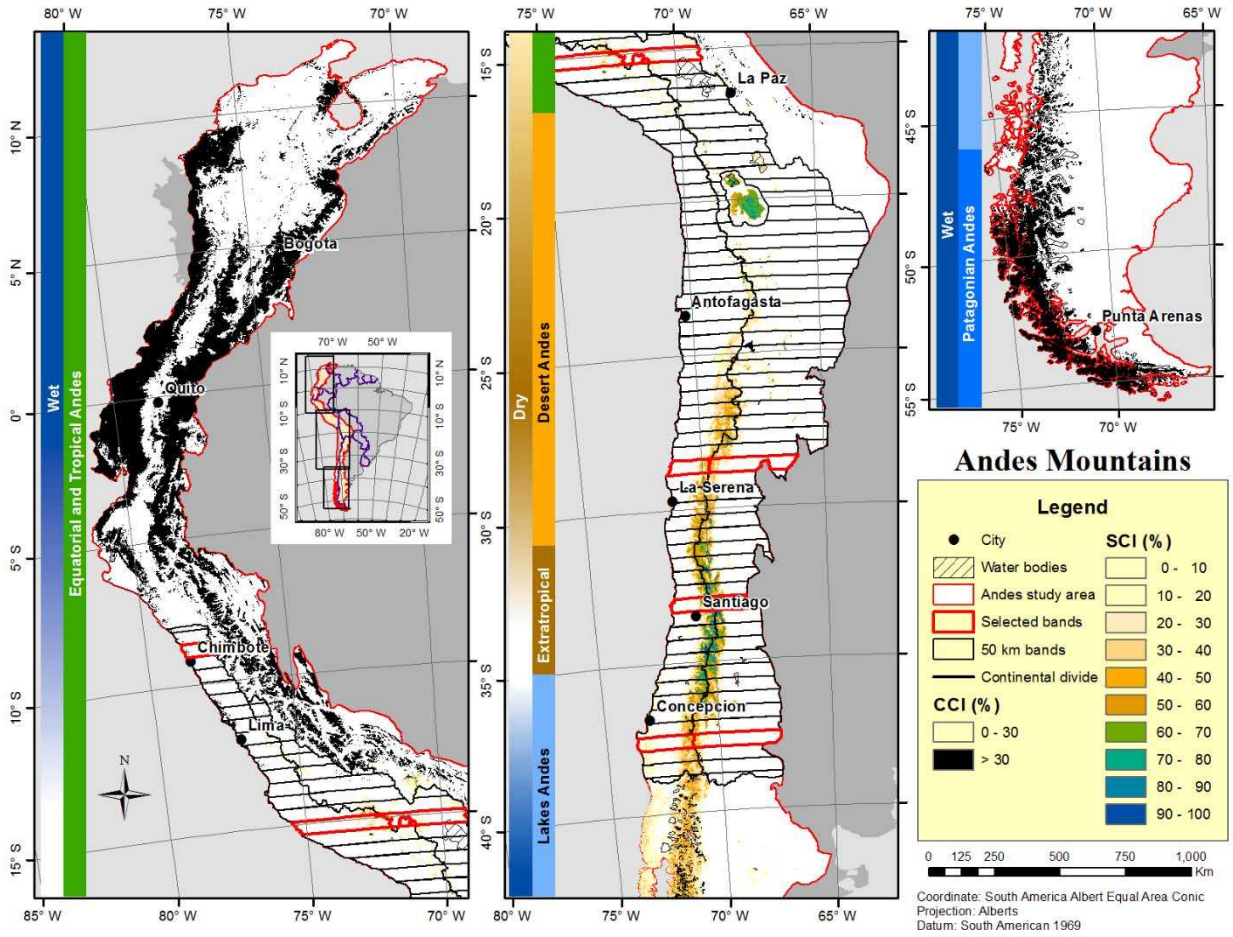

Figure 2.3. Andes Mountains with maximum 2000-2014 SCI for any 8-day interval in the year. Areas with CCI > 30% are masked in black. Areas with latitude bands marked (horizontal lines) were used for further data analysis, whereas those to the north and south were excluded due to high cloud cover impairment. Areas around salt flats (20°S) were also masked from the study area (see polygon surrounding excluded area).

2.4.2. SCI patterns

The spatial-seasonal patterns of SCI reveal dominant features in the snow covered area. These patterns are shown as raster plots of the 2000-2014 SCI (with CCI>30% masked) in nine selected 50 km bands named by center latitude (number and first letter) and side of the Andes Mountains (last letter) (Figure 2.3). For example 9SW is the band centered at 9°S Lat. on the West side of the Andes. We present some examples of these plots to illustrate the regional

variability (objective 1) and snow zones (objective 2). Each selected band shows an increase of SCI with elevation (Figure 2.4), but the seasonality and elevation patterns of SCI differ from North to South. The two northern bands are located in the Equatorial and Tropical Andes region (Barry, 2008), but the patterns of snow cover are different. The 9SW band has a high elevation snow cover, with SCI ≥10% at 4,800 m throughout the year; this indicates that snow accumulates during some years at 4,800 m and is rarely observed at lower elevations. SCI values of ≥90% are found at 5,800 m in the austral summer, shifting down to 5,200 m during the austral winter season (middle year in Southern Hemisphere). These high SCI values indicate snow is present nearly every year at these dates and elevations. SP values for the lower elevation boundaries of intermittent, seasonal, and permanent snow zones are 4,800, 5,000, and 6,000 m, respectively. A little further south, 16S bands (both West and East) show a high elevation snow cover, with SCI 10% at 4,700 m on both west and east sides and SCI 90% in the west side at 5,300 m. The elevation boundaries for intermittent snow zones are equal to those of the 9SW band, but seasonal and permanent snow zone boundaries are higher than in the 9SW band (5,400 m and 5,800 m, respectively). SCI values extend to their lowest elevations during the first 100 days of the year in these latitudes, indicating that snow covered area tends to be greatest in the austral summer due to the enhanced easterly flow from the lowlands of Amazonia and convection that produces the "*invierno altiplanico*" (plateau winter) (Garreaud et al., 2003) (Figure 2.4).

The Desert Andes region (Barry and Seimon, 2000; Vuille and Ammann, 1997; Williams and Ferringo, 1998) is represented by 27S bands. On the west side the minimum elevation of SCI 10% decreases from 4,800 m at 16SW to 2,900 m in the 27SW band. On the east side decreasing minimum SCI elevation from North to South was also detected, but the difference between 16SE and 27SE bands was lower (from 4,800 m to 3,600 m). The lowest elevation for any SCI >10%

category occurred during winter months (day of year 160 -200) on both sides of the mountains. SP values indicate a lower frequency of snow in the 27S desert bands compared to the tropical bands because just intermittent and seasonal snow thresholds are reached. The lower elevation boundary of the intermittent snow zone is 3,500 m on the west side and 4,100 m on the east side. The seasonal snow threshold on the west side is 5,000 m, and the east side does not have seasonal snow, as the maximum SP is 30% (Figure 2.4).

The extratropical and Lakes Andes regions (Barry and Seimon, 2000; Vuille and Ammann, 1997; Williams and Ferringo, 1998) are represented by 33S and 38S bands. In this range of latitudes, the lower elevations of each SCI category decrease from North to South, and the elevation is consistently lower on the west side. SCI 10% decreases from 1,200 m in the 33SW band to 300 m in the 38SW band on the west side of the Andes and from 2,700 m to 1,300 m on the east side. For 33S bands snow zone boundaries were consistently at lower elevation on the west side compared to the east side (1,900 m and 2,800 m for intermittent, 2,800 and 4,700 m for seasonal, and 5,200 and 5,300 m for permanent). The 38S bands show similar patterns to the 33S bands, but snow zone boundaries were at lower elevations (1,000 m, 1,500 m, and 2,700 m for intermittent, seasonal and permanent snow zones on the west side). The east side again had higher elevation values for each category (1,600 m and 2,000 m for intermittent and seasonal snow zones). The permanent snow zone was not present in this band on the east side. All 33S and 38S bands show similar seasonal patterns, with the minimum elevation of SCI 10% during winter around day of year 200 (Figure 2.4).

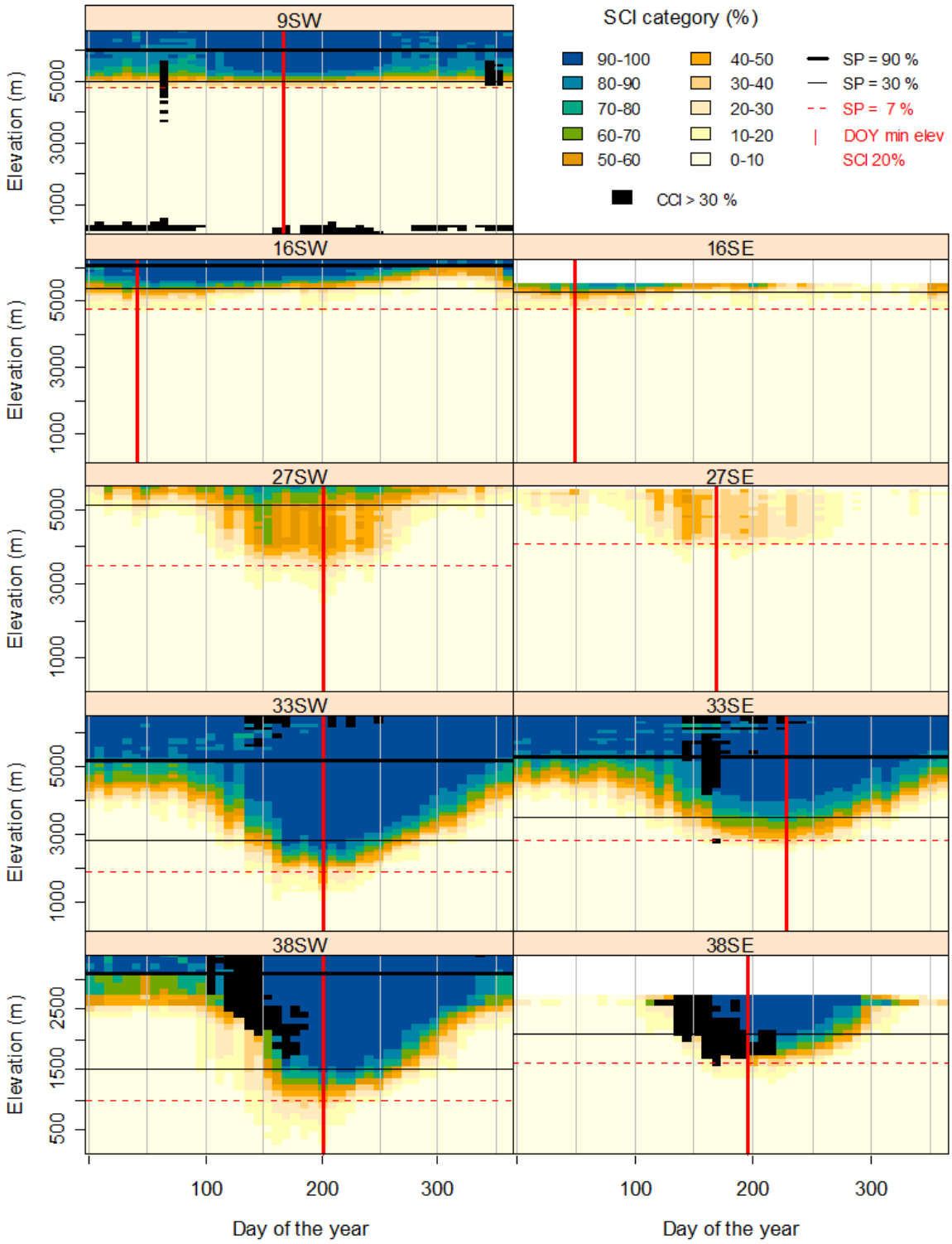

Figure 2.4. Raster plots of the 2000-2014 8-day time step SCI for 100 m elevation bands in nine 50 km latitude bands including 15 years of data. Elevations >5,300 m are excluded for the 16SE band, and > 2,600 m for 38SE band due the small (< 1 km^2) surface areas of these elevation bands.

2.4.3. Snow regions

Three parameters were derived to identify regions with similar snow accumulation elevations and seasonality. First, the minimum elevations of each SCI decile category were defined by taking the lowest elevation across the year using the SCI raster plot (Figure 2.2a) and plotting these values for each latitude band in Figure 2.5.

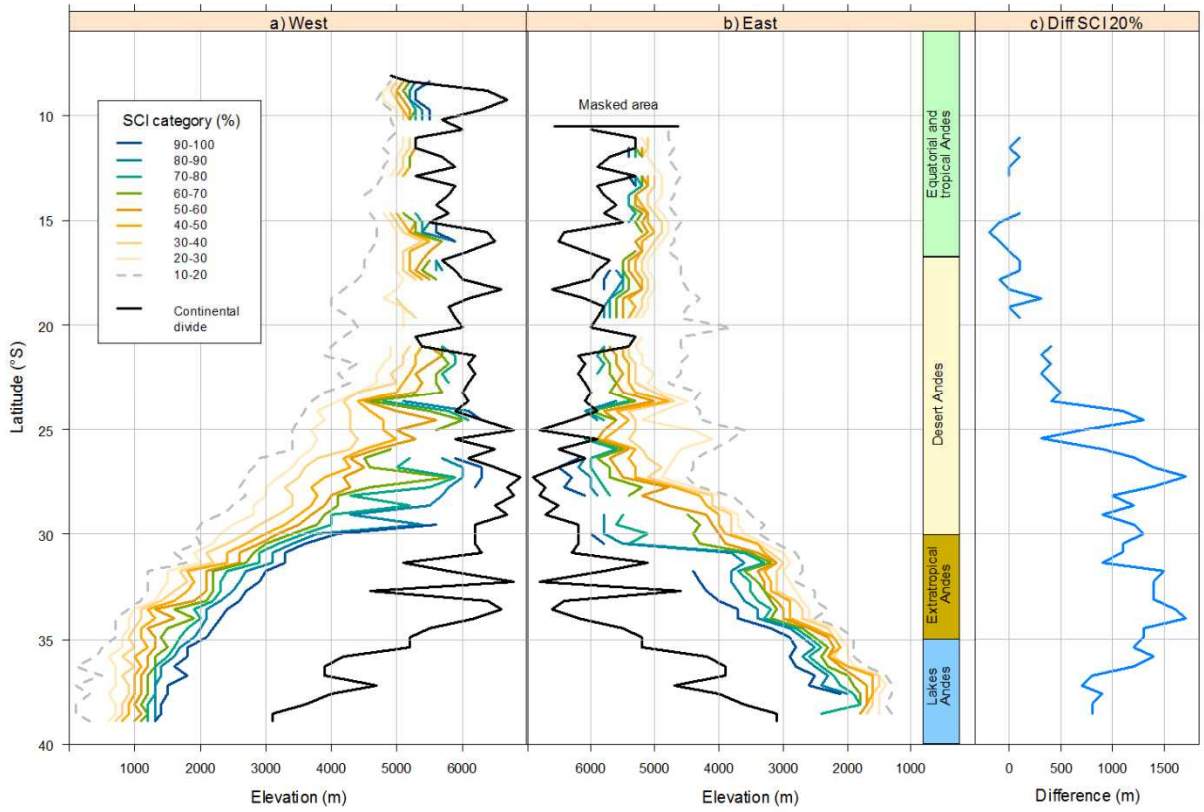

Figure 2.5. Minimum elevation of each 2000-2014 SCI decile category by latitude band for (a) west and (b) east side of Andes Mountains. (c) Difference between minimum elevations for SCI 20% (East minus West).

In the northern (between 8°S and 23°S) and central (between 25°S and 36°S) regions mountain peaks can exceed 6,000 m, and further south the mountain peaks decrease to 3,000 m. Cluster analysis of the minimum elevation of SCI = 20% divided the general pattern of minimum snow elevation into three main regions: high-stable, middle-variable, and low-stable snow elevation (Figure 2.6a). In the west side, the high-stable elevation begins at 8°S. In this region snow cover begins to accumulate at 5,000 m (SCI 10%), and high snow cover (SCI 90%) is present above 5,500 m. These elevations of snow accumulation are similar between 8-15°S, although some bands around 11°S and between 13°S and 14°S do not have enough snow data to define SCI per elevation (Figure 2.5). South of 15°S the higher SCI (≥30%) increases a little in elevation, but lower SCI (10 and 20%) decreases in elevation. The middle-variable region begins at latitude 23°S. In this region, the elevation of all SCI categories decreases with latitude, but lower values of SCI (<50%) decrease at a lower rate than higher SCI categories (>50%). South of 30°S all categories continue decreasing in elevation at similar rates. In the low stable region south of 35°S all SCI categories maintain similar elevations, with only a slight decline in elevation with latitude.

The east side has a similar pattern to the west but with two main differences. The latitude boundaries for the high-stable, middle-variable, and low stable regions are further south than on the west side (25°S and 37°S). The other main difference between sides is the value of elevation for each SCI category. To compare this elevation difference across latitude bands, SCI 20% (snow line) is shown in Figure 2.5 (East minus West side snow line elevation). In the northern part of the study area (north of 20°S), no difference between west and east sides is evident. South of 20°S, the difference between sides increases with latitude to a maximum of 1,700 m at 27 and 34°S, meaning that the western side of the Andes had 1,700 m lower elevation of snow cover

than the east side. South of 34°S, the difference between sides decreases with latitude because the height of the mountain range decreases and reduces the orographic effect on precipitation.

The second parameter used to define snow regions is the inverse slope of the snow persistence curve (SPC), which was calculated for each band (Figure 2.2b) to determine the rate of change in snow persistence with increasing elevation. Two clusters were defined using the inverse slope values (Figure 2.6b): (1) Steep, and (2) Gradual. The steep cluster has an average value of 0.069 SP/m and wide range of slope values (std. deviation of 0.025). It is located between 8°-22°S on the west side and 10°-24°S on the east side; the north boundary was limited by the cloud masked area. The gradual cluster has an average value of 0.025 SP/m and a narrower range of slopes (std. deviation of 0.008). This cluster extends from the southern boundary of the steep cluster to 39°S, the southern boundary of study area.

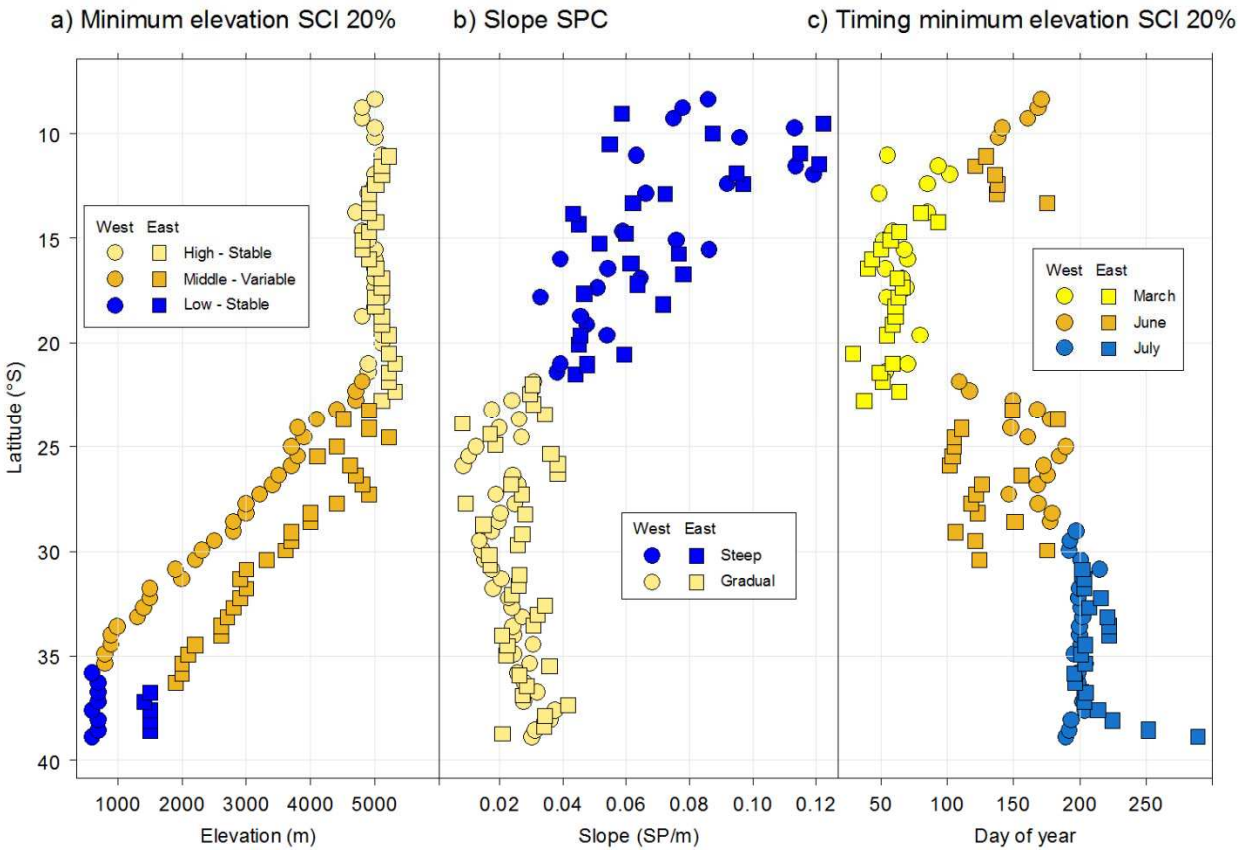

Figure 2.6. Cluster analyses results over 50 km latitude bands by (a) minimum elevation of SCI 20%, (b) inverse slope of SPC, and (c) day of year of minimum elevation for SCI 20%.

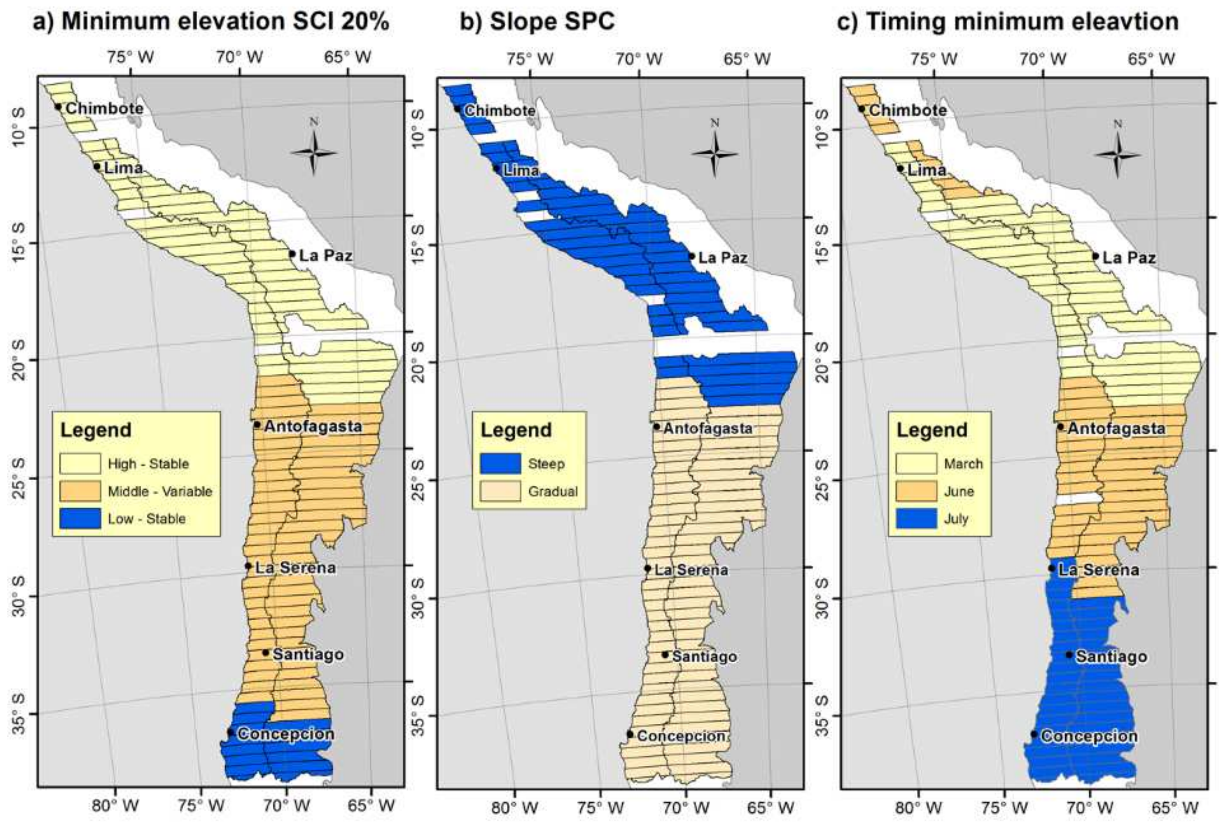

Figure 2.7. Maps of cluster analysis results for 50 km latitude bands by (a) minimum elevation of SCI 20%, (b) inverse slope of SPC, and (c) day of year of minimum elevation of SCI 20%.

The third parameter for defining snow regions is the day of the year of lowest elevation of SCI 20% (timing minimum elevation). A cluster analysis defined four clusters of minimum elevation of SCI 20% (Figure 2.6c). Two clusters were aggregated into one because they have similar timing but are geographically separated. In the March group (fall maximum snow), the average day of minimum elevation SCI 20% is day 76 (March 17th). This cluster extends from 11°S to 23°S. In the north this cluster has greater representation in the west side, whereas in the southern area the presence of the cluster is more on the east side. The June group (early winter maximum snow) cluster includes two areas from 8° to 14°S and 23° to 31°S. The average timing of minimum elevation of snow cover was day 163 (June 12th), but the minimum elevation tended to occur earlier in the year on the east side than on the west side. Finally, the July cluster (late

winter maximum snow) extends from 29°S to 38°S with an average minimum elevation of day 199 (July 18th).

The spatial extent of the regions defined by the three snow parameters is illustrated in Figure 2.7. Latitude bands with no presence of SCI 20% were excluded from analyses for minimum elevation SCI and timing of minimum elevation, and latitude bands that had <3 elevation bands with snow cover were excluded from the slope SPC analyses. Collectively the three region classification parameters show that in tropical latitudes (8°S to 23°S), snow cover is found at the highest elevations, with a steep change in SP with elevation and peak snow cover in March, except at the northernmost extent of the region. Overlapping of the three cluster maps divides this area into two snow regions (Figure 2.8, Table 2.1). The northernmost region, Tropical-latitude1, covers 4% of the study area. This region has high snow cover elevation, a steep change in snow accumulation with elevation, and austral winter maximum snow cover. The region extends from 8°S to 10.5°S on the west side of the Andes and from 11°S to 13.5°S on the east side. The next tropical region, Tropical-latitude 2, covers 35% of the study area. This region differs from Tropical latitude 1 primarily in the timing of snow cover, which peaks in austral fall. The region extends from 11°-21.5°S in the west and from 13.5°-23°S in the east side.

In mid-latitudes south of the tropics, the snow cover drops in elevation, and the change in snow cover with elevation becomes more gradual. These regions all have winter maximum snow cover, but the timing of peak snow cover shifts later in the winter further south (Figure 2.7). Combining the extent of the cluster zones defined in Figure 2.7, the mid-latitude snow regions are separated into three sub-groups (Figure 2.8, Table 2.1). Mid-latitude 1 extends from the southern boundary of region 2 to 29°S in the west and to 30.5°S in the east. This region has middle elevation snow accumulation and early winter peak snow cover. Mid-latitude 2 extends

from the southern boundaries of Mid-latitude 1 to 35.5°S in the west and 36.5°S in the east. This region differs from Mid-latitude 1 only in the later timing of peak snow cover. Finally Mid-latitude 3 extends to 39°S, the southern boundary of the data analysis. It differs from Mid-latitude 2 in that it has lower elevation of snow accumulation.

Table 2.1. Summary characteristics of five Andes snow climatology regions. SCI numbers give areas (km^2) of each SP category per region.

Parameter	Tropical-latitude 1	Tropical-latitude 2	Mid-latitude 1	Mid-latitude 2	Mid-latitude 3	Total
Minimum elevation of SCI 20% (m)	High 5,010 ± 99	High 5,032 ± 132	Middle 4,067 ± 646	Middle 2,018 ± 725	Low 977 m ± 417 m	
Inverse slope of SPC (SP/m)	Steep 0.093 ± 0.023	Steep 0.061 ± 0.020	Gradual 0.024 ± 0.008	Gradual 0.024 ± 0.006	Gradual 0.031 ± 0.005	
Timing of minimum elevation of SCI 20%	June 155 ± 12	March 83 ± 41	June 166 ± 21	July 201 ± 13	July 198 ± 28	
Little or no snow (km^2)	63,017	483,475	416,721	186,980	125,158	1,275,351
Intermittent (km^2)	1,159	17,333	47,651	29,081	23,024	118,248
Seasonal (km^2)	664	1,166	7,058	39,555	13,113	61,556
Permanent (km^2)	22	71	84	1,110	20	1,307
Total area (km^2)	64,863	502,044	471,514	256,727	161,315	1,456,463

2.4.4. Snow zones

Analyses of seasonal patterns of SCI and SP across latitudes bands exhibited four distinct levels of SP that were used to delineate snow zones. A summary of snow zone areas for each snow climatology region is shown in Table 2.1, and a map of the distribution of snow zones within each snow climatology region is shown in Figure 2.8. In the study area as a whole, 12% of the area has intermittent, seasonal or permanent snow. The intermittent snow zone covers the largest area (8%), seasonal snow cover 4% and just 0.8% has permanent snow. The mid-latitude

region 1 has the largest area of intermittent snow, which covers 10% of this region and 40% of the total intermittent snow zone in the study area. The mid-latitude region 2 has the largest areas of seasonal and permanent snow, which represent 16% of this region, 64% of seasonal snow, and 85% of permanent snow in the study area.

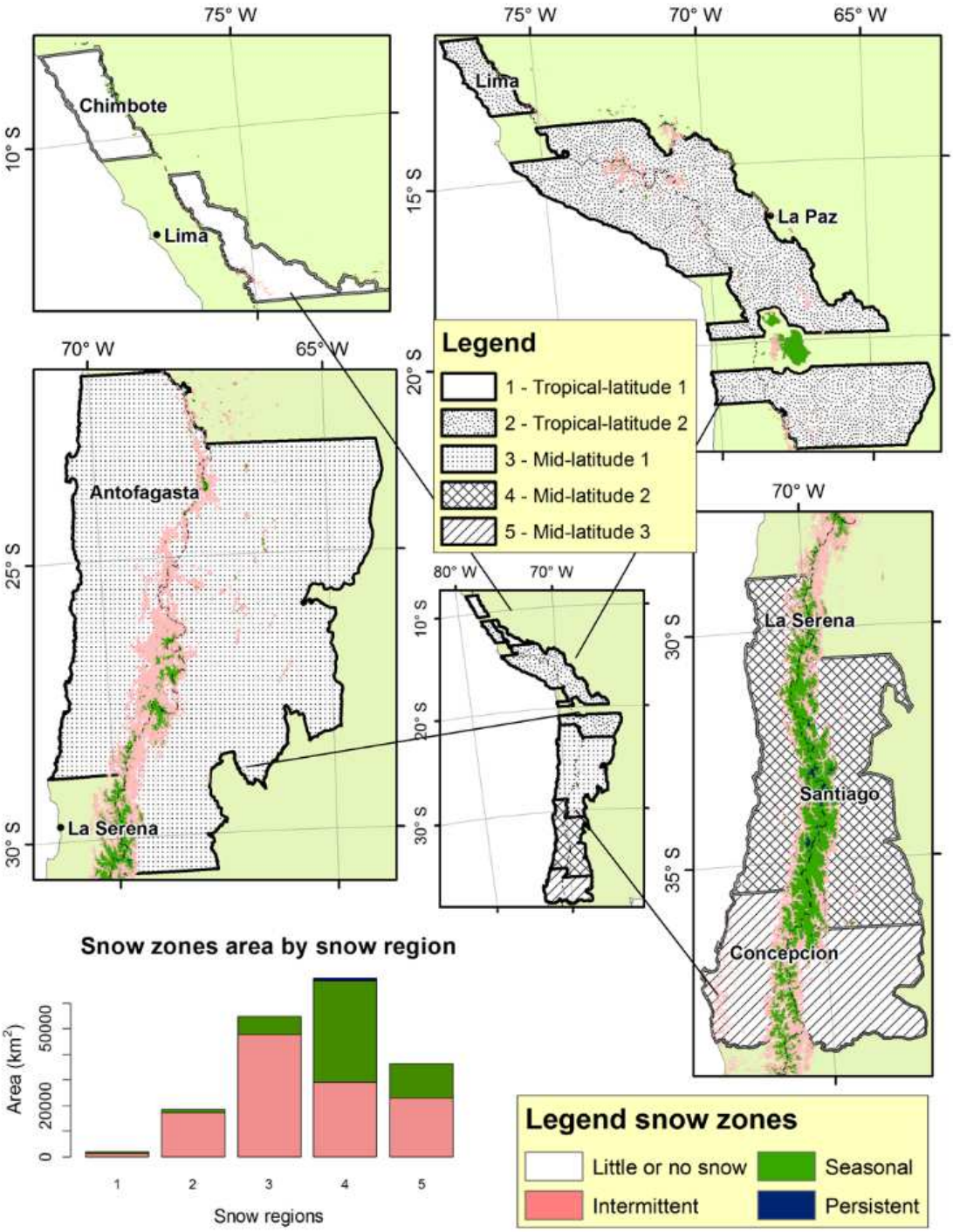

Figure 2.8. Distribution of snow zones by snow region.

2.5. DISCUSSION

We used MODIS data to document connections between the patterns of spatial and seasonal snow cover and climate conditions across the Andes, identify locations of snow lines, and quantify rates of changes in snow persistence with elevation. Overall, the snow line elevation (SCI 20%) decreased with latitude from 5,000 m at 10°S to 700 m at 38°S. Snow cover extended to the lowest elevations during austral winter (JJA) except in tropical latitudes between 12° to 23°S. The rate of change in snow persistence with elevation has a break point at Tropic of Capricorn, with a steep slope north of this limit and a more gradual slope to the South.

North of 23°S two snow regions are defined: Tropical-latitude 1 (TL1) and Tropical-latitude 2 (TL2). TL1 exhibits less seasonal variability in snow line elevation (band 9SW in Figure 2.4), but there is some evident seasonality in high SCI categories, with a decrease in the elevation of high SCI during austral winter (JJA). The slightly greater SCI during JJA is inconsistent with seasonal patterns of precipitation in these latitudes. TL1 is located in an outer tropic climate zone, which is characterized by low seasonal temperature variability, high solar radiation influx all year round, and high seasonality in precipitation (Rabatel et al., 2012). The dry season lasts from May to September and wet season from October to March (Garreaud, 2009; Rabatel et al., 2013). Most of the snow falling during the wet season lasts for a short duration (hour to days) due high solar radiation in austral summer (Lejeune et al., 2007; Wagnon et al., 2009). Due to this short duration of snow on the ground, brief periods of snow cover in TL1 during the wet season may not have been detected during the times of MODIS sensor overpass. It is also possible that snow was mis-classified as cloud during the wet season, although we have no reason to expect that mis-classifications of snow vs. cloud were greater in

this area than elsewhere. It is more likely that cloud cover occurs more regularly, as seen by the CCI>30% across most elevations around day 70 and 350 in band 9SW (Figure 2.4), and this may alter the SCI due to the short period of observation. During the dry season, although less snow falls than in the wet season, any precipitation that falls at high elevation is typically snow, and any snowfall occurring in May–August may persist longer due to more limited ablation (Rabatel et al., 2012). Therefore, the dry season snow cover peak (day of year 155) probably relates to greater persistence of snow, which made it more likely to be detected by MODIS. The timing of highest snowline elevation is similar to transient snowlines documented in prior studies in the area (Hanshaw and Bookhagen, 2014; Rabatel et al., 2012).

Tropical-latitude 2 (TL2) is located in the Desert Andes, where the semi-permanent high pressure zone in the Pacific is a primary cause of extremely dry conditions on the west side of the Andes. This region does have a peak in snow accumulation following the tropical wet season, consistent with the timing of maximum positive mass balance of glaciers in the area (Arnaud et al. 2001). During the austral summer (DJF), elevated precipitation during the "*invierno altiplanico*" leads to peak snow cover in March between 11-23°S (Garreaud et al., 2003). The easterly winds lead to greater precipitation on the east side than the west (Houston and Hartley, 2003), but this does not create a difference in snow cover elevations on either side of the Andes (Figure 2.5c). This lack of difference in snow cover elevation may indicate the presence of snow is limited by temperature in the tropics, although prior glacier studies in the region highlight the importance of both precipitation and temperature patterns in snow line elevation (Arnaud et al., 2001). Snow line elevations in this region are similar to those documented in prior glacier-focused research (Arnaud et al., 2001; Hanshaw and Bookhagen, 2014). These studies have

examined longer periods of time than in our MODIS analysis and have found increases in snow line elevations over the past several decades.

South of 23°S, air temperatures cool, leading to a greater rate of decline in snow cover elevation with latitude than in the tropics. The dominant wind direction also shifts to westerly, and the interaction of orography with the westerly prevailing winds has major consequences for snowline elevation and differences in snow on west and east sides of the Andes (Figure 2.5c). In this area, the ascending westerlies bring moisture from the Pacific Ocean, and the Andes act as a barrier to produce a marked rain/snow shadow (Quintana, 2012b). This leads to substantial differences in snow accumulation elevations on the west and east sides of the Andes, suggesting that reduced precipitation on the east side leads to higher elevations of snow accumulation. The difference between snow line elevations in both sides of the Andes is proportional to the highest elevation at certain elevation bands, with a peak difference at around 34°S, where mountains are highest, and a decrease further south where the height of the mountains declines (Figure 2.5c). Throughout the mid-latitude snow regions, the lowest elevation of the snowline is reached in winter, when temperatures are coolest and precipitation is highest in this area.

These climate regions developed from snow cover provide more details on regional differences than previous climatology patterns developed for the Andes area. Prior classifications have been based on vegetation and distributions of mean temperatures (annual and monthly) (Kottek et al., 2006), precipitation, ecological criteria (Borsdorf and Stadel, 2015), or glacier distribution (Williams and Ferringo, 1998). Kottek et al. (2006) updated the climate division based on vegetation and temperature to define five main areas at a global scale following the Köppen-Geiger approach. Three main Köppen-Geiger climates are present in the Andes Mountain (8-39°S) : (1) Desert climate (BW) on the east side of the Andes, and extending to

30°S on the west side, (2) Warm temperate climates dry summer (Cs) extending to 30°S on the west side, and (3) Polar tundra climate (ET) at the highest elevations.

The approach presented by Borsdorf and Stadel (2015) defined five areas based on vegetation: (1) subtropical-tropical desert that extends from the northern part of the study area to 28°S on the west side and 35°S on the east side, (2) Mediterranean from 28°S to 36°S just on the west side, (3) dry between 35°S and 36°S on the east side, (4) humid-temperate forest from 36°S on the west side, and (5) cold forest steppe south of 36°S on the east side. Because it uses vegetation as an indicator of climate, this approach integrates the factors that affect vegetation patterns such as precipitation, evapotranspiration, state (rain/snow), and other climate variables (temperature, radiation, relative humidity). However, the adaptive capacity of vegetation means that similar types of vegetation may be present over a range of climate conditions. Additionally, in areas where we identified different spatial and seasonal patterns of snow, the vegetation-based classification grouped all together as desert.

Finally, glacier distributions have been the focus of studies in persistent snow zones. Williams and Ferringo (1998), define the Dry Andes as extending to 30°S with no difference between sides of the Andes. Our snow climatology approach identifies three different regions in the same area and provides information on differences between sides of the Andes. Because the presence of snow integrates precipitation, temperature, and topography, it is a useful indicator of climate patterns. These patterns can be derived directly from remote sensing data, which is particularly useful in areas with limited in situ climate monitoring. Snow covered areas do include glaciated parts of the region, but the snow-based analysis covers a larger geographic extent than glacier-focused classifications. The snow zone analysis defined thresholds for snow

zones using data from a wide range of latitudes (8-39°S), so these zone thresholds may be transferable to other parts of the world.

Any spatial analysis must consider the quality of product itself and scales used. The MODIS snow product has uncertainties and limitations in the snow definition reported by several studies (Arsenault et al., 2014; Hall et al., 2010; Stroeve et al., 2006; Wang et al., 2012). Changes in the threshold used in the snow definition algorithms has improved the accuracy of the MODIS snow product, but misclassification between cloud and snow still remain (Rittger et al., 2013). Our approach of using cloud thresholds to mask areas with high cloud impairment likely eliminated the majority of misclassifications. The high frequency of cloud presence was a large limitation in wide areas (Northern and Southern Andes). This limitation could be decreased by using some cloud removal algorithms in a daily product before calculating snow climate indices (Gafurov and Bardossy, 2009; Gao et al., 2010; Gu et al., 2011; Hall et al., 2010).The temporal resolution of 8-days used in this study will not capture snow cover variability during a quick snow melting season (Rittger et al., 2013), but it is sufficient for identifying seasonal patterns (Figure 2.2), except possibly in areas with snow cover that lasts only a few hours and may be missed by the satellite overpass. On the other hand, the 8-day maximum product can also over-estimate snow persistence in areas with low or intermittent snow if the satellite overpass does occur during a brief window of snow cover. The spatial resolution of the MODIS snow product (500 m) is acceptable for the regional scale presented in this study, but particularly in areas such as TL1 that lack in situ snow observations, added ground observation would be helpful for reducing uncertainties in snow cover patterns. Additionally, weather and topographic variables such as precipitation, wind, slope, aspect, or shading will affect snow cover patterns at finer scales (Richer et al., 2013). Thus a study with finer scale of interest may require additional

remote sensing information (e.g. Landsat). The snow indices developed in this study can continually be updated with new MODIS data, refined snow cover retrieval algorithms, different sources of snow cover data such as fractional snow cover (Salomonson and Appel, 2004) or MODSCAG (Painter et al., 2009; Raleigh et al., 2013), and higher frequency snow cover images. Use of a fractional product can also be merged with a SWE product to yield bulk snowpack estimates (Bales et al., 2008).

The maps of snow patterns produced in this study have a number of potential applications. The current sparse in situ snow monitoring network can be improved by using these maps to identify areas that are representative of regional snow patterns and areas with high inter-annual variability for new snow stations. The definition of snow zones with 15 years of information could be the basis for evaluating snow change or abnormal snow events in the future. From the hydrologic perspective, snow cover time series can be used in hydrologic modeling (Parajka and Bloschl, 2008), and the snow climatology information can help hydrologists determine how stream flows relate to snow melt timing.

2.6. CONCLUSIONS

This study developed a method for mapping the spatial and seasonal variability of snow cover in the Andes using MODIS SCA data. Cloud cover reduced the ability to use MODIS snow product in the northernmost and southernmost portions of the Andes. The analysis of the SCI by bands of latitude (50 km) and elevation (100 m) led to defining five snow climate regions. In the tropical latitudes (north of 23°S) two regions were defined (Tropical-latitude 1 and 2), both with snow cover restricted to the highest elevations and a steep rate of change of

snow persistence with elevation. There were minimal differences in the elevation of snow accumulation on both sides of the mountains, which suggests that temperature is a primary control on snow presence. Although seasonal changes in snow cover were minimal in tropical latitudes, snow persistence was slightly greater in the austral winter in Tropical-latitude 1 due to lower radiation in this season, whereas tropical-latitude 2 snow region had peak snow cover in the fall following the wet season.

In Mid-latitudes (south of 23°S), snow cover dropped in elevation, and the rate of change of snow persistence with elevation was more gradual. Mid-latitude snow regions had peak snow cover in the winter, when temperatures were lowest, and precipitation was high. Differences in elevations of snow accumulation between sides of the mountains were greatest in Mid-latitude region 2, where high mountains lead to a pronounced orographic effect on precipitation. This suggests that precipitation had a greater effect on snow accumulation elevation in these latitudes than in the tropics, leading to lower snow lines on the west side where precipitation was higher. This snow cover approach to analyzing climate patterns provides more details on regional differences than previous maps of climate zones in the region, which used mean annual and monthly temperatures, precipitation, and ecological criteria, and it helps quantify where and when snow accumulates throughout the region.

Maps of snow zones show that snow cover extent was limited in the tropics and Atacama Desert, with the largest areas of seasonal (winter) and permanent snow in Mid-latitude 2 (28-36°S) as result of higher precipitation than areas further north and higher elevation than mountains further south. Seasonal and permanent snow are both important sources of water production, and results of this study can help identify watersheds where snowmelt is likely a strong contributor to stream flow. Tracking changes in these snow zones over time can help

identify geographic variability in the sensitivity of the Andes Mountain snowpack to climate change.

CHAPTER 3: CHANGES IN THE ANDES MOUNTAINS SNOW COVER FROM MODIS DATA 2000-2014.

3.1. INTRODUCTION

The influence of changing climate on snow cover has been studied across the world (Adam et al., 2009; Barnett et al., 2005; Brown and Mote, 2009; Dahe et al., 2006; Masiokas et al., 2006). In snow-dominated basins, snowpack provides the largest reservoir of water (Adam et al., 2009; Masiokas et al., 2006), which influences stream discharge, affecting erosion, sediment transport, hydropower production, and potential water storage (Hall et al., 2012). These basins are particularly sensitive to climate change due to both precipitation and temperature changes. At global scale, warming temperatures cause decreases in snow cover by increasing the elevation of the 0°C isotherm in mountain regions and/or decreasing the fraction of precipitation falling as snow (Barnett et al., 2005; Brown and Mote, 2009). The magnitude of this effect decreases with increasing elevation (López-Moreno et al., 2009). However, snow cover changes can be difficult to predict in areas where the temperature increase is accompanied by increased precipitation (Adam et al., 2009; Dahe et al., 2006). Decreases in the duration of snowpack cause negative feedbacks due to decrease in albedo, which leads to increased absorption of solar radiation, intensification of warming trends, and further reductions in snowpack. In mountain environments, the persistence of snow affects the plant growing season and the amount of water available for soil moisture (Stewart, 2009).

In the Southern Hemisphere, seasonal snow cover is primarily confined to southern South America, where extensive winter snow cover may occur (Foster et al., 2009). The impacts of climate change on snow covered areas in South America have not been studied in detail due to

sparse and unevenly distributed climate data. (Aravena and Luckman, 2009; Cortés et al., 2011; Masiokas et al., 2006). Masiokas et al. (2012) conducted one of the most extensive snowpack temporal trend studies in this region, but the high spatial variability in mountain areas and the few stations used (15 stations) limited their ability to draw solid conclusions about snowpack trends across the region. Remote sensing offers the opportunity to document snow cover change throughout the region in the last 15 years. The primary objectives of this chapter are to (1) quantify changes in the snow cover and their spatial patterns with latitude and elevation, and (2) explore how these changes relate to climate variables.

3.2. STUDY SITE

The Andes Mountains cross seven countries (Venezuela, Colombia, Ecuador, Peru, Bolivia, Chile, and Argentina) along more than 8,000 km (10º N to 57º S) (Figure 2.1) (Barry, 2008). They represent the highest mountain system out of Asia, the longest in the world, and have a strong effect on atmosphere circulation (Llamedo et al., 2016). Local climates vary greatly depending on latitude, altitude, and proximity to the sea (Garreaud, 2009).

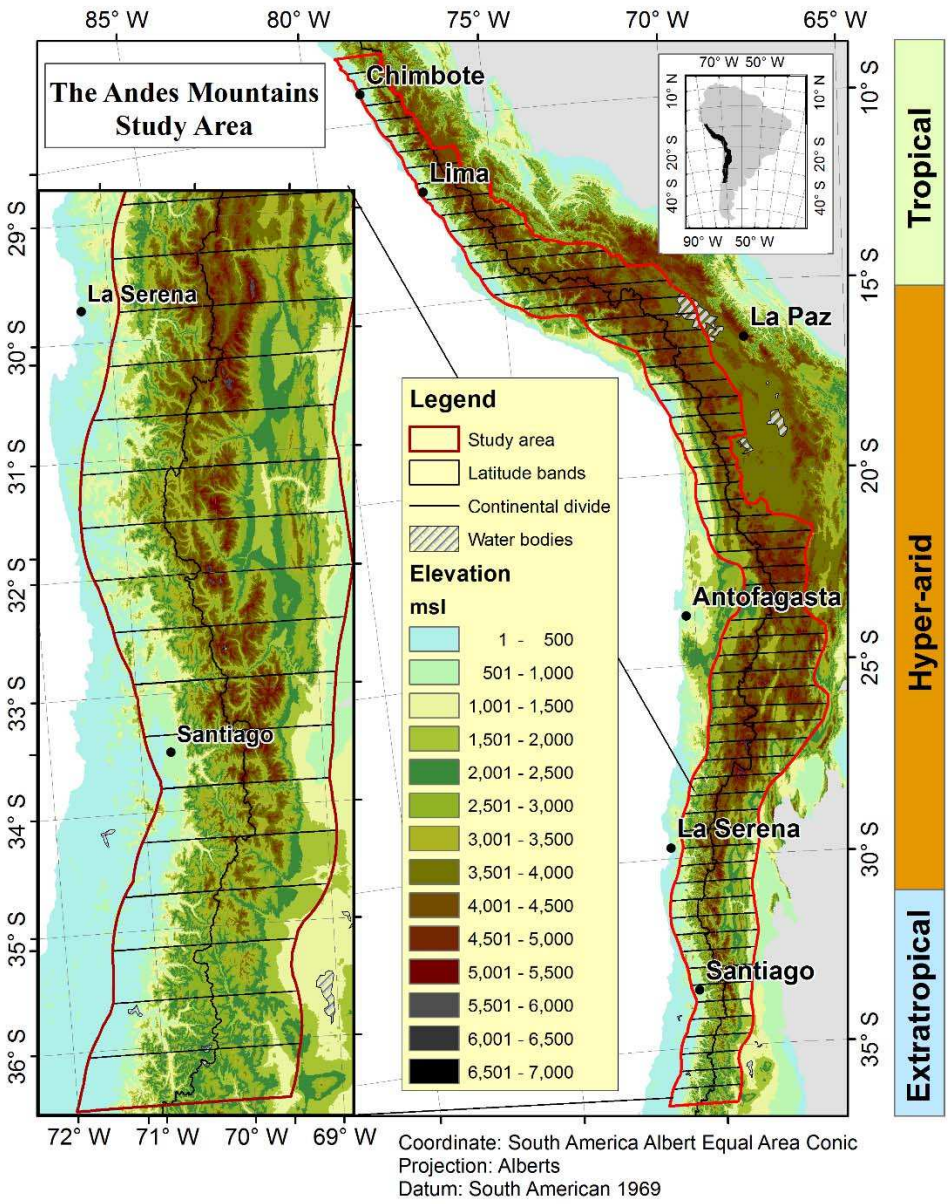

Figure 3.1. Study area (red line) over digital elevation model of the Andes Mountains and subdivided into latitudes bands (black line).

Figure 3.2a shows the monthly precipitation patterns in both sides of Andes (see the continental divide in Figure 3.1) by latitude using the University of Delaware dataset 2000-2014 (Matsuura and Willmott, 2015). The overall pattern is an increase in precipitation to the south and on the windward of the Andes due to the orographic effect (Garreaud et al., 2009; Quintana, 2012b). In the northern area (north of 20°S), precipitation is concentrated in the austral summer

(DJFM), with higher precipitation on the east side. Areas between 20-30°S have hyper-arid conditions with limited precipitation all year on the west side and greater precipitation on the east side. During the austral summer, wet episodes tend to occur due to strong upper-level easterly winds that enhance moisture transport from Amazonia (Garreaud et al., 2003). South of 30°S, precipitation has a well-defined annual pattern with a peak of precipitation in austral winter (JJA) and higher precipitation on the west side (Quintana, 2012a, b; Valdés-Pineda et al., 2015a). In these latitudes, air masses come from the west (Pacific), so the west side of the Andes receives higher precipitation than the east side (Garreaud, 2009; Matsuura and Willmott, 2015).

The monthly air temperature from the University of Delaware gridded dataset 2000-2014 is shown in Figure 3.2b (Matsuura and Willmott, 2015). Lowest temperatures are during austral winter (JJA) but there is less seasonal variability in the tropics than in higher latitudes. Mean annual temperature decreases from North to South and with increasing elevation. The combined precipitation and temperature patterns affect snow cover duration in the region. Snowfall patterns have been mapped in detail for this region using remote sensing, but high cloud cover limited this mapping to the area between 8°S to 36°S (Saavedra et al., 2016). Figure 3.2c shows the monthly average snow covered area between years 2000 and 2014 for each latitude band using Moderate Resolution Imaging Spectroradiometer (MODIS) snow product (MOD10A2) across the year on both sides of the Andes. Most of the high snow cover (>30%) is south of 24°S. On the west side the snow season lasts from around day 110 (April 20th) to 280 (October 7th) between 24-33°S. Between 33-35°S the snow season can last all year in high elevation areas. South of 36°S, the snow season starts around day 110 but lasts longer into the summer until around day 320 (November 16th). The latitude variability of snow cover can be summarized using snow persistence (SP), which is the fraction of a year with snow cover. North of 25°S,

average snow persistence is lower than 10%, and the snow line (SP=20%) is over 5000 m (Saavedra et al., 2016). The snow line decreases in elevation with increase in latitude south of 25°S with a consistently lower snow line on the west side than on the east side (Barry and Seimon, 2000; Saavedra et al., 2016; Vuille and Ammann, 1997; Williams and Ferringo, 1998).

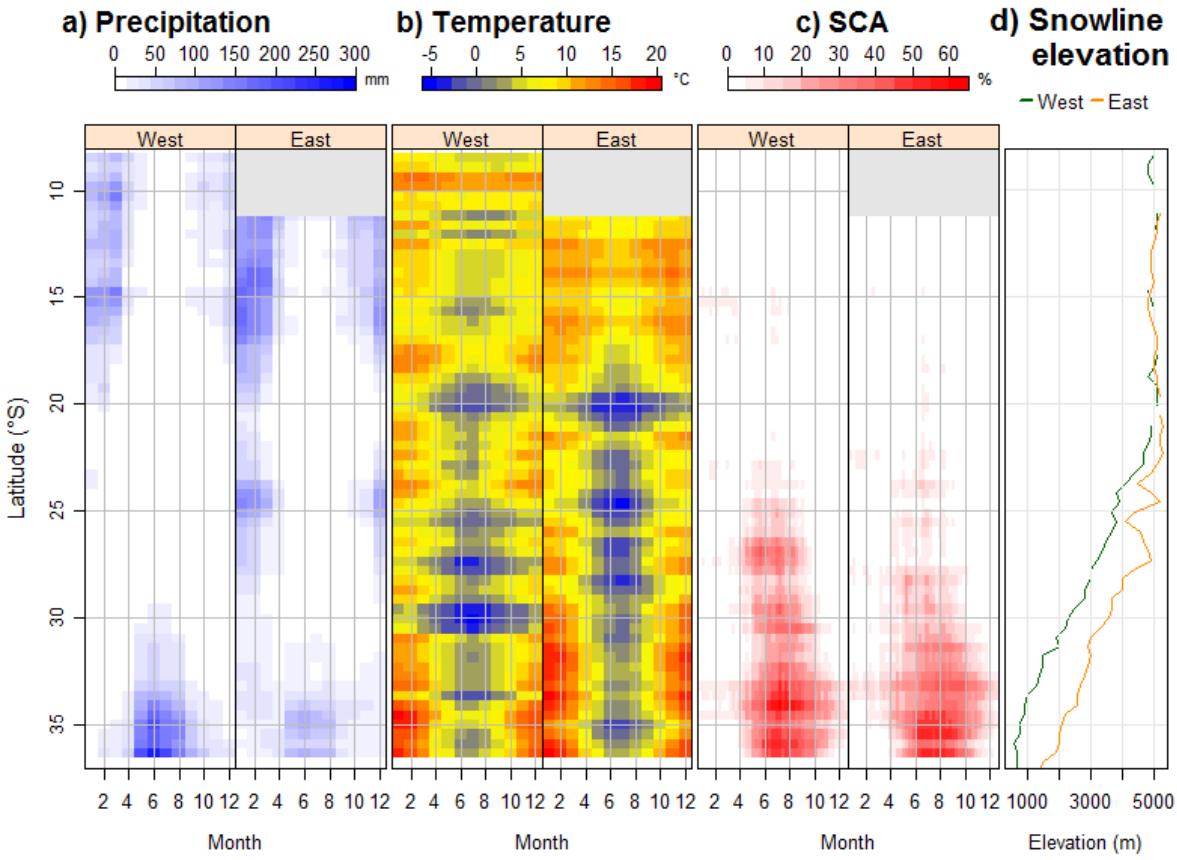

Figure 3.2. Mean monthly precipitation (a) and temperature (b) from the University of Delaware dataset 2000-2014. Mean fraction of area with snow cover by latitude band calculated from the binary 8-day product from MODIS (MOD10A2) 2000-2014 (c), and snow line elevation following Saavedra et al. (2016) methodology (d). Grey areas represent latitudes masked due to high frequency of cloud cover in snow covered area analysis (>30% time period).

3.3. METHODS

3.3.1. Data

We used the MODIS eight-day 500m binary snow cover products Collection 5 Level 3. MODIS is a passive 36-band spectrometer on board two satellites (Terra and Aqua) (Hall et al., 2002). One of the spectral bands used to calculate the snow products for the Aqua satellite has malfunctioned, so our research is based on Terra products. Because of high cloud impairment in daily MODIS snow cover products, we use the eight-day maximum product (MOD10A2), which represents the maximum snow cover and minimum cloud during each eight-day interval (Riggs et al., 2006). The study area is covered by 7 MODIS images (tiles), which we downloaded for the time period from 2000 to 2014 (MOD10A2) (http://reverb.echo.nasa.gov), giving a total of 5,147 tiles of MOD10A2.

We collected monthly precipitation and temperature from the University of Delaware dataset version 4.01 (UDelv4) with a grid resolution of 0.5° from 2000-2014 (Legates and Willmott, 1990) (http://www.esrl.noaa.gov/psd/data/gridded/data.UDel_AirT_Precip.html). For the study area, UDelv4 compiled data from ground stations at a monthly time step from several sources including Global Historical Climatology Network Monthly, Daily Global Historical Climatology Network, Global Synoptic Climatology Network, and Global Surface Summary of Day. The monthly averages of station data were interpolated to a 0.5 degree by 0.5 degree latitude/longitude grid using the spherical version of Shepard's distance-weighting method (Willmott and Robeson, 1995). In addition, station-by-station cross-validation was employed to evaluate the spatial interpolation errors (Matsuura and Willmott, 2015).

An important source of interannual climate variability in the region is El Niño/Southern Oscillation (ENSO). We collected the multivariate ENSO Index (MEI) that is based on the six main observed variables over the tropical Pacific (http://www.esrl.noaa.gov/psd/enso/mei/table.html). Negative values of the MEI represent the cold ENSO phase (La Niña), while positive MEI values represent the warm ENSO phase (El Niño) (Wolter and Timlin, 1998).

We used a digital elevation model (DEM) developed from a combination of Shuttle Radar Topographic Mission (SRTM) and Advanced Spaceborne Thermal Emission and Reflection Radiometer (ASTER) elevation data to divide the study area into 100 m elevation bands and 50 km latitude bands (Saavedra et al., 2016). The continental divide was defined by using the drainage side (East or West) of the Andes determined from the Watershed Tool in ArcGIS. All geospatial data were mosaicked and projected into the South American Alber's equal area azimuthal projection to minimize shape distortion (Kennedy and Kopp, 1994).

3.3.2. Analysis

To document snow cover patterns and their changes over time from 2000-2014, we calculated the annual snow persistence (SP) for each pixel in the study area as the fraction of the images in a year with snow cover (Saavedra et al., 2016). We masked areas with mean annual SP<7% to avoid potential misclassifications in MODIS snow products (Figure 3.2a) (Hall et al., 2002). This threshold excludes the little to no snow zone (SP<7%) as defined in Saavedra et al. (2016). For the remaining pixels we used the non-parametric Mann-Kendall analysis to test for trends in annual SP (Khaled and Ramachandra, 1998) and quantified the rate of change using the

linear Theil-Sen's slope, which determines the slope as the median of all possible slopes between data pairs (Sen, 1968; Theil, 1950). We ran the Mann-Kendall analysis using the "Kendall" package for R (McLeod, 2011). Trends were considered significant at a p-value ≤ 0.05. We also calculated a standardized Theil-Sen's slope by dividing the original slope by the mean annual SP. This allowed us to compare the rate of SP change (slope) in different snow zones. For each year, we estimated the elevation of the snow line using a SP value of 20%, following Saavedra et al. (2016) and evaluated the trends in snow line elevation for each latitude band on the west and east sides. Finally, we calculated trends in SP for individual months and elevation bands and examined how the magnitude of trends varied seasonally and with elevation across the study area. We conducted all geo-statistical analyses using statistical computing R software (RCoreTeam, 2013).

To explore how climate variables relate to snow persistence trends we used the University of Delaware annual data set (air temperature T, and precipitation P) and the Multivariate ENSO Index (MEI). For each of these variables, we ran the same trend analyses described for SP. Additionally, we evaluated the linear correlation between each climate variable (T, P, MEI) and SP using Pearson's correlation coefficient (r). We also ran multiple linear regressions at a monthly time step to define the proportion of variability of SP explained by each climate variable. The strength of these regressions was quantified using the coefficient of determination (r^2). Finally, we calculated the relative importance of independent variables on annual SP using de Lindeman, Merenda and Gold (lmg) approach included in the relative importance for linear regression "relaimpo" R package (Groemping and Matthias, 2013). The lmg method evaluates the individual contribution of each regressor to the full r^2 of the model

(Grömping, 2006).We visualized all statistical analyses by pixel mapping and as latitude-elevation charts.

3.4. RESULTS

3.4.1. Annual snow persistence and snow line trends

The mean annual snow persistence across the Andes Mountains varies with both latitude and elevation (Figure 3.3a). The total area with mean annual SP≥7% is 178,330 km^2 and is distributed in three main zones. The northern area (8-11°S) has just 2% of this snow area (2,992 km^2); latitudes14-16°S contain 9% (16,231 km^2) of the snow area, and the remaining snow covered areas are all south of 23°S (159,107 km^2). Mann-Kendall trend analyses of annual SP (Figure 3.3b) shows significant decreasing trends south of 29°S, where 2-5 fewer days of snow every year (-1.5 to -0.5 % year) are the most common values. Small areas registered an increase of SP (blue range colors in Figure 3.3b) south of 34°S at lower elevations. The standardized slope shows the magnitude of the slope normalized by mean annual SP (Figure 3.3c). North of 34°S the standardized slopes are elevation-dependent on both sides of the mountains, with greater changes (more negative trends) at lower elevations. South of 34°S the relative changes in SP are greater (more negative) on the east side than on the west side of the Andes.

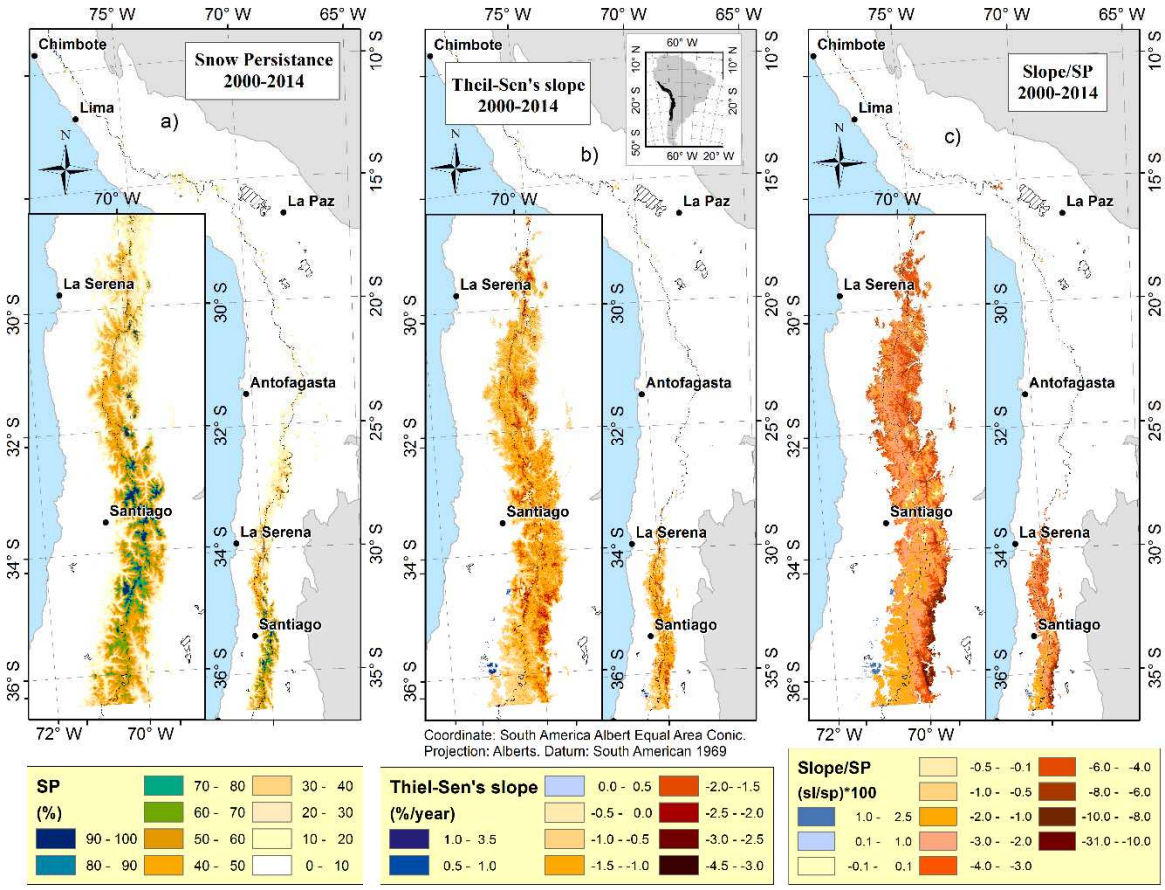

Figure 3.3. Snow pattern of (a) mean annual snow persistence (SP) 2000-2014, (b) Theil-Sen's slope of trend in annual SP from Mann-Kendall test 2000-2014, and (c) standardized slope of SP trend (slope/mean SP); pixels are only colored if the trend is significant at $p \leq 0.05$ and if $SP \geq 7\%$; the SP threshold excludes areas with little to no snow.

The latitude-elevation band analysis of SP reveals how the pattern of snow varies across the region. North of 23°S the snow is confined to over 5000 m, with a steep change of SP with elevation. South of 23°S, areas with similar SP values are found at lower elevations with increasing latitude. The west side has consistently lower elevation snow than the east side for SP values under 90%. For a more detailed description of these patterns see (Saavedra et al., 2016) (Figure 3.4a). The trend of annual SP is shown in Figure 3.4b as Sen's slope values. North of 19°S, decreasing SP is confined to over 5000 m on both sides of the Andes, and south of 29°S areas with declining SP drop in elevation and vary between west and east sides (Figure 3.4b).

The west side has a lower elevation of each category of Theil-Sen's slope compared to the east side at the same latitude. The maximum decreases in trend slopes are located at middle-high elevations, between 4000-5000 m at 29°S and declining to 3000-4000 m at 36°S for both sides. The inset boxes in Figure 3.4b shows the relation between Theil-Sen's slope and SP for all latitude-elevation bands south of 23ºS. In this latitude range, the maximum rates of SP decline are in the seasonal snow zone, which is defined as mean annual SP between 30-90% (Saavedra et al., 2016). The standardized Theil-Sen's slope shows greater declines at lower values of SP on both sides, except in a few anomalous areas. This means that the greatest absolute declines in SP south of 23ºS have been in the seasonal snow zone (Figure 3.4b), whereas the greatest relative declines have been in the intermittent snow zone (SP<30%; Figure 3.4c).

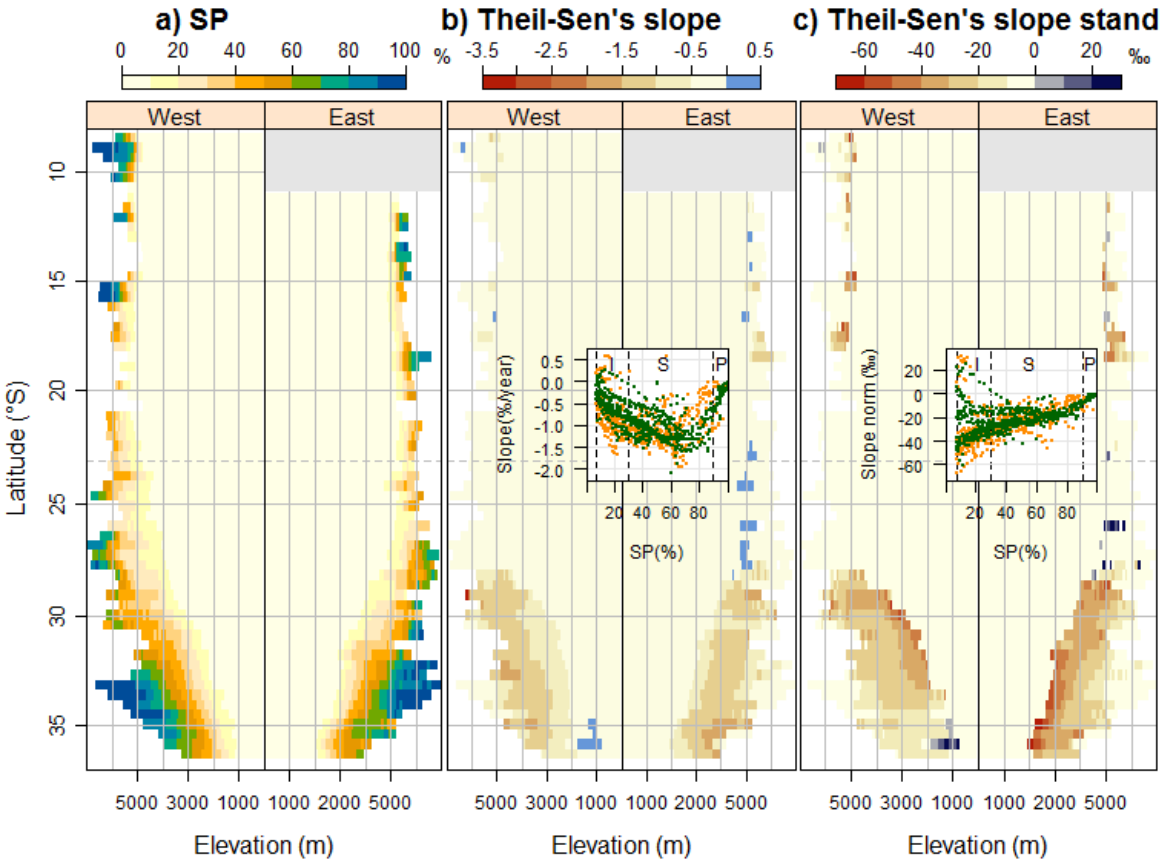

Figure 3.4. Latitude-elevation band analysis of (a) mean annual SP for 2000-2014 (b), Theil-Sen's slope of Mann-Kendall trend in annual SP from 2000-2014, and (c) standardized Theil-Sen's slope (slope/mean SP); only areas with significant trends ($p \leq 0.05$) and SP≥7% are colored. Inset boxes show the relation of SP with Theil-Sen's slope (b), and standardized Theil-Sen's slope (c) for each latitude-elevation band south of 23°S (grey dashed line) on West (green) and East (orange) sides. Within inset plots, vertical dashed gray lines represent thresholds for intermittent (I), seasonal (S), and persistent (P) snow zones. Grey areas represent latitudes masked due to high frequency of cloud cover in snow covered area analysis (>30% time period).

The amount of area affected by significant changes in snow persistence also shows a strong difference between sides of the Andes (Figure 3.5a). South of 29°S the total area with slopes lower (more negative) than -0.5 (%/year) is 70,515 km^2 with 38% in the west side. The most common slopes of decreasing SP are in the range of -2.0 to -0.5 %/year. For areas with the steepest declining trends in SP (-3.0 to -2.5 % year), 86% of the affected area is on the east side (inset boxes in Figure 3.5a). Trends in snow line elevation were only significant south of 29°S on

the west side and south of 30°S on the east side (Figure 3.5b), where the snow line is increasing in elevation at a rate of about 10-30 m/year. Rates of increase in snow line elevation are higher for the west side than for the east side between 30-32°S, but south of 34°S the east side snow line elevation changes are higher and significant compared with a non-significant trend on the west side.

The seasonality of SP change is shown in Figure 3.5c. North of 23°S the greatest changes in snow persistence were in early months, during austral summer (DJFM) on both side of the Andes. South of 23°S, the largest changes were in late austral winter (JJA) for lower values of SP (7<SP<30%), which represent the intermittent snow zone and lower boundary of the seasonal snow zone (Figure 3.4a). For middle values of SP (30<SP<70%), which represent the seasonal snow zone, the largest changes in snow persistence were during the melting season in austral spring (SON). For intermittent and seasonal snow zones, there are no major differences in the seasonality of change between west and east sides. Finally at the upper boundary of the seasonal snow zone and into the persistent snow zone at the highest values of SP (>70%), the largest changes in snow persistence were observed during austral fall (AM) on the west side associated with the accumulation season and the austral winter (JJA) on east side.

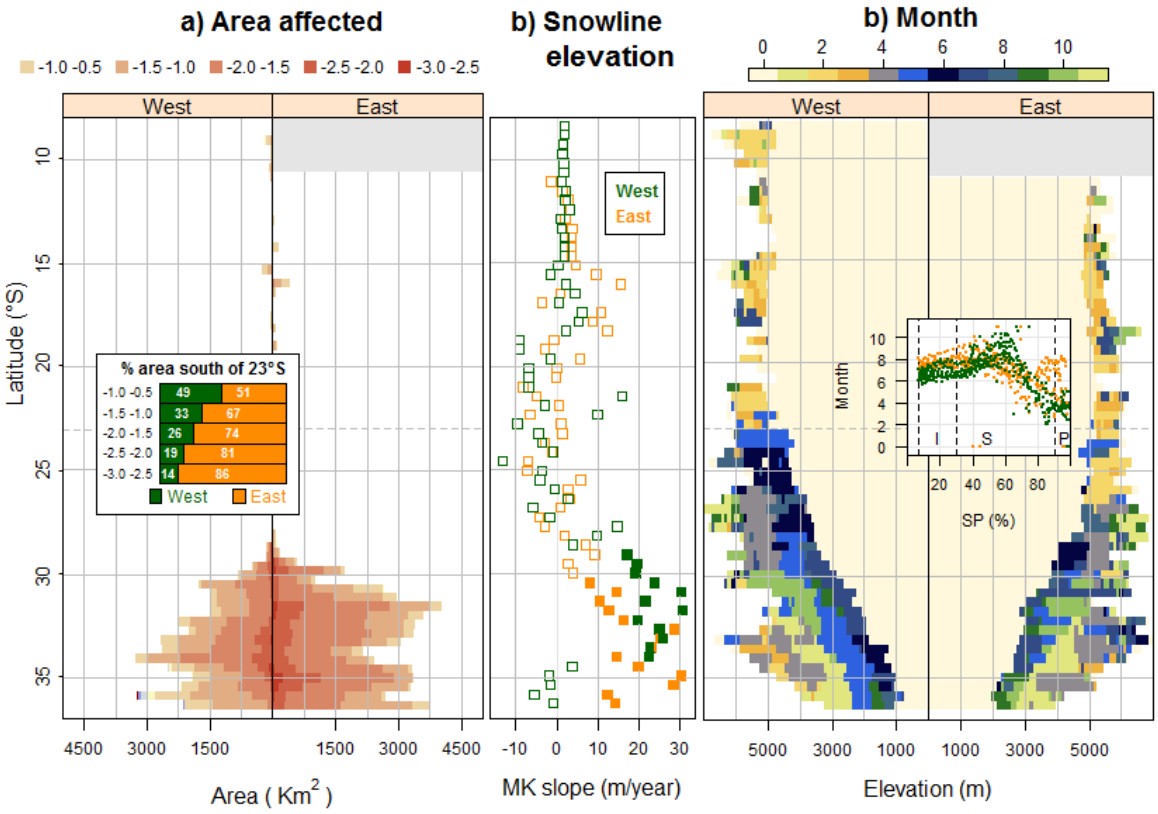

Figure 3.5. Areas with significant change in annual SP by latitude band (a), (b) slope of Mann-Kendall trend in elevation of snow line (SP=20%), solid symbols have significant trends ($p \leq 0.05$), and (c) months with the highest significant Sen's slope from Mann-Kendall trend analysis of SP. Inset box in Figure (a) shows percentage of area in each Sen's slope category for West and East sides, and inset box in (c) shows the variability in the range of months with greatest SP changes for each latitude-elevation band south of 23°S (dashed grey line) on West (green) and East (orange) sides. Within the inset box, vertical dashed gray lines represent thresholds for intermittent (I), seasonal (S), and persistent (P) snow zones. Grey areas represent latitudes masked due to high frequency of cloud cover in snow covered area analysis (>30% time period).

3.4.2. Climate connection

Many parts of the study area had significant trends in annual precipitation and mean annual temperature from 2000-2014 (Figure 3.6). Trends in annual precipitation were mostly not significant north of 25°S but showed a significant decrease from 2-4 mm/year at 26°S to 15-20 mm/year at 36°C (Figure 3.6a). The standardized decrease of precipitation (Theil-Sen's

slope/mean annual P; Figure 3.6b) is low north of 31°S (1%) and increases to the south, with higher values on the east side. This indicates greatest impacts of decreasing precipitation on the east side. The seasonality of decreasing P (Figure 3.6c) shows that the austral winter (JJA) is the most affected season on the west side, and early austral fall (March) is most affected on the east side.

The temperature shows significant increases north of 16°S on both sides of the Andes in the range of 0.08 to 0.16 °C per year (Figure 3.6d). In the west side and latitudes 17-30°S there were significant decreasing temperature trends in the range of -0.08 to -0.04°C per year. In most of the rest of the study area, temperatures had increasing trends. These trends extended from 31-35°S on the west side and 26-35°S on the east side. The standardized change of temperature (Theil-Sen's slope / mean annual temperature) shows a homogeneous rate of increase (10%) in all of the areas with increasing temperature trends (Figure 3.6e). The seasonality of increase of temperature change varies across the region (Figure 3.6f); areas with decreasing temperature trends were masked in this plot. North of 15°S the highest increase occurred in June; between 15-20°S the highest values are usually in winter (June and July), and south of 25ºS, the greatest increases are mainly in fall months.

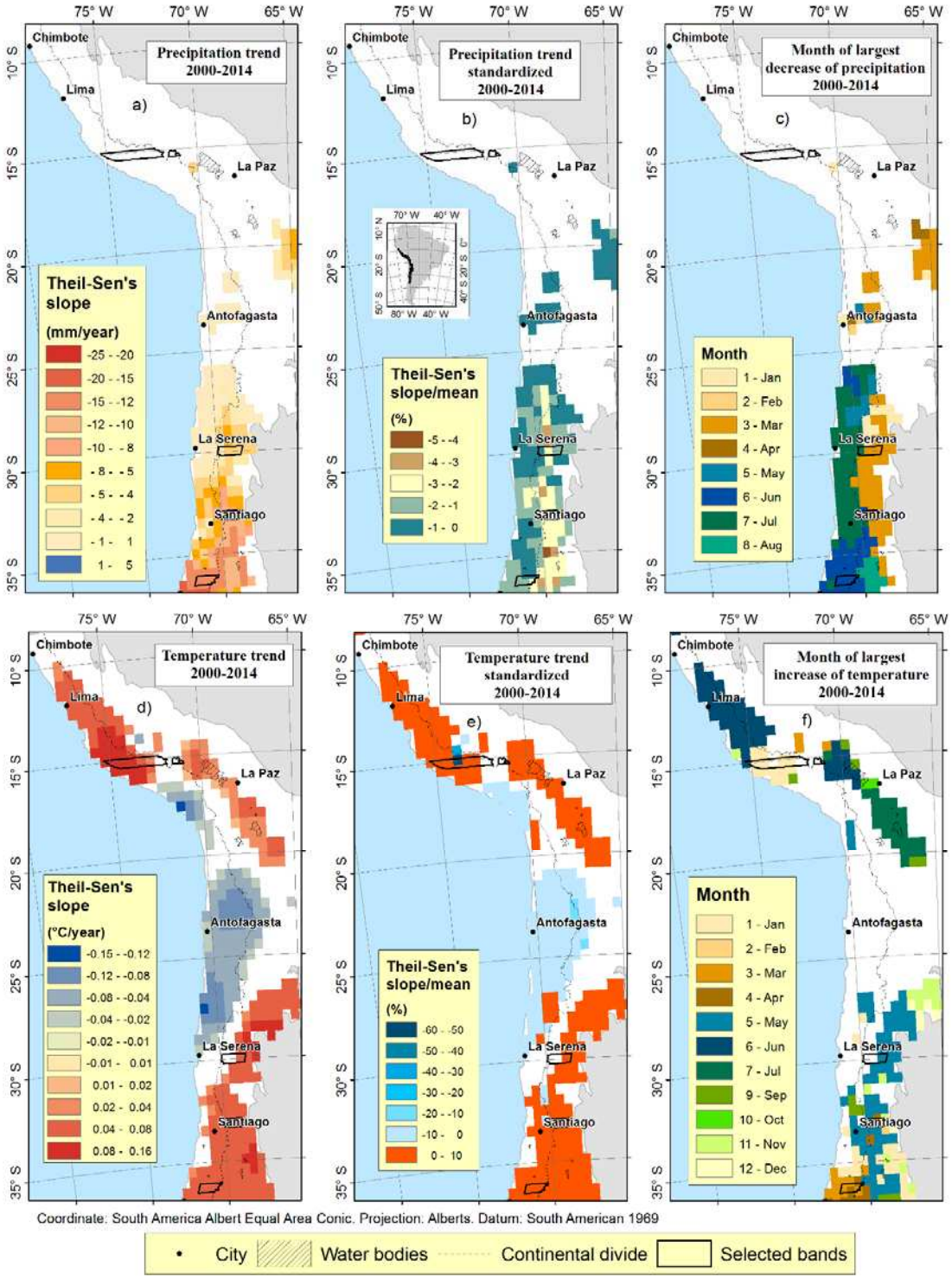

Figure 3.6. Theil-Sen's slope of Mann-Kendall trend from 2000-2014, standardized Theil-Sen's slope, and month of the greatest change (largest increase of temperature or largest decrease of precipitation) at an annual time scale for precipitation (a, b, and c) and air temperature (d, e, and f); only pixels with significant trends ($p \leq 0.05$) are colored. Black polygons highlight selected bands used to describe in detail the evolution of temperature, precipitation, and snow from 1960-2014 (Figure 3.7).

Figure 3.7 shows the evolution of MEI in the study time period relative to annual time series of snow covered area (SCA), temperature and precipitation in selected latitude bands. The years 2000 and 2008 had a strong Niña conditions (-0.87, -0.68, and -0.7 MEI respectively), and years 2002 and 2015 had a strong Niño condition (0.62, and 1.26 MEI respectively). These MEI patterns do not appear to relate strongly to T, P, or SCA in the selected latitude bands. The band in the tropics (Lat15 °S – West, Figure 3.6c.1) had no significant change in precipitation but a significant increase in temperature from 2000-2014. The other bands further south both had significant decreases in precipitation and snow persistence and increases in temperature. In a longer time analysis (1960-2014), all band show an increasing temperature trend, but the trend in precipitation is not clear. MEI values show alternating Niña-Niño conditions before 1978 and then a high frequency of Niño conditions (MEI>0) between 1978 and 2000.

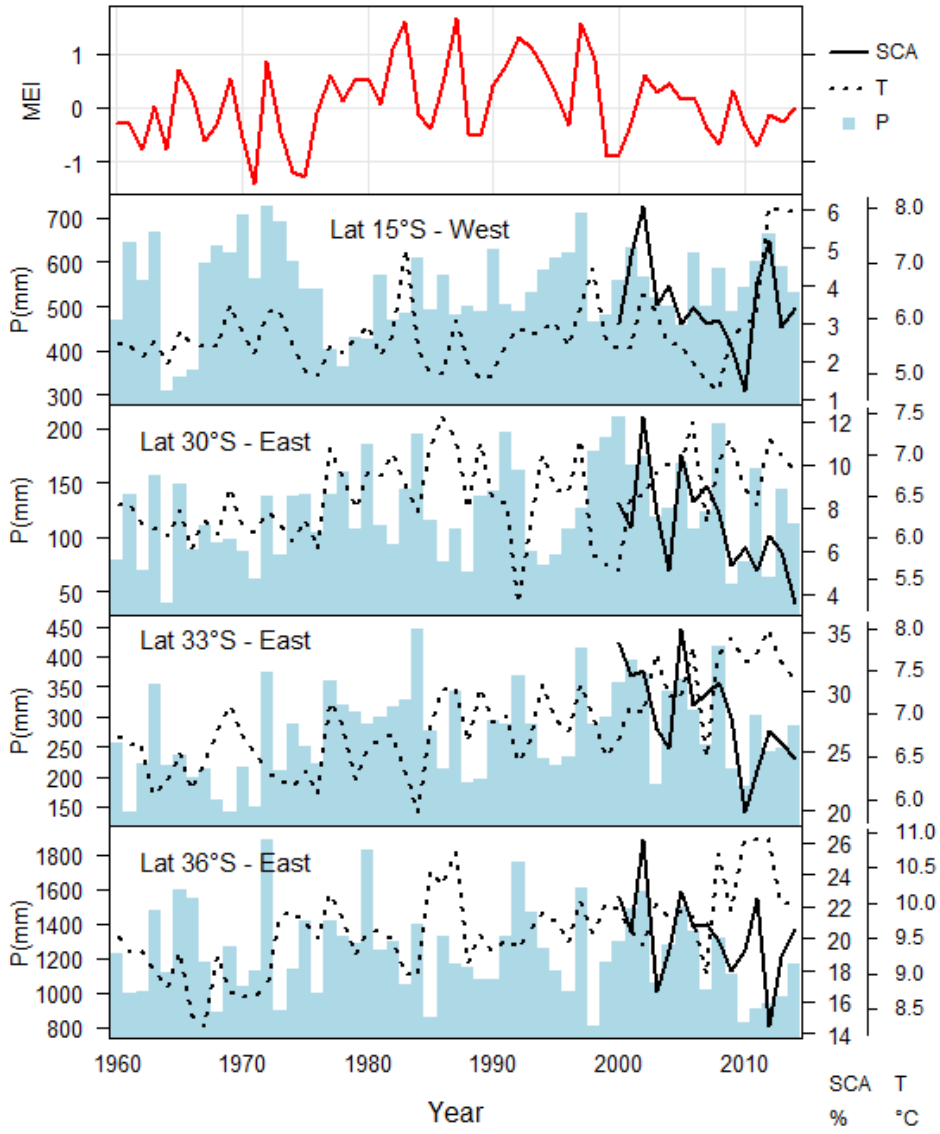

Figure 3.7. Time series of 1960-2014 MEI compared to temperature, precipitation from UDelv4 dataset and average SCA from MODIS dataset as percentage of whole latitude band (2000-2014) for select latitude bands.

Correlations between annual snow persistence and air temperature, precipitation, and MEI for each pixel are illustrated in Figure 3.8. Both air temperature and precipitation are strongly correlated with SP, but with opposite signs. Air temperature has an inverse relationship with SP, whereas precipitation has a direct correlation with SP. MEI has a direct but weak correlation with SP.

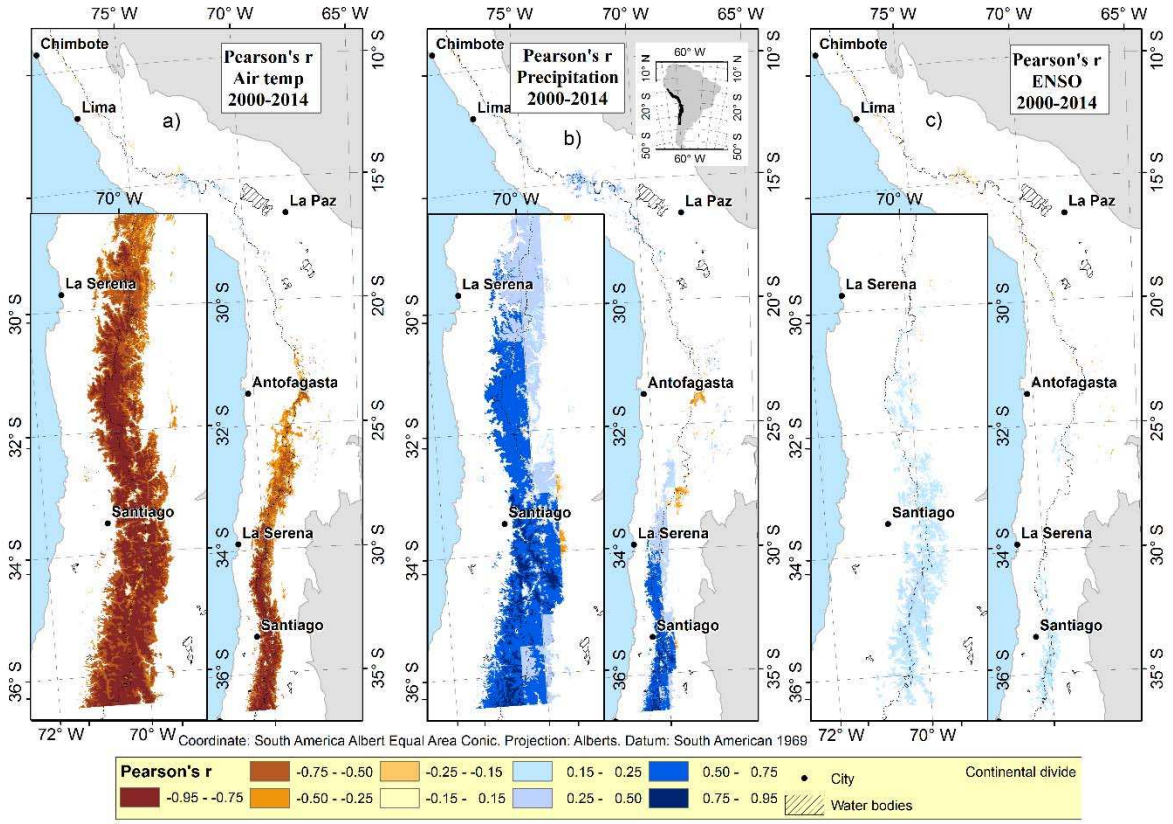

Figure 3.8. Map of Pearson's correlation coefficient between annual SP and (a) mean annual temperature, (b) annual total precipitation, and (c) annual MEI 2000-2014.

The variability in correlation strength between climate variables and SP is shown in Figure 3.9. The strongest correlations are located south of 23°S for air temperature and south of 25°S for precipitation. Significant correlations extend to lower elevations, with stronger correlation coefficients on the west side than the east side. Between 30-35°S, the strongest values of air temperature correlations with SP are located at middle elevations (3000-4000 m) where there are intermediate values of SP (around 50%) (inset boxes in Figure 3.9a). Strongest values of precipitation correlations with SP are located at lower elevations (2000-3000 m) on the west side where SP is around 30%; this is the boundary between intermittent and seasonal snow zones (inset boxes in Figure 3.8b). Correlations between MEI and SP are negative but weak north of

23°S at high elevations (over 5000 m). South of 30°S the relation is inversed, with moderate positive correlations (0.3-0.4).

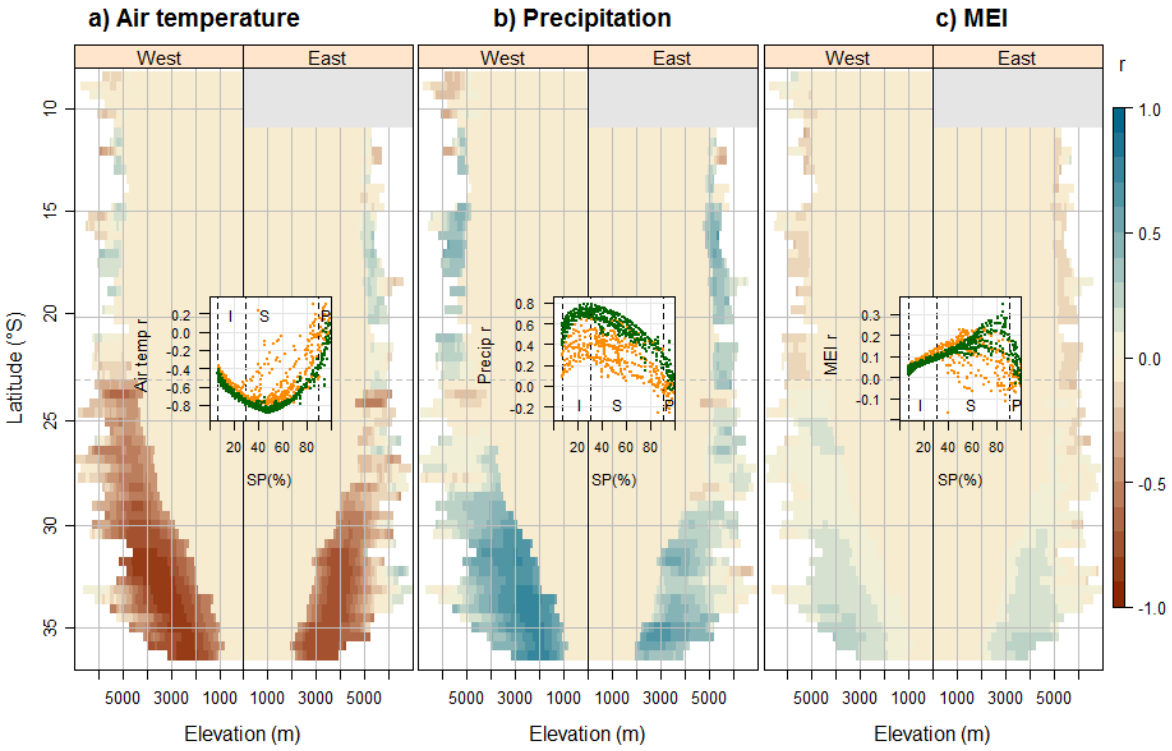

Figure 3.9. Latitude-elevation band analysis of Pearson's correlation coefficient (r) between annual snow persistence and a) air temperature, b) precipitation, and c) MEI. Inset boxes show how the correlation values for latitude-elevation bands south of 23°S (dashed gray line), vary with SP in West (green) and East (orange) sides. Within inset boxes, vertical dashed gray lines represent thresholds for intermittent (I), seasonal (S), and persistent (P) snow zones. These indicate that correlations between air temperature and SP are highest (most negative values) in the seasonal snow zone (high SP), whereas correlations between precipitation and SP are highest in the intermittent snow zone (low SP). Grey areas represent latitudes masked due to high frequency of cloud cover in snow covered area analysis (>30% time period).

Due to the low values of r between MEI and SP, we used just air temperature and precipitation to run a Multiple Linear Regression (MLR). Maps of coefficient of determination and latitude-elevation band distributions in areas with SP≥7% 2000-2014 are shown in Figures 3.10a and 3.11a. High values of r^2 are present in extended areas south of 25°S, and values increase with increasing SP up to 50%. At higher values of SP, r^2 values decline (inset box

Figure 3.11a). To explore which parameter (air temperature or precipitation) most influences SP in each location, we computed the relative importance for the MLR variables (Figure 3.10b and 2.11b). North of 23°S precipitation has a more important role, and south of this latitude the combined effects of air temperature and precipitation change with latitude and elevation. On the east side temperature is more important than precipitation at all elevations, whereas on the west side precipitation is more important for lower SP (<40%) areas at middle-lower elevations (4000 m at 25°S down to 2000 m at 35°S).

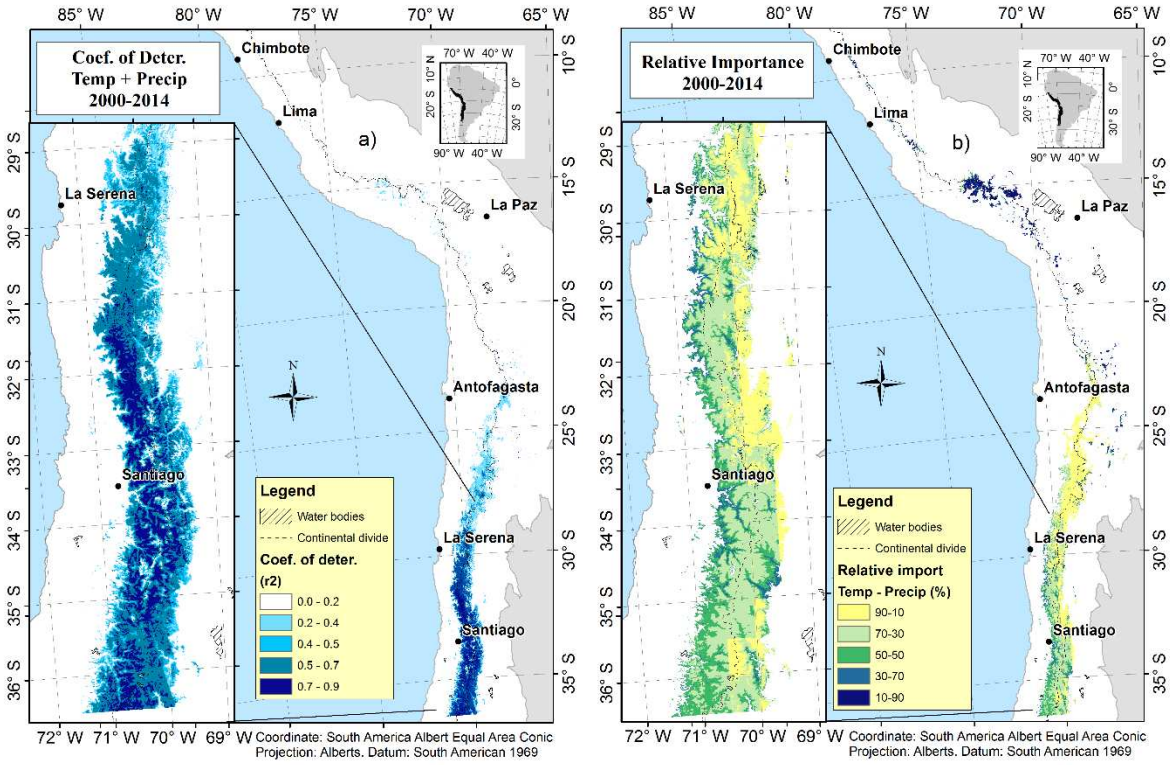

Figure 3.10. Multiple linear regression analysis by pixel (a) showing the coefficient of determination (r^2) for SP predictions using annual precipitation and mean annual air temperature b) relative importance of air temperature and precipitation in the multiple linear regression; blue colors indicate greater importance of precipitation, and yellow colors indicate greater importance of temperature. Blocky pattern results from coarser resolution climate data compared to snow data.

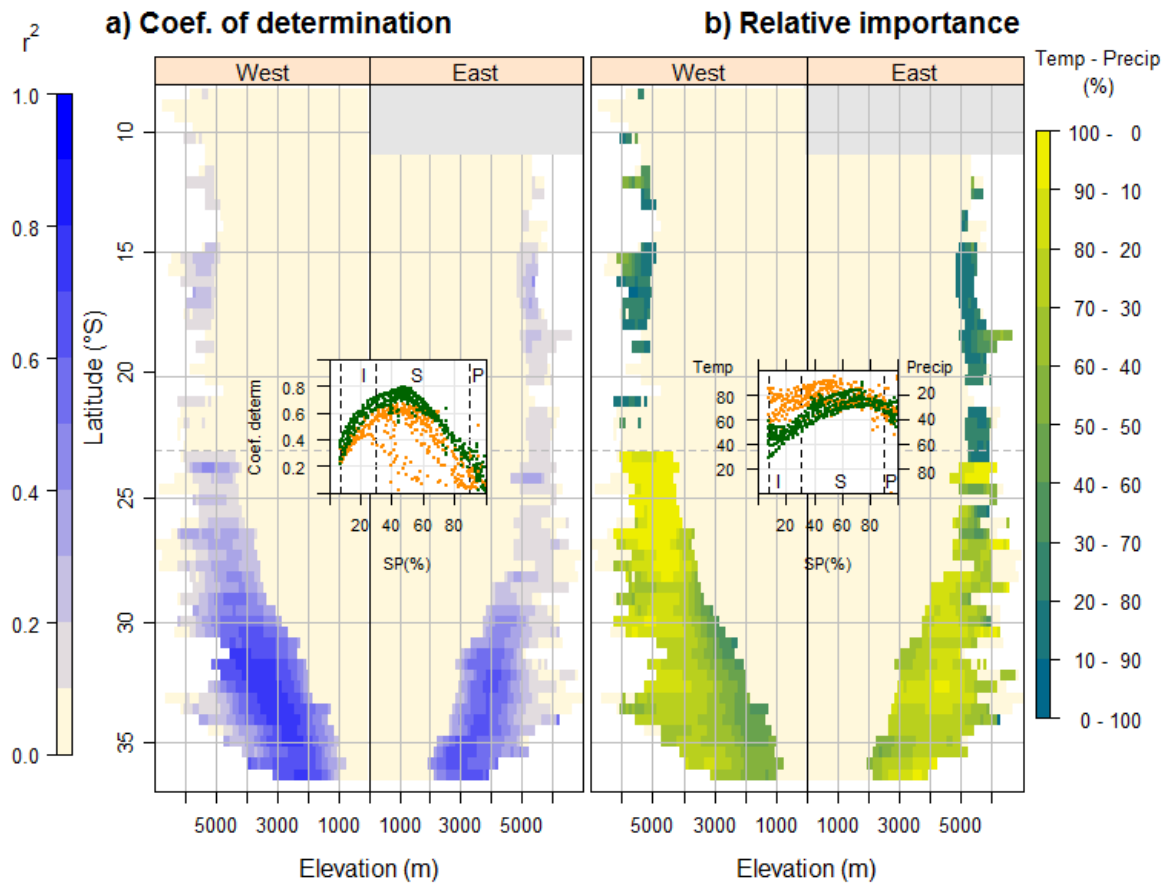

Figure 3.11. Latitude-elevation band analysis of. (a) coefficient of determination (r^2) for multiple linear regression of annual precipitation and mean air temperature over SP 2000-2014, (b) relative importance of air temperature (left color bar label) and precipitation (right color bar label) in the multiple linear regression. Inset box in a) shows the change in r^2 south of 23°S in West (green) and East (orange) vs SP values for latitude-elevation bands, indicating temperature and precipitation best predict SP in the seasonal snow zone. Inset box in b) shows temperature relative importance (left y-axis) and precipitation relative importance (right y-axis). Vertical dashed gray lines inside inset boxes represent thresholds for intermittent (I), seasonal (S), and persistent (P) snow zones. Grey areas represent latitudes masked due to high frequency of cloud cover in snow covered area analysis (>30% time period).

3.5. DISCUSSION

3.5.1. Spatial variability in snow persistence trends

We used MODIS snow data to quantify the change in the frequency of snow and its connection with climate conditions across the central Andes. North of 25°S, the snow-covered areas are small, making it difficult to track trends in SP (Figure 3.3a). This low snow presence is probably related to a combination of temperature and precipitation effects. Figure 3.2a shows the seasonality in patterns of precipitation, which is concentrated during austral summer synchronous with the highest temperatures during the year (Figure 3.2b). Thus, the precipitation falls mostly as rain, and snow is limited to elevations over 5000 m (Figure 3.5a). A limited trend is SP shown in this area (Figure 3.3b and Figure 3.4a), likely because the variation in SP is more related to precipitation than temperature (Figure 3.10b), and no trends in precipitation were detected in those areas (Figure 3.6a).

South of 25°S, we detected a significant decrease of SP (Figure 3.3b). The rates of decline vary across the range of elevation and latitudes. Areas with intermittent winter snow show a moderate decrease (-0.5 to -1.0 % per year) (inset box Figure 3.4b), with the largest decrease during winter (inset box Figure 3.5a). However, these areas have the greatest relative rates of snow loss (standardized slope in SP), particularly on the east side. Areas with seasonal winter snow show the steepest rate of change (-1.5 % per year) around SP=60%, with the largest decreases during spring. These declines in SP in the seasonal snow zone were not as high as those in intermittent snow zones when considering the standardized slope of SP. Persistent snow areas have moderate decreasing trends, which vary in timing. On the east side the greatest decline is during winter and on the west side during fall.

Previous studies had shown inconsistent findings related to snow changes for the same latitude range where we detected declining snow persistence (30°–37°S). Masiokas et al. (2006) showed a positive trend (not significant) of annual maximum snow water equivalent in five ground stations located in the same area between years 1951–2005, whereas higher studies focus on glaciers found a general decrease in areas of snow/ice during time periods from 1983-2011 located in elevation range of 1500-5800 m (Cortés et al., 2014), 1955-1997 (Pellicciotti et al., 2013), and a longer time period over the last 100 years (Masiokas et al., 2009). These inconsistencies could relate to: (1) the limited in situ observations used in Masiokas et al. (2006) were not representative of the region as a whole, (2) the longer time period covered for Masiokas et al. (2006) (54 years) has a different trend than the 2000-2014 time period examined here, and (3) generally lower elevations of stations used in Masiokas et al. (2006) (three stations over 3000 and just one over 3500m) compared with areas that have the largest declines in SP (over 3000m at 35°S to over 4000 at 30°S; Figure 3.4b).

The magnitude of significant decreases in SP south of 25°S ranges from 0.5% to 3.5%, which corresponds to 2-13 fewer days with snow per year during the study time (2000-2014). Prieto et al. (2001) constructed a series of the annual number of snow days in the Mendoza area of Argentina (32.5°S, elevation 750 m) from newspaper weather reports. The study shows a strong inverse relationship between temperature and snow occurrence and registered a reduction in days with snow between years 1885-2000. The inverse relation between the seasonal snow days and temperature has also been documented in other mountainous areas. Wang et al. (2008) in Northern Xinjiang (China) showed an inverse association between temperature and snow season duration at different elevations. Snow seasons were longer at higher elevation, but the relationship between temperature and snow season was weak at the highest elevations (over

4000m). This elevation dependence is also present in the San Francisco estuary and its upstream watershed (California, USA), where the greatest loss of snowpack was identified in the 1300–2700 m elevation range (Knowles and Cayan, 2004) in the seasonal snow zone (Moore et al., 2015). Our work shows a similar pattern south of 23°S where we documented that the elevation range of greatest loss in snow persistence is in seasonal snow zones (inset box in Figure 3.4b). This area of greatest snow persistence loss has a strong latitude dependence, and it varies in elevation from over 4000 m between 28-30°S down to 3000-4000m at 35°S on both sides of the mountain range.

The decreasing trend of snow persistence in the intermittent snow zone affected the trend of snow line elevation. The average snow line elevation decreases with latitude from 5000 m at 10°S to 700 m at 38°S (Saavedra et al., 2016), and it showed a significant increase in elevation of 10-30 m per year south of 30°S on the east side and between 29-35°S on the west side (Figure 3.5b). Previous glacier work used an empirical model to reconstruct annually the equilibrium-line altitude (ELA) in five points of Chilean Andes and documented a significant positive trend of the 0°C isotherm has occurred in the northern (24°S) and central (36°S) regions, indicating an ELA rise due to regional warming from 1958 to 2006 (Carrasco et al., 2008). Our work does not show an increase in snowline in the northern region, probably due to the precipitation dependence of snow cover in this area (Saavedra et al., 2016). The climatic factors affecting snow lines are likely somewhat different from those that affect glacier ELA, although snowline elevation increase has been documented in Andes tropical areas as well over 1961–2012 (Pepin et al., 2015). In the central area (32-34°S), Carrasco et al. (2008) found an increase of elevation of isotherm 0°C of 23 m/year that is consistent in both magnitude and trend direction with our results (Figure 3.5b), probably due to the temperature-dependence of snowline in this area.

3.5.2. Climatic causes of snow persistence trends

Trends in SP were greatest south of 23°S, where temperature is increasing while precipitation is decreasing (Figure 3.6), suggesting the combined influence of both of these variables leads to detectable loss of snow. Similar results were shown by Dedieu et al. (2014) in Central Asia using remote sensing data. In a warmer world, less winter precipitation falls as snow, and the melting of winter snow occurs earlier in spring (Barnett et al., 2005). Additionally, both T and P are modulated by ENSO in the region (Masiokas et al., 2006; Meza, 2013; Santos, 2006; Valdés-Pineda et al., 2015b; Zamboni et al., 2011). The trends in P and T we detected are generally consistent with those found in previous studies (Bradley, 2004; Quintana, 2012a; Salzmann et al., 2013; Vuille and Bradley, 2000). However, our results show that SP is only weakly correlated with ENSO (quantified by MEI) (Figure 3.8), which is inconsistent with other studies (Kluver and Leathers, 2015). This may be explained by the short time period of our research (15 years), which is insufficient for capturing the effect of this long-term temporal climate modulation. Future work could include other ENSO indices and varying time lags into the analysis to explore the influence of ENSO on snow persistence in greater detail. Other climate cycles such as the southern annular mode could also be examined to evaluate whether they affect the snow trends in the region.

Because snow persistence varies with elevation, the timing of greatest snow loss is also variable. In intermittent snow zones, where snow is not consistently present throughout the year, the greatest decreases in SP occur in austral winter. Here, a decline in winter precipitation leads to decline in snow and an increase in the elevation of the snow line. Higher up in the seasonal snow zone, where snow is present every year, the negative trends in SP are strongest in spring. These trends are explained primarily by temperature changes that accelerate the spring loss of

snow. The largest absolute changes in snow persistence are found in the seasonal snow zones mainly because of the larger amounts of snow in these areas compared with intermittent snow zones. Persistent snow zones are at the highest elevations, where temperatures are usually under freezing level, so changes in SP at these elevations are not as high as in lower elevation snow zones. When rates of SP change are divided by mean annual SP, the intermittent snow areas have the greatest declines around 4% on average; seasonal snow areas have values around 3%, and permanent snow areas lower than 1% (inset box Figure 3.4c), indicating that the highest elevations have experienced minimal changes in snow over the study time period.

Several studies have suggested that higher elevations are warming faster than lower elevations around the world (Liu et al., 2009; Oyler et al., 2015; Pepin et al., 2015), and climate models indicate that the largest temperature changes will be at high elevation in South American Mountains (Bradley, 2004). However, the available datasets for South America do not include high elevation stations, and the spatial resolution of the gridded temperature and precipitation products (0.5°) cannot capture the high topographic variability in mountains areas. Use of remote sensing could be helpful to incorporate higher spatial resolution information into future studies, although the snow cover-based approach may not capture changes in temperature at high elevations where snow cover is relatively permanent. Trends identified in this study may also be affected by the use of the MODIS 8-day maximum snow product, and future testing could evaluate whether these trends are consistent using daily or fractional SCA products. These finer resolution products face greater problems with cloud cover, so trend analyses with finer resolution products will likely need to incorporate cloud removal algorithms in many areas.

3.6. CONCLUSIONS

This work quantifies trends in snow persistence across a large range of latitude (9-36°S) and elevation (0-7000m) on both sides of the Andes Mountains from 2000-2014. North of 29°S (tropical latitudes and desert Andes), minimal change in SP was registered because the areas with snow are small, and there were limited changes in precipitation from 2000-2014. South of 29°S, significant loss of SP was recorded due to the combination of increased temperature and decreased precipitation. 62% of the area with significant SP loss was on the east side of the Andes Mountains. The absolute magnitude of these losses is greatest in areas with seasonal winter snow, whereas the greatest relative loss of snow persistence is in areas with intermittent winter snow, where the snow line has increased in elevation. The relative importance of precipitation and temperature to losses in SP varies with latitude and elevation. South of 23°S, precipitation has more relative importance at lower elevations than temperature on the west side, whereas temperature has greater relative importance at higher elevations and on the east side. The connection of SP with both temperature and precipitation are clear across the region, and climate modeling studies suggest that the trend of increasing temperature and declining precipitation will continue in this area (Bradley, 2004; GCOS, 2003). Loss of snow has consequences for streamflow in the region, where many of the rivers have a snowmelt-derived regime (Cortés et al., 2011). Improved understanding of the connections between change climate, snow, and streamflow production can aid in future water supply planning.

CHAPTER 4: STATISTICAL MODEL FOR PREDICTING WATER YIELD AND PEAK FLOW IN CHILEAN RIVERS

4.1. INTRODUCTION

In central Chile (30-37°S), rivers flowing from the west side of the Andes to the Pacific Ocean and are the main source of water supply for energy generation, irrigation, and drinking water and have great importance for the Chilean economy (Cortés et al., 2011; Vergara et al., 2007). In this region, runoff comes from winter rains or from snowmelt during spring and early summer (Cortés et al., 2011; Masiokas et al., 2013; Pellicciotti et al., 2013; Ragettli et al., 2013). Throughout the second half of the 20th century, the Central Andes Mountains experienced significant climatic and environmental changes characterized by a persistent warming trend (Falvey and Garreaud, 2009), an increase in elevation of the 0ºC isotherm (Vicuña et al., 2010), reduced precipitation (Le Quesne et al., 2009; Quintana, 2012a), sustained glacier shrinkage (Morales et al., 2012), and increase of drought frequency (Meza, 2013; Squeo et al., 2007). Additionally, Masiokas et al. (2006) presented a significant correlation between streamflow and snowpack variability on both sides of the central Andes (30°–37°S). In this changing environment, water resource management requires predictions of both current and future water yield.

Prediction of water yield is important for water resource planning. The ability to produce robust and accurate streamflow forecasts earlier in the season enhances the ability to manage the scarce resource (Kennedy et al., 2009). Many streamflow forecasting approaches are statistical models that relate predictor variables (climate, geographic) to the streamflow variable of interest. Since the early 1900's the Natural Resources Conservation Service (NRCS) in the United States

has produced statistical regression-based forecasts of water yield throughout the western US. This forecasts are based on varying combinations of current snowpack, previous soil moisture and streamflow, and autumn precipitation (Pagano and Garen, 2006). Hydrologic simulation models attempt to represent physical processes that affect streamflow generation. These models can also be used to predict water yield. For example, the US NRCS has implemented the Precipitation Runoff Modeling System (PRMS) for streamflow forecasts in some basins (Pagano et al., 2005). In Chile, the most used hydrologic model is Water Evaluation And Planning (WEAP) because of the ease of implementation and few parameter requirements (Cortes, 2010). Other models have been used such as SNOW-17, FTXZ, MSND, and TopNet to predict the volume of snowmelt runoff (Cartes, 2008; Mendoza, 2010).

A primary limitation to water yield prediction with both empirical and process-based hydrologic models is the availability and accuracy of input data. Ragettli et al. (2013) found that accurate simulation of streamflow in both WEAP and Topographic Kinematic Wave Approximation and Integration ETH Zurich (TOPKAPI-ETH) models required more information on precipitation than was available in a snow-dominated watershed at 33°S in the Andes Mountains. In central Chile, estimates of precipitation can be obtained from the Global Climate Observing System (GCOS) and Global Historical Climatology Network (GHCN), but these products usually underestimate values at high altitudes in central and northern Chile (Falvey and Garreaud, 2007; Favier et al., 2009; Rojas, 2005). When these data have been used to calculate runoff ratios (flow/precipitation), ratios sometimes exceed 100% in high elevation watersheds (Favier et al., 2009), an indication that the precipitation values are likely inaccurate. Inaccuracies in these climate data products stem from the quality and distribution of ground-based meteorological data used to develop the products. In the Andes mountains, precipitation,

temperature, and discharge are poorly observed especially at high elevation (>3000m) and too scarce to capture the variability in this high mountain region (Favier et al., 2009). This lack of data makes it difficult to predict water yield in the region.

Remotely sensed data on snow covered area (SCA) may potentially be useful for improving streamflow forecasts in this data-sparse region. Previous studies have used SCA to force hydrologic models of runoff production (Martinec et al., 2008; Molotch and Meromy, 2014; Rango et al., 1977). Hall et al. (2012), studied ten years of MODIS snow cover and 30 years of discharge and show that MODIS snow cover maps were a useful tool to predict streamflow in the Wind River Range, west Central Wyoming. Snow cover data are routinely used as part of streamflow forecasts in some regions. Given the limitations in available precipitation and snowpack data for the region, the main objective of this work is to develop a statistical hydrological model to predict water yield and peak flow in the central Chilean Andes using available data sources.

4.2. STUDY SITE

The study area is located in the central Chilean Andes between 30-37°S. In this area the Andes reach peak elevations over 7000 m at 33°S, with peak elevations decreasing to 4000 m at the southern boundary (Figure 4.1a). The regional snow line decreases from north to south from 4000 m at 29°S to 1900 m at 36°S (Saavedra et al., 2016) (Figure 4.1b). The study area has a Mediterranean-type climate, dry summers and wet winters. Temperature has a strong variability with elevation. The mean annual temperatures range from 10-20°C in the coastal area and drop to less than -10°C at the highest elevations (Figure 4.1c). Annual precipitation above 2500 m ranges from less than 500 mm in the north (31°S) to as much as 2000 mm further south at around

36°S (Rivera et al., 2000) (Figure 4.1d). Precipitation and streamflow are monitored by the "Dirección General de Aguas" (DGA), the Chilean government entity responsible for measuring and managing water resources. The study area has 79 streamflow measurements located in the headwaters of the all river basins and 215 points of precipitation monitoring. The DGA has recorded more than 600 diversion points, and there are 42 documented reservoirs, which are mostly located downstream from snow-covered areas (Figure 4.1e).

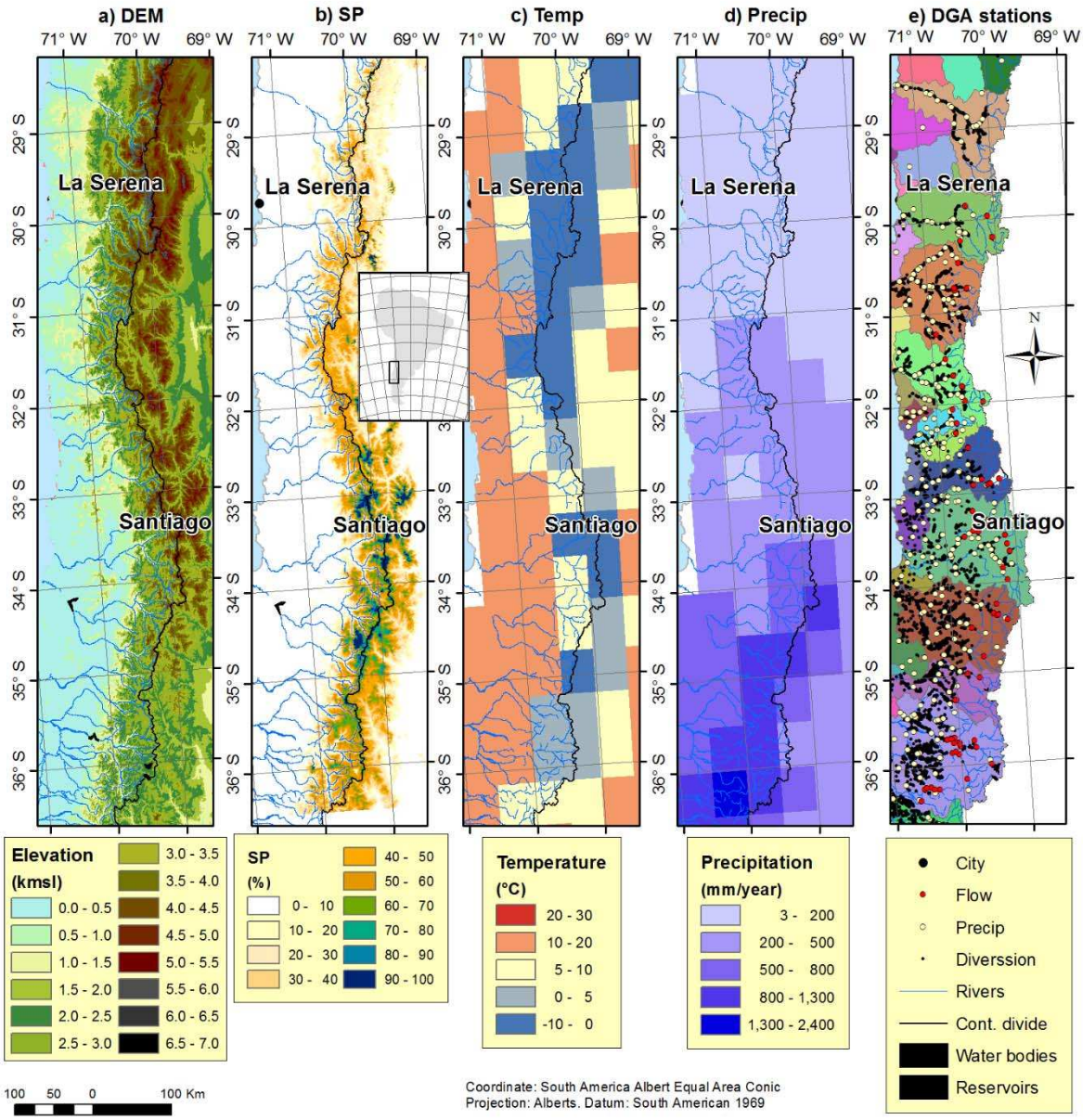

Figure 4.1. Study Area showing the: a) Digital Elevation Model (DEM), b) mean annual 2000-2014 snow persistence (SP) from (Saavedra et al., 2016), c) mean annual temperature, d) mean annual precipitation 2000-2014 from University of Delaware dataset (0.5° gridded), and e) ground stations for streamflow (red circles), precipitation (yellow circles), and diversions (black circles) from Chilean DGA dataset over major watershed boundaries.

4.3. METHODS

4.3.1. Data

Discharge

We selected flow prediction sites from the stream discharge (Q) stations monitored by the DGA, (http://snia.dga.cl/BNAConsultas/reportes). Of these stations, if more than one station was located on the same river, we selected the highest elevation streamflow station. To minimize the effects of flow modifications on water yield, we also excluded stations with more than five flow modifications (reservoirs and diversions) located upstream from the station selected. The watersheds selected are in headwater locations, and their high slope, relatively small agriculture areas, and low temperature mean that they have little or no human intervention (Cortés et al., 2011; Mendoza et al., 2014). For each of the selected stations we evaluated the quality of data from 2000-2014 at a monthly scale. In Chile, most of the climate and streamflow data are affected by gaps in information (Cortés et al., 2011). We discarded stations with more than 10% missing data. This led to a total sample size of 29 stream discharge stations (Figure 4.2). Streamflow station identification, location, and drainage area are summarized in Table 4.1.

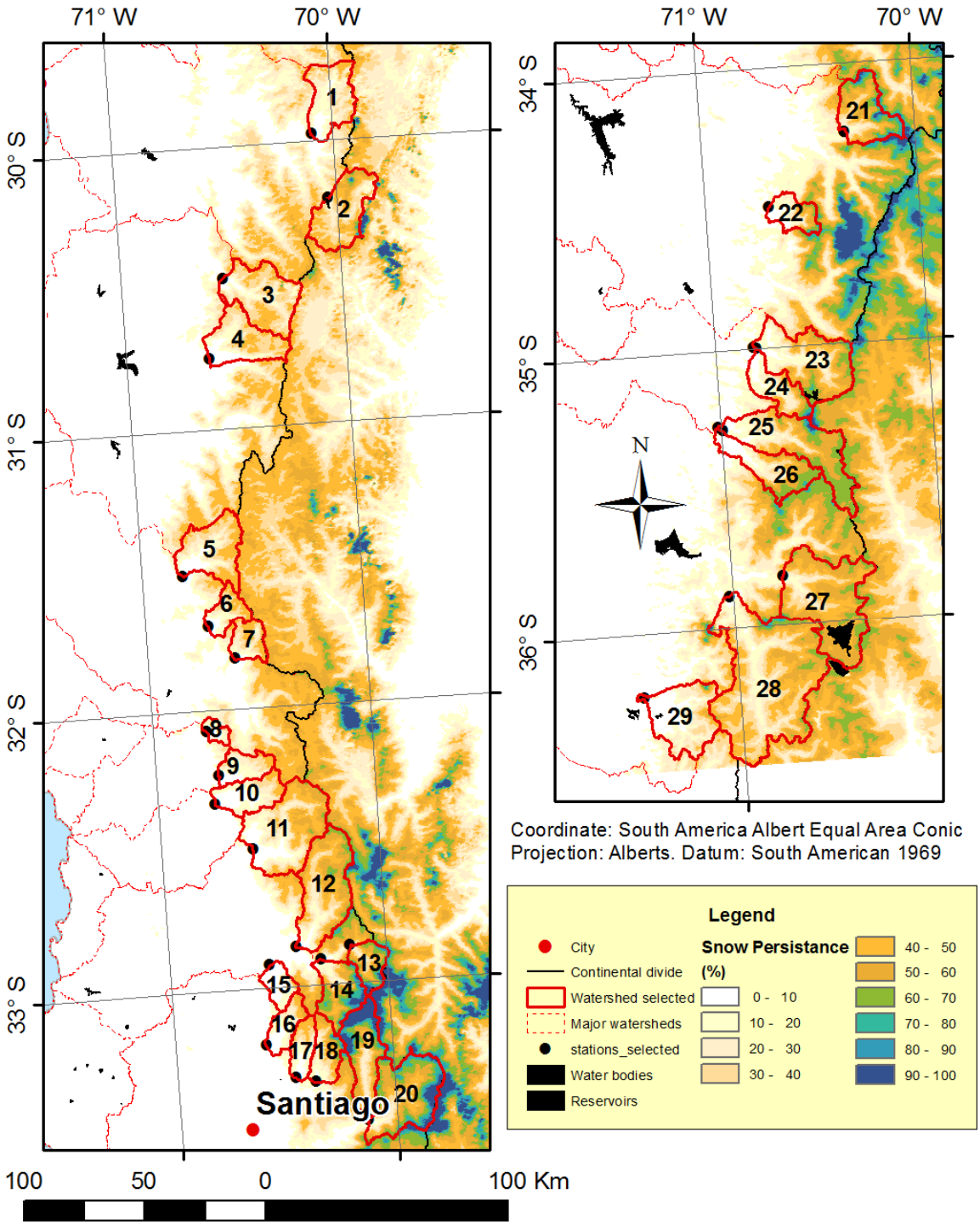

Figure 4.2. Location of selected streamflow stations (black circles) over mean annual snow persistence (SP) from 2000-2014 (Saavedra et al., 2016). Areas with greater SP are more likely to have snowmelt-dominated streamflow. The watersheds contributing to each streamflow station are shown in red polygons. These watersheds are located in the headwaters of major watersheds (dashed red polygons).

Table 4.1. Location and drainage area of streamflow stations used. Cod BNA refers to the Chilean identification of streamflow stations.

id	Cod BNA	Name	lat	long	Area (ha)
1	04302001-3	Rio Toro antes junta rio La Laguna	-29.97	-70.09	48,842
2	04301002-6	Rio La Laguna salida embalse La Laguna	-30.20	-70.04	56,662
3	04501001-5	Rio Hurtado en San Agustín	-30.46	-70.54	65,761
4	04520002-7	Canal central Los Molles en Cámara DGA	-30.75	-70.62	53,171
5	04721001-1	Rio Illapel en Las Burras	-31.51	-70.81	56,299
6	04712001-2	Rio Chalinga en La Palmilla	-31.70	-70.71	22,634
7	04704001-9	Rio Cuncumen junta Choapa (Chacay)	-31.82	-70.60	21,699
8	05101001-9	Rio Perdernal en Tejada	-32.07	-70.76	8,075
9	05100001-3	Rio Sobrante en Pinadero	-32.23	-70.71	24,174
10	05200001-7	Rio Alicahue en Colliguay	-32.33	-70.74	35,048
11	05414001-0	Rio Putaendo en reguardo Los Patos	-32.50	-70.58	94,609
12	05406001-7	Rio Colorado en Colorado	-32.86	-70.41	83,519
13	05401003-6	Rio Juncal en Juncal	-32.87	-70.17	23,498
14	05403002-9	Rio Aconcagua en Rio Blanco	-32.91	-70.30	40,917
15	05411001-4	Estero Pocuro en El Sifón	-32.92	-70.54	18,221
16	05735001-6	Canal Colina en Peldehue	-33.20	-70.58	22,788
17	05722001-5	Estero Arrayan en La Montosa	-33.33	-70.46	21,637
18	05721001-k	Estero Yerba Locan junta San Francisco	-33.34	-70.36	28,252
19	05706001-8	Rio Olivares antes junta Rio Colorado	-33.49	-70.14	54,320
20	05705001-2	Rio Colorado antes junta Rio Olivares	-33.49	-70.13	78,882
21	06006001-0	Rio Pangal en Pangal	-34.25	-70.33	51,869
22	06013001-9	Rio Claro en Hacienda Las Nieves	-34.50	-70.70	24,379
23	07104002-k	Rio Teno después de junta con Claro	-35.00	-70.82	85,349
24	07103001-6	Rio Claro en Los Quenes	-35.00	-70.81	35,407
25	07115001-1	Rio Palos en Junta con Palos	-35.28	-71.02	49,706
26	07112001-5	Rio Colorado en junta con Palos	-35.28	-70.99	88,669
27	07303000-5	Rio Maule en los Banos	-35.82	-70.76	117,674
28	07317005-2	Rio Melado en El Salto	-35.88	-71.02	214,072
29	07350001-k	Rio Longavi en la Quiriquina	-36.23	-71.46	67,601

From DGA streamflow data we calculated the annual water yield by water year and by season for each of the 29 watersheds selected. The Chilean water year starts in April and is divided into four seasons: fall includes April and March (AM), winter covers June, July, and August (JJA), spring includes September, October, and November (SON), and summer is December, January, February, and March (DJFM). We calculated snowmelt-dominance categories (SDC) for each watershed as the ratio between spring + summer and annual total

water yield: (SON + DJFM)/(annual water yield). We classified the watersheds into four categories from 1 to 4 according SDC level (0.3, 0.5, and 0.7). SDC 1 (<0.3) is clearly rain dominated; SDC 2 (0.3-0.5) mostly rain dominated; SCD 3 (0.5-0.7) mostly snowmelt dominated, and SCD 4 (>0.7) clearly snowmelt dominated (Fritze et al., 2011).

Physiographic characteristics

For each of the selected watersheds, we compiled information about the physiographic characteristics. To delineate the contributing area for each stream discharge station, we used a digital elevation model (DEM) developed from a combination of Shuttle Radar Topographic Mission (SRTM) and Advanced Spaceborne Thermal Emission and Reflection Radiometer (ASTER) elevation data (Saavedra et al., 2016). We used the watershed tool in ArcGIS to define the contributing areas from the DEM (Figure 4.2). Additionally, we calculated: centroid latitude (°) of the watershed, elevation of station (in meters), watershed mean elevation (in meters), maximum elevation of each watershed as the average of the 100 highest pixels (in meters), mean aspect, mean slope, northness to capture the influence of aspect and slope in the solar exposure as cos(aspect)*sin(slope), and Gravelius's index (Kg), which is as a ratio between perimeter (P) and area (A) of watershed, Kg=0.28*P/square root(A)(Bendjoudi and Hubert, 2002). A summary of physiographic variables is shown in Table 4.2.

Table 4.2. Summary of physiographic parameters for each selected watershed.

id	Centroid latitude (°)	Station elevation (m)	Mean elevation (m)	Max elevation (m)	Mean aspect	Mean slope	Mean Northness	Kg
1	-29.85	3,135	4,301	6,193	187	25	-0.41	1.4
2	-30.25	2,080	3,904	5,954	198	20	-0.32	1.4
3	-30.53	2,041	3,723	5,543	182	23	-0.39	1.4
4	-30.69	1,211	3,225	4,727	197	24	-0.39	1.6
5	-31.42	1,471	3,198	4,722	202	23	-0.36	1.3
6	-31.65	1,433	2,995	4,430	210	22	-0.32	1.4
7	-31.76	1,158	3,146	4,370	187	23	-0.38	1.5
8	-32.07	1,137	2,619	3,674	199	21	-0.33	1.4
9	-32.21	1,355	2,445	3,450	213	22	-0.31	1.3
10	-32.30	838	2,404	3,972	199	21	-0.34	1.4
11	-32.44	2,144	3,637	5,900	183	30	-0.49	1.3
12	-32.66	1,302	3,433	5,894	187	29	-0.48	1.4
13	-32.94	1,082	3,265	5,085	195	25	-0.41	1.4
14	-33.03	1,078	1,995	3,510	206	19	-0.30	1.3
15	-32.99	1,192	2,901	4,666	196	23	-0.37	1.4
16	-33.13	1,527	3,753	6,559	194	28	-0.45	1.5
17	-33.22	1,578	3,695	5,990	181	28	-0.46	1.6
18	-33.24	1,320	3,144	5,364	213	26	-0.37	1.4
19	-33.25	1,051	2,515	3,766	188	22	-0.37	1.3
20	-33.41	900	2,343	3,744	220	20	-0.27	1.4
21	-34.18	1,464	3,082	5,092	200	29	-0.45	1.4
22	-34.53	713	2,083	3,693	203	26	-0.41	1.4
23	-35.06	656	1,852	4,078	194	23	-0.38	1.7
24	-35.15	654	2,197	3,956	193	25	-0.41	1.5
25	-35.36	596	2,297	4,077	193	18	-0.30	1.9
26	-35.43	596	1,976	3,449	184	18	-0.31	1.8
27	-35.93	961	2,332	3,823	180	19	-0.33	1.7
28	-36.19	717	1,973	3,618	183	22	-0.37	1.7
29	-36.31	417	1,393	3,195	195	22	-0.37	1.5

Climate variables

We characterized the climate of each selected watershed using snow cover, precipitation, and temperature. For snow cover, we used the MODIS 500m binary snow cover products Collection 5 Level 3 eight-day product (MOD10A2) (Hall et al., 2002). MOD10A2 summarizes the maximum snow cover and minimum cloud during each eight-day interval (Riggs et al., 2006). The study area is covered by 5 MODIS images (tiles), which we downloaded for the time

period from 2000 to 2014 (MOD10A2) (http://reverb.echo.nasa.gov). From the MOD10A2 data, we calculated the annual snow persistence (SP) for each pixel in the study area as the fraction of the images in a year with snow cover (Saavedra et al., 2016).

We collected monthly temperature (T) and precipitation (P) with a 0.5° grid resolution from the University of Delaware dataset version 4.01 (UDelv4) from 2000-2014 (http://www.esrl.noaa.gov/psd/data/gridded/data.UDel_AirT_Precip.html) (Legates and Willmott, 1990). UDelv4 uses ground stations to compute a spherical version of Shepard's distance-weighting interpolation method (Willmott and Robeson, 1995). For comparison, we collected precipitation data from the 29 closest DGA stations to the streamflow station; usually the precipitation data are from the same location as the streamflow data. We also collected the Land Surface Temperature (T_s) from MODIS snow product (MOD11A2).

We summarized all predictor variables in monthly, seasonal, annual, and all period (2000-2014) time steps for each watershed. For the gridded variables (SP, T, P, T_s) these values represent the average of all pixels in the watershed contributing area. We also computed the snow covered area for the watershed (SCA) averaged over each time step. The annual climate and streamflow summary for each watershed is shown in Table 4.3.

Table 4.3. Summary of mean annual climate variables and water yield for selected watersheds, 2000-2014.

Id	SP watershed (%)	SCA (ha)	T Udelv4 (°C)	T_s MODIS (°C)	P UDelv4 (mm)	P DGA (mm)	Q (m^3/s)	Q (mm)
1	39.0	19,048	-8.20	18.2	154	112	1.6	88
2	23.3	13,202	-3.79	18.2	90	87	0.6	40
3	31.4	20,649	-4.89	13.4	163	134	2.4	113
4	26.7	14,197	0.32	17.3	179	171	0.7	39
5	32.2	18,128	2.99	16.7	238	262	0.4	62
6	27.7	6,270	5.27	17.8	220	255	0.8	108
7	29.3	6,358	-3.32	15.9	194	239	1.9	108
8	21.7	1,752	6.22	22.7	233	224	0.8	105
9	16.4	3,965	7.53	21.2	259	215	0.3	101
10	19.1	6,694	5.24	22.6	204	232	1.0	88
11	56.7	53,643	4.67	18.8	489	308	5.6	743
12	54.8	45,768	-0.26	14.2	489	356	7.1	537
13	41.8	9,822	4.39	9.6	353	304	4.3	152
14	11.8	4,828	6.96	10.2	283	283	0.8	130
15	31.0	5,649	2.60	26.4	260	263	7.0	232
16	58.0	13,217	-1.60	22.2	427	375	6.4	260
17	59.8	12,939	-6.08	19.6	427	404	2.8	158
18	39.0	11,018	-6.08	13.9	476	404	0.9	104
19	24.4	13,254	-6.08	8.5	476	404	1.4	198
20	21.3	16,802	0.23	8.3	230	348	1.8	244
21	53.1	27,542	7.46	11.1	896	803	14.2	864
22	29.6	7,216	11.09	17.1	537	695	7.4	950
23	30.1	25,690	3.18	15	1,252	1,029	17.5	1,540
24	37.8	13,384	4.88	17	1,165	899	54.8	2,013
25	43.9	21,821	2.69	13	1,051	927	43.0	1,519
26	36.2	32,098	3.07	15.1	1,051	1,028	27.4	1,720
27	46.5	54,718	4.22	12.9	1,546	814	58.1	1,608
28	37.7	80,705	5.66	15.1	1,546	1,231	84.5	1,250
29	19.5	13,182	9.42	15.6	2,146	1,335	46.8	2,132

4.3.2. Model development

Individual watershed models

First, we examined how independent climate variables relate to water yield for individual watersheds. To do this, we ran a univariate linear regression to relate each independent variable:

snow persistence (SP), snow covered area (SCA), mean temperature (T and T_s) (from UDelv4 and MODIS datasets) and total precipitation (P) (from UDelv4 and DGA datasets) to each dependent variable: total water yield (WY) and peak flow (PF) by water year. Each independent variable was tested using annual, seasonal (AM, JJA, SON, and DJFM), and monthly values. We computed the coefficient of determination (r^2) from each univariate linear regression per watershed to compare the proportion of WY and PF variance predicted from univariate analysis.

Next, we ran a multivariate analysis including snow, precipitation, and temperature independent variables. We selected the variable with the highest r^2 between SP and SCA for snow, between MODIS and UDelv4 datasets for T, and between UDelv4 and DGA for P. Then, we ran a multivariate regression using annual, seasonal, and monthly independent variables. For multivariate analysis, we also developed a cumulative monthly model. This approach begins with data from the first month of the each water year (April) to define the baseline forecast (step 1). Then we added a consecutive month of climate information and averaged these values with those of the previous month to run the multivariate analysis again. This process repeated until March to complete the water year (12 steps).

All watersheds model

Next, we examined how independent variables relate to WY and PF across all watersheds together. We first explored the univariate regressions for all independent variables (physiographic, streamflow, and climate presented in Table 4.4). Before conducting the multivariate analysis for all watersheds, we conducted a cross-correlation analysis between independent variables and computed a matrix of correlation coefficients (r). When two variables were highly correlated (absolute value of $r > 0.6$), we selected the one with the highest univariate

r^2 to include in the multivariate regression model. For both univariate and multivariate analysis, we applied climate variables using all period, annual, seasonally, monthly, and cumulative monthly values. For the monthly cumulative analysis we computed the relative importance of each independent variable to quantify the change in the relative weight of each variable across the water year. We followed the relative importance developed by Lindeman, Merenda and Gold (lmg) included in the relative importance for linear regression "relaimpo" R package (Groemping and Matthias, 2013) to test the individual contribution of each regressor to the full r^2 of the model (Grömping, 2006).

Table 4.4. Summary of independent variables explored in statistical models of water yield and peak flow for all watersheds combined.

Category	Predictor		Individual watershed model	All watershed model	Units
Physiography	Area			x	ha
	Station elevation			x	m
	Mean elevation			x	m
	Max elevation			x	m
	Mean aspect			x	°
	Mean slope			x	°
	Mean northness			x	
	Centroid Latitude			x	°S
	Kg			x	
Streamflow	SDC all period			x	
	Variable	*Time step*			
Climate	SP and SCA	All period		x	% and ha
		Annual	x	x	
		Seasonal	x	x	
		Monthly	x	x	
	T and T_s*	All period		x	°C
		Annual	x	x	
		Seasonal	x	x	
		Monthly	x	x	
	P**	All period		x	mm
		Annual	x	x	
		Seasonal	x	x	
		Monthly	x	x	

* MODIS and UDelv4 dataset, ** UDelv4 and DGA dataset

4.4. RESULTS

We selected six example watersheds to illustrate the variability of climate and streamflow in the study area (Figure 4.3; for watershed number refer to Figure 4.2). Precipitation has a similar seasonal pattern in all watersheds, with the maximum amount around austral winter (between April and September). The northern watersheds (1 and 2) also have a second

precipitation peak in late spring. The magnitude of precipitation ranges from less than 100 mm/year in the northern watersheds to 1600 mm/year in the southern watersheds. Temperature is highest in austral summer and lowest in austral winter, with a range from -15 to 10°C in the northern watershed and from 0-20°C in the southern watersheds. Snow cover is highest in austral winter (blue areas in Figure 4.3) and lowest during austral summer (yellow areas in Figure 4.3). Some watersheds (2 and 20) have snow present all year at high elevations. The streamflow seasonal patterns vary between watersheds selected. Some have peak flow in spring after the peak in snow cover and precipitation (watersheds 2 and 20). Other watersheds (1 and 28) have both a spring streamflow peak and relatively high flow during the winter. Finally, watersheds 15 and 29 have peak streamflow during winter.

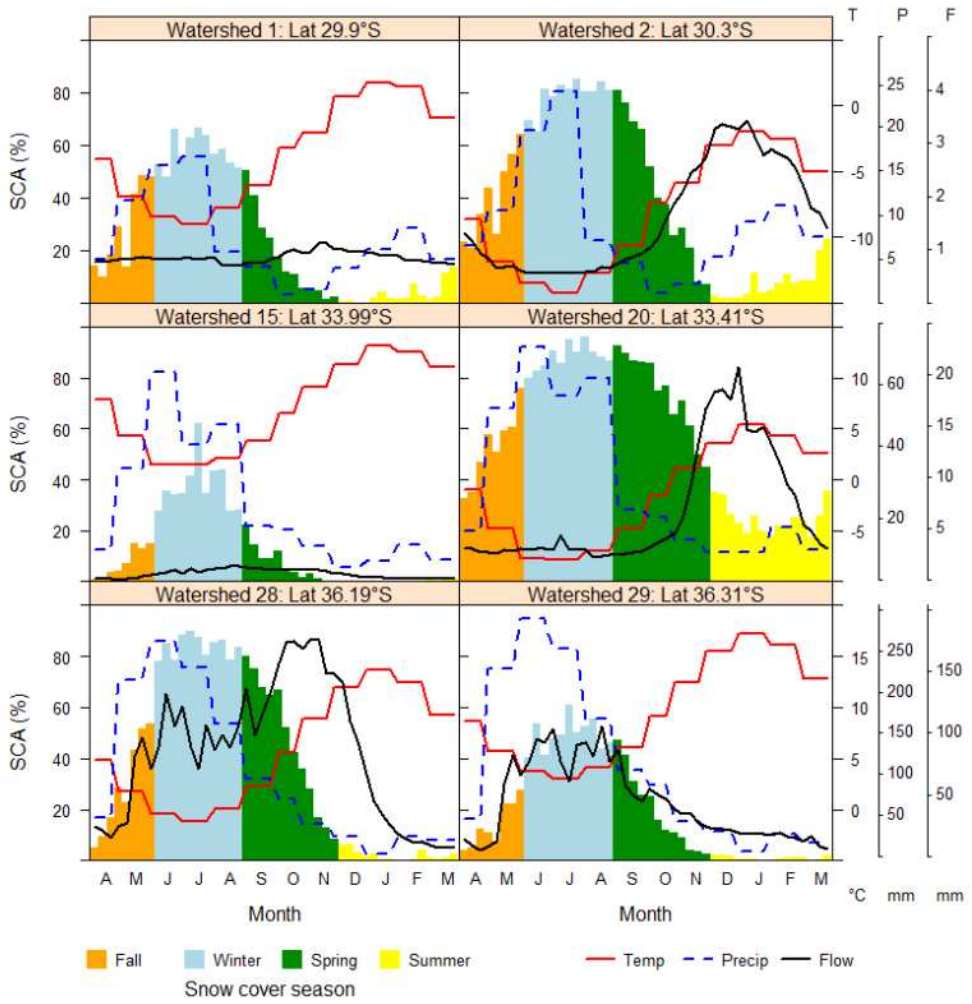

Figure 4.3. Example watersheds illustrating the seasonal patterns of temperature and precipitation from University of Delaware dataset, streamflow from DGA record, and snow covered area from MODIS snow product divided in four seasons following the Chilean hydrologic division. Mean values across all years (2000-2014).

The average monthly streamflow magnitude has a large range from 0.3 to 90 m^3/s from North to South (Figure 4.4a). When normalized by drainage area, the water yield in mm also has a large range from arid (<100 mm/year) to humid conditions (>2000 mm/year) (Figure 4.4b). The snow dominance category (SDC) is used to classify the streamflow regime (Figure 4.4c). Most of the watersheds have a moderate to strong snow connection. The clearly snowmelt-dominated watersheds (category 4) are concentrated between 32-34°S, whereas most of the

watersheds further north and south are mostly snowmelt dominated (category 3). We calculated the runoff ratio (Q/P) from UDelv4 and DGA datasets to evaluate the regional variability in runoff export and the quality of precipitation data. The runoff ratio generally increases from North to South, and some of the values are greater than one south of 34°S (Figure 4.4d and e).

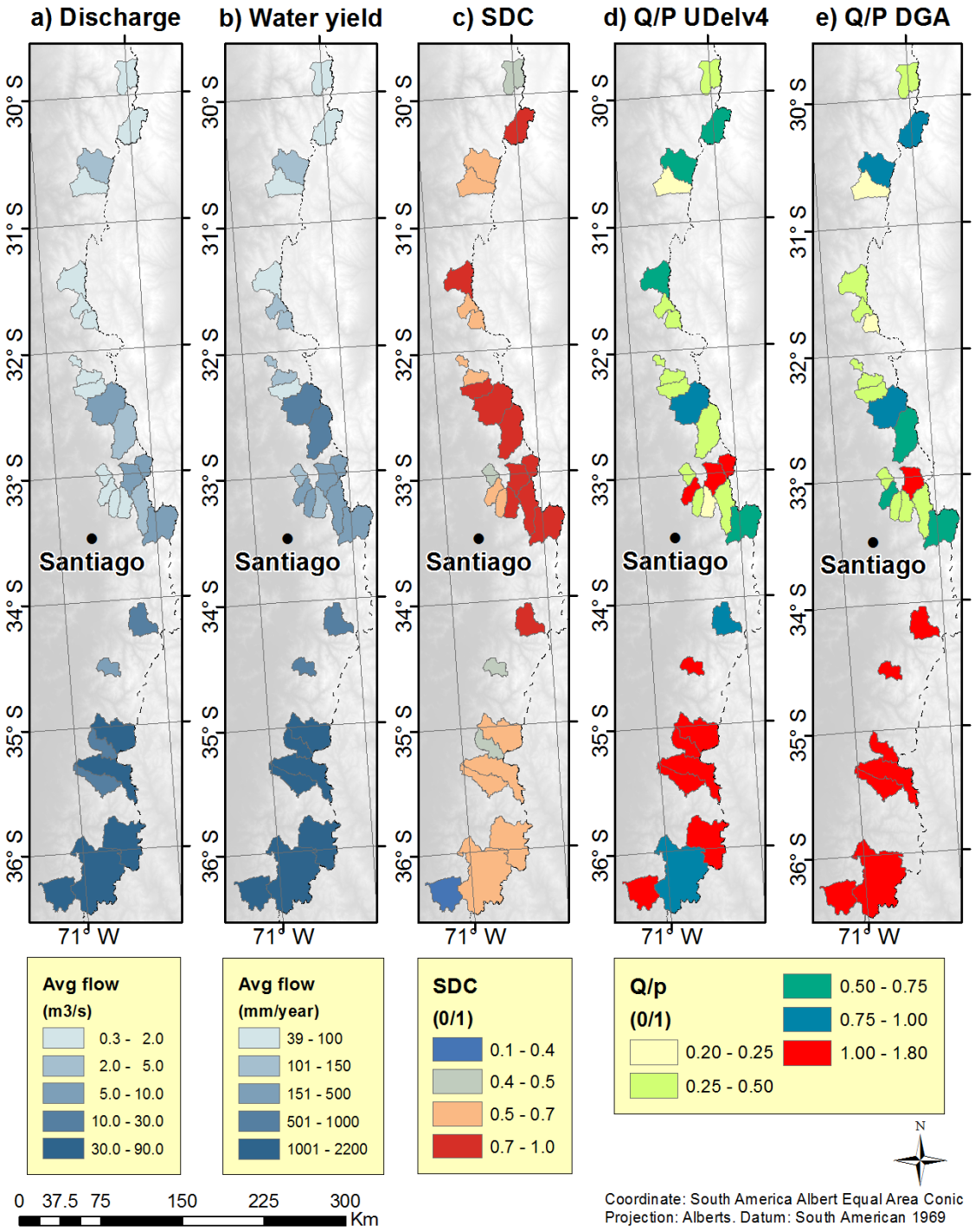

Figure 4.4. a) Annual mean discharge, b) water yield (mm), c) snow dominance category (SDC), d) runoff ratio (Q/P) using precipitation data from University Delaware dataset (UDelv4) and e) runoff ratio using precipitation from DGA stations.

4.4.1. Individual watershed model

The univariate analysis by watershed reveals a seasonal and spatial variability of regression performance. To illustrate how snow relates to flow in the individual watersheds Figures 4.5 and 3.6 show the geographic distribution for the r^2. Per each water year we computed the average SCA over the whole watershed in annual and seasonal time scales (SCA_{annual}, SCA_{AM}, SCA_{JJA}, SCA_{SON}, and SCA_{DJFM}) to and related these values to total WY (Mm^3) and PF (m^3/s). SCA has a stronger correlation with water yield volumes than SP because it represents the area in the watershed with snow. SCA_{annual} and SCA_{SON} correlate strongly with WY and PF. The correlation is weaker using SCA input data from the other seasons (SCA_{AM}, SCA_{JJA}, or SCA_{DJFM}). The relations become weaker in the southernmost watersheds. The other univariate analyses between WY, PF, and the other climate variables did not have evident geographic patterns (data not shown).

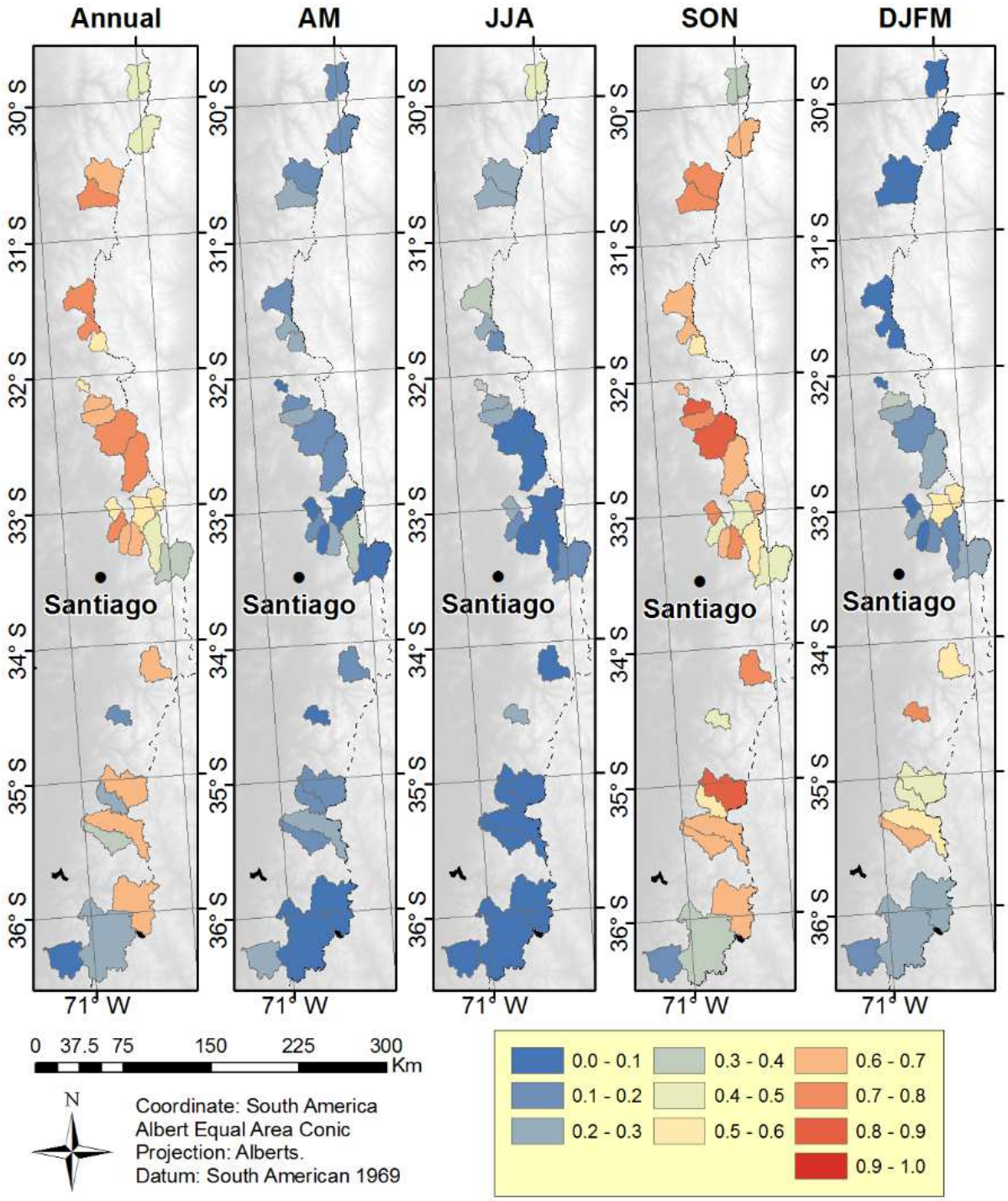

Figure 4.5. Coefficient of determination (r^2) for predictions of WY for each watershed using (SCA_{annual}, SCA_{AM}, SCA_{JJA}, SCA_{SON}, and SCA_{DJFM}) values.

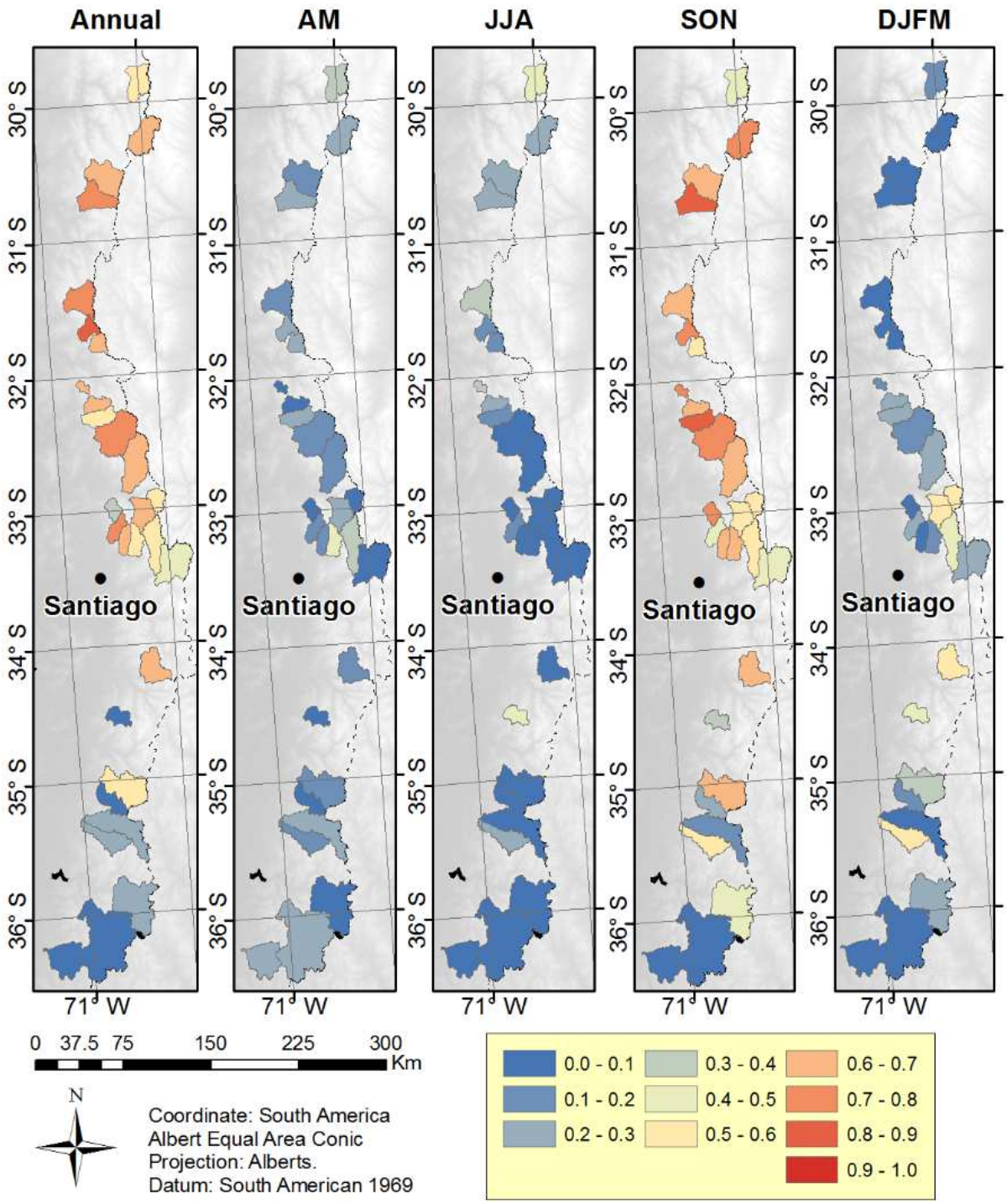

Figure 4.6. Coefficient of determination (r^2) for predictions of PF for each watershed using annual and seasonal (SCA_{annual}, SCA_{AM}, SCA_{JJA}, SCA_{SON}, and SCA_{DJFM}) values.

To illustrate how each of the climate variables relate to WY and PF, Figure 4.7 shows the distribution of r^2 using annual and spring (SON) season input values for univariate analysis. Watersheds are stratified by either SDC or 2000-2014 mean watershed SP. For these analyses, we used P and T from UDelv4 dataset because this dataset has consistently better performance (higher r^2) than alternative datasets (P from DGA and T_s from MODIS). The univariate correlations to WY and PF using SCA (annual and SON season) and T (annual and SON season) are affected by the snow dominance category (SDC). Lower values of SDC (<0.6) have lower values of r^2 (<0.4), indicating that SCA and T are only strongly correlated with WY and PF in clearly or mostly snowmelt-dominated watersheds. Annual P is highly correlated with WY in some watersheds but not in others. The predictive strength of P has no apparent connection to SDC. Spring (SON) precipitation is always poorly correlated with WY and PF. When SCA, T, and P are combined in a multivariate analysis, predictions of WY and PF in SDC 2 improve over the univariate r^2 values, but the predictions of WY and PF for the mostly and clearly snowmelt dominated watersheds (SDC 3,4) are only slightly improved over their values using SCA alone.

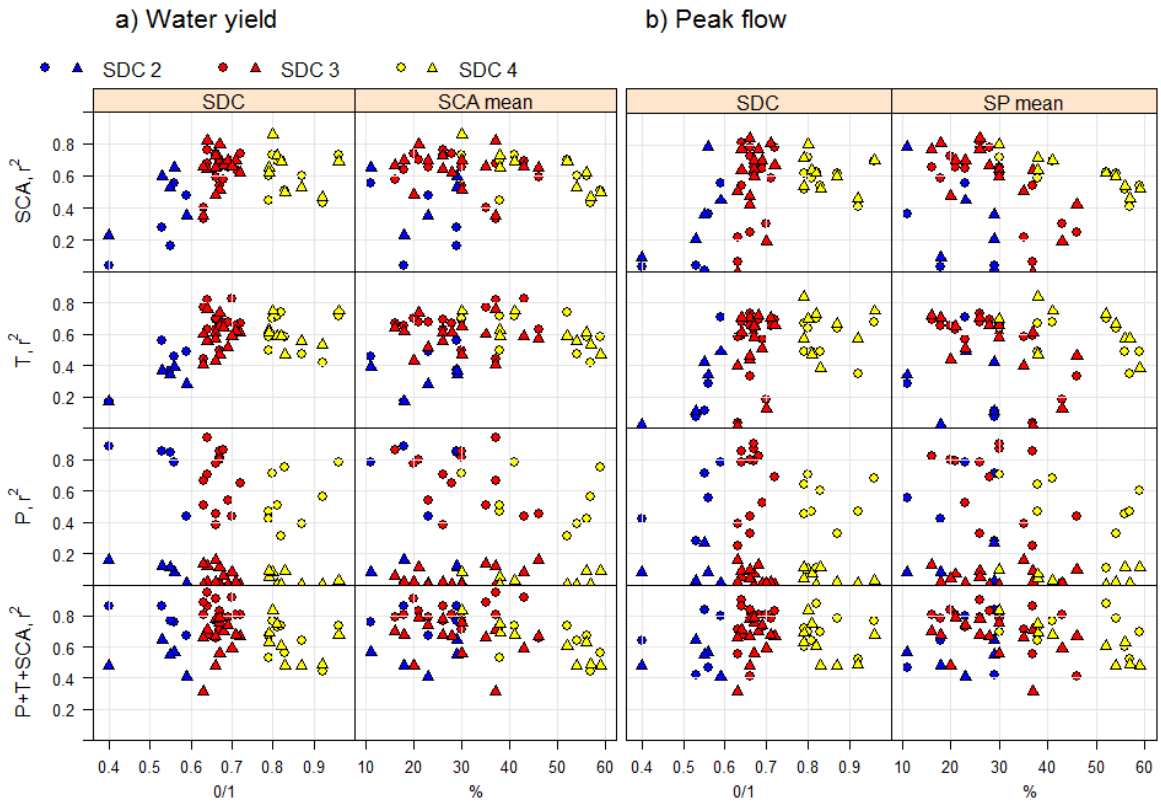

Figure 4.7. Coefficient of determination of (a) water yield predictions and (b) peak flow per watershed using snow covered area (SCA), temperature (T), and precipitation (P) separately, and a combined linear regression using all input variables combined (SCA+T+P). Each column represents a distribution of r^2 results by 2000-2014 mean SDC and SCA_{mean} over all time period (2000-2014). Each point represents the r^2 for an individual watershed; Annual input values are shown in circles, and SON season input variables are shown in triangles.

The monthly cumulative analysis illustrates how well water yield and peak flow can be forecasted as the water year progresses (Figure 4.8). The time evolution of r^2 to predict WY for each watershed (Figure 4.8) has an s-curve shape with a steep increase between July and August followed by stable values after September. At the beginning of the water year (April), forecasts of WY and PF are poor, but these predictions improve as the water year progresses to a maximum in September or October, the spring snowmelt season. Averaging in additional months of climate information in late spring or summer (November-March) does not improve the WY

predictions, and in some cases it decreases the strength of the PF prediction. Watersheds classified in SDC 3 tend to have higher r^2 values all year, although some watersheds in this category are also poorly predicted. Table 4.5 shows the coefficients of determination for each watershed with cumulative information at September for the water yield (WY) expressed in millions of meter cubic (Mm^3) per year, when the temperature is input in Celsius degree (°C), precipitation as depth in millimeters (mm), and the SCA in hectares (ha). Table 4.6 shows the regression coefficients for peak flow (PF) in meter cubic per second (m^3/s) using the same units inputs as in the WY regressions.

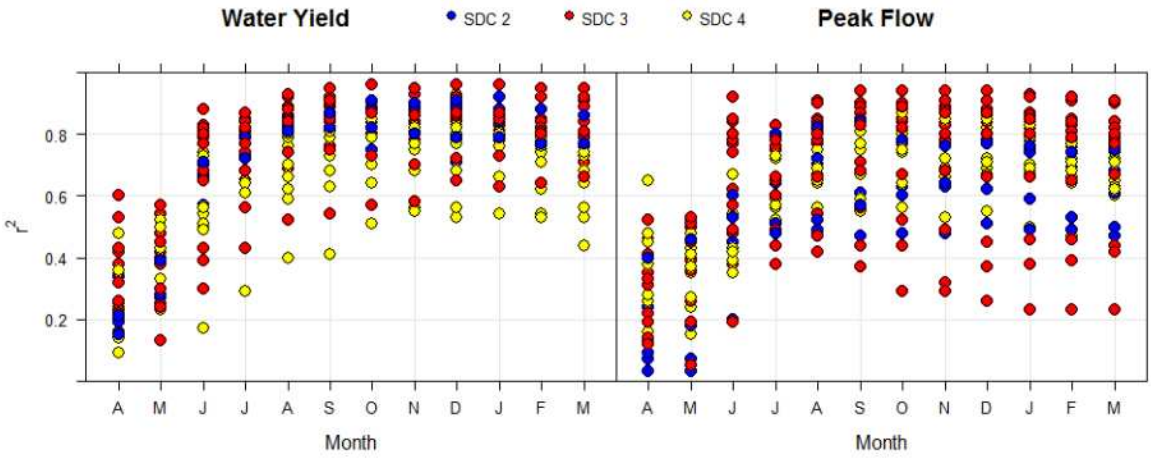

Figure 4.8. Coefficient of determination (r^2) to predict water yield and peak flow from multivariate regressions using monthly accumulated data of combined variables (SCA+T+P) for each watershed.

Table 4.5. Water yield (WY) regression coefficients for cumulative months until September. WY expressed in Mm^3, and the units for input are defined in column labels.

Watershed	Intercept	T (°C)	P (mm)	SCA (ha)	r^2
04302001-3	2.28	-0.254	0.110	4.00E-05	0.75
04301002-6	78.70	9.801	0.423	1.59E-03	0.41
04501001-5	-42.20	10.010	0.931	2.76E-03	0.82
04520002-7	-22.92	1.023	0.145	1.05E-03	0.76
04721001-1	-253.70	0.887	0.844	5.31E-03	0.86
04712001-2	-37.30	-2.874	0.142	3.45E-03	0.90
04704001-9	-47.90	-4.880	0.183	1.79E-03	0.84
05101001-9	-14.46	-0.342	0.080	3.95E-03	0.86
05100001-3	-57.99	4.310	0.196	3.53E-03	0.89
05200001-7	-62.18	2.676	0.244	3.43E-03	0.92
05414001-0	-746.80	114.800	1.040	1.73E-02	0.84
05406001-7	-934.10	72.290	0.988	1.41E-02	0.82
05401003-6	-110.30	30.480	0.400	8.98E-03	0.63
05403002-9	-519.57	67.985	1.208	2.22E-02	0.79
05411001-4	-63.29	8.044	0.139	6.89E-03	0.86
05735001-6	-92.54	5.821	0.276	1.00E-02	0.90
05722001-5	6.52	7.048	0.164	5.20E-03	0.84
05721001-k	-13.93	3.731	0.063	3.40E-03	0.73
05706001-8	-192.60	17.490	0.328	8.03E-03	0.68
05705001-2	-181.20	-11.970	1.349	-1.19E-03	0.63
06006001-0	-617.90	17.240	1.244	4.17E-03	0.81
06013001-9	68.24	12.783	0.625	-2.64E-02	0.82
07104002-k	-2232.00	79.870	4.229	1.47E-02	0.95
07103001-6	-536.30	79.910	1.185	9.01E-03	0.87
07112001-5	-1167.00	87.930	2.771	9.68E-03	0.91
07115001-1	-477.40	39.360	1.664	-2.21E-03	0.86
07303000-5	-1648.00	-75.410	3.246	1.82E-02	0.54
07317005-2	-3162.00	351.900	4.829	5.75E-03	0.75
07350001-k	-2976.00	294.600	2.381	1.34E-02	0.87

Table 4.6. Peak flow (PF) regression coefficients for cumulative month until September. PF expressed in m^3/s, and the units for input are defined in column labels.

Watershed	Intercept	T (°C)	P (mm)	SCA (ha)	r^2
04302001-3	-1.04	-0.12	0.0064	4.14E-05	0.61
04301002-6	-0.80	0.62	0.0651	2.16E-04	0.67
04501001-5	-8.31	0.66	0.0917	2.34E-04	0.81
04520002-7	-1.75	-0.11	0.0069	6.32E-05	0.71
04721001-1	-32.60	-0.09	0.0917	6.74E-04	0.85
04712001-2	-2.78	-0.17	0.0093	2.25E-04	0.94
04704001-9	-4.71	-0.18	0.0136	2.31E-04	0.87
05101001-9	-1.31	-0.07	0.0074	5.00E-04	0.90
05100001-3	-8.70	1.09	0.0218	3.64E-04	0.90
05200001-7	-4.64	0.24	0.0190	2.27E-04	0.89
05414001-0	-103.60	15.06	0.1065	2.39E-03	0.85
05406001-7	-132.80	10.05	0.1204	2.14E-03	0.75
05401003-6	-13.32	4.37	0.0637	4.42E-04	0.59
05403002-9	-63.60	0.70	0.2079	1.25E-03	0.81
05411001-4	-12.08	2.17	0.0174	8.65E-04	0.68
05735001-6	-8.19	1.05	0.0257	1.05E-03	0.87
05722001-5	-1.27	0.63	0.0188	4.90E-04	0.85
05721001-k	-0.79	0.39	0.0070	2.99E-04	0.59
05706001-8	-5.49	3.22	0.0450	8.73E-04	0.59
05705001-2	-40.15	-1.48	0.1810	8.18E-05	0.55
06006001-0	-31.40	0.04	0.1437	-6.46E-04	0.77
06013001-9	64.51	0.66	0.0834	-8.13E-03	0.84
07104002-k	-291.90	16.44	0.4961	1.82E-03	0.83
07103001-6	-145.60	47.73	0.3693	-1.38E-03	0.47
07112001-5	-196.10	8.42	0.2032	3.21E-03	0.56
07115001-1	-16.83	-0.52	0.1565	-2.00E-03	0.68
07303000-5	97.00	37.33	0.4012	-2.20E-03	0.44
07317005-2	-480.40	36.76	0.4093	2.77E-03	0.37
07350001-k	-1007.00	76.76	0.7129	5.97E-03	0.57

4.4.2. All watersheds model

For all watersheds combined, we computed the univariate predictions of WY and PF using all period, annual, seasonal and monthly time scale input variables (Table 4.7). Of the physiographic variables, area and latitude have the higher r^2 values. Of the climatic variables, SCA and P give higher r^2 values than T and T_s.

Table 4.7. Coefficient of determination (r^2) for univariate regressions between independent variables and WY and PF. Values of r^2>0.4 are in red.

			WY			PF		
Category	Predictor		All period	Annual	SON	All period	Annual	SON
Physiography	**Area**		0.64	0.50	0.50	0.43	0.50	0.50
	Station elevation		0.24	0.20	0.20	0.29	0.20	0.20
	Mean elevation		0.29	0.23	0.23	0.39	0.23	0.23
	Max elevation		0.16	0.13	0.13	0.18	0.13	0.13
	Mean aspect		0.15	0.11	0.11	0.11	0.11	0.11
	Mean slope		0.06	0.04	0.04	0.04	0.04	0.04
	Mean northness		0.01	0.00	0.00	0.00	0.00	0.00
	Centroid Latitude		0.60	0.49	0.49	0.62	0.49	0.49
	Kg		0.37	0.19	0.19	0.30	0.30	0.30
Streamflow	SDC all period		0.20	0.08	0.08	0.23	0.08	0.08
Climate	**SCA**	MODIS	0.54	0.45	0.49	0.30	0.45	0.49
	SP	MODIS	0.07	0.04	0.12	0.04	0.03	0.05
	T_s	MODIS	0.06	0.07	0.04	0.07	0.16	0.16
	T	UDelv4	0.20	0.09	0.14	0.09	0.26	0.26
	P	**UDelv4**	0.69	0.63	0.86	0.63	0.54	0.54
	P	**DGA**	0.63	0.59	0.81	0.59	0.31	0.31

Before integrating variables into a multivariate regression, we first tested the correlation between the possible independent variables (Table 4.8). From Table 4.7 we selected the most relevant variables ($r^2 > 0.4$), and from these we compared the correlations between the possible predictors; the independent variables that correlated best with WY and PF are highlighted in bold in the cross-correlation matrix (Table 4.8). When the absolute value of correlation was greater than 0.6 we selected the variable with the greater r^2 in the univariate predictions of WY and PF (Table 4.7). Following this approach, we selected area, SCA, and P from UDelv4 dataset, ran a multivariate regression, and computed the relative importance of each independent variable. Table 4.9 summarizes the values of coefficient of regression and r^2 for the selected independent variables in a multivariate regression at all period, annual, and monthly time scales. Relative importance for each selected variable in each model is shown in Table 4.10. Precipitation has

always the higher relative importance (44-63%) and SCA the lower (14-28%). For both univariate (Table 4.7) and multivariate models, the r^2 is greater for WY than for PF for most time scales of input variables. Multivariate models best predict WY for the input variables averaged over the entire time period ($r^2 = 0.89$), but performance of WY models using annual and spring input variables are also strong ($r^2 = 0.80$ for annual and 0.73 for SON season time scales). For PF the entire time period has the highest value ($r^2 = 0.89$), whereas annual ($r^2 = 0.69$) and SON season ($r^2 = 0.62$) models have poorer performance (Table 4.9).

Table 4.8. Cross-correlation matrix between independent variables (r). Variables that correlate best with WY and PF in univariate analysis (Table 4.7) are highlighted in bold. Cross-correlation values >0.6 are shown in red.

		Elevation station	Watershed mean elev	Watershed max elev	Aspect	Slope	Northness	**Latitude**	Kg	SDC all period	**SCA**	SP	T_s MODIS	T UDelv4	**P UDelv4**	**P DGA**
Physiography	**A**	-.20	-.13	-.03	-.51	-.11	.02	-.43	.51	.06	.31	.16	-.33	.06	.50	.44
	St. elev		.88	.77	-.14	.36	.04	.72	-.46	.41	.26	.12	-.16	-.56	-.66	-.57
	Mn elev			.92	-.19	.50	.03	.74	-.32	.67	.47	.21	-.39	-.66	-.71	-.65
	Mx elev				-.26	.64	.05	.50	-.20	.68	.65	.37	-.59	-.62	-.46	-.42
	Mn aspect					-.14	-.14	.19	-.37	-.15	-.52	-.38	.55	.27	-.24	-.28
	Mn slope						-.14	.08	-.31	.56	.65	.42	-.62	-.13	-.13	-.08
	Mn northness							-.07	.36	-.02	.15	.04	-.14	-.02	.06	.08
	Centroid latitude								-.56	.28	-.22	-.07	.27	-.49	-.93	-.86
	Kg									-.12	.29	.12	-.34	.04	.62	.50
SDC all period											.67	.27	-.48	-.40	-.43	-.46
Climate	**SCA**	**MODIS**										.48	-.92	-.24	.14	.12
	SP	MODIS											-.25	-.07	.05	.00
	T_s	MODIS												.22	-.26	-.28
	T	UDelv4													.45	.43
	P	**UDelv4**														.94
	P	**DGA**														

Table 4.9. Equation coefficients for multivariate regression and the r^2 of regressions. Area, SCA, and P (UDelv4) are independent variables for computing WY in Mm^3 and monthly PF in m^3/s.

		Intercept	Area (ha)	SCA (ha)	P (mm)	r^2
WY	All period	-598.7	1.004E-02	-2.487E-03	1.133	0.89
	Annual	-608.7	7.179E-03	3.489E-03	1.217	0.80
	SON	-418.5	4.799E-03	7.776E-03	5.500	0.73
PF	All period	-776.3	1.843E-03	-2.442E-03	0.163	0.89
	Annual	-796.6	1.449E-03	-1.619E-03	0.177	0.69
	SON	-579.0	1.120E-03	-5.562E-04	0.862	0.62

Table 4.10. Relative importance of each independent variable in the regression analysis for WY and PF prediction in all period, annual and SON time scales.

		WY			PF		
Category	Predictor	All period	Annual	SON	All period	Annual	SON
Physiography	Area	31	26	28	29	23	25
Climate	SCA	23	22	28	17	14	15
	P - UDelv4	46	52	44	54	63	60

Finally, we ran a monthly cumulative multivariate regression using the independent variables shown in Table 4.10. We computed the evolution of r^2 for each climate variable as a univariate regression as compared to the combined multivariate regression that includes area, SCA, and P combined (Figure 4.9). As expected, the combined multivariate regression always has the best performance compared to independent climate variables. Similar to the individual watershed models, the r^2 of the multivariate regression increases from the beginning of the water year (April) until spring (September), at which point additional months of climate information do not improve predictions of WY and PF. The r^2 for predicting WY is greater than for PF. The physiographic variable (Area) contributes most to the regression early in the water year, but its relative importance declines as the water year advances while the importance of SCA and P increases. P has greater relative important in PF prediction than WY at any cumulative month.

Table 4.11 shows the coefficients of regressions in the first part of the water year (May to October) with WY in Mm^3 and PF in m^3/s.

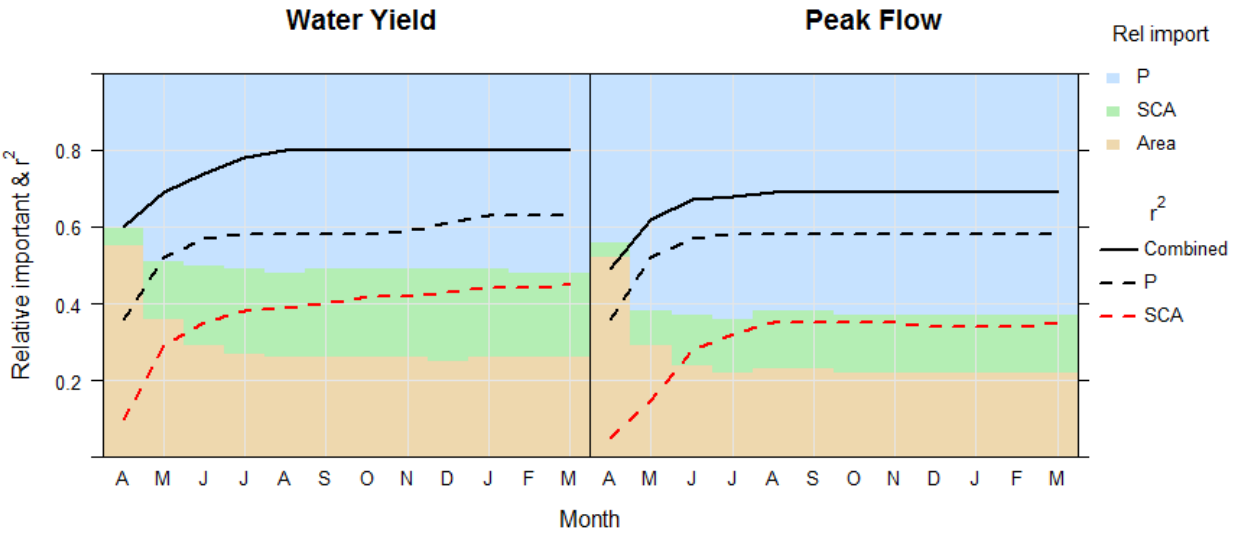

Figure 4.9. Coefficient of determination (r^2) to predict water yield and peak flow using monthly accumulated data of combined variables and independent SCA and P using all watershed data. The combined model uses SCA, P and area as independent variables. Background color shows the relative importance of each variable by time.

Table 4.11. Coefficients of regressions for WY (Mm^3) and PF (m^3/s) predictions using monthly cumulative input values between May and October.

	Month	Intercept	Area (ha)	SCA (ha)	P (mm)	r^2
WY	M	-524.80	9.55E-03	-1.10E-03	4.62	0.76
	J	-592.30	8.35E-03	1.70E-03	2.59	0.79
	J	-589.80	7.62E-03	2.24E-03	1.88	0.79
	A	-619.70	8.55E-03	6.69E-04	1.55	0.80
	S	-604.20	7.35E-03	2.41E-03	1.40	0.80
	O	-591.10	6.34E-03	3.85E-03	1.33	0.80
PF	M	-64.26	1.10E-03	-8.65E-04	0.69	0.65
	J	-74.85	1.17E-03	-6.93E-04	0.38	0.67
	J	-75.71	1.31E-03	-8.65E-04	0.27	0.68
	A	-80.22	1.67E-03	-1.33E-03	0.22	0.69
	S	-79.66	1.65E-03	-1.24E-03	0.20	0.69
	O	-79.90	1.60E-03	-1.22E-03	0.19	0.69

4.5. DISCUSSION

Most of the 29 watersheds selected for analysis in this study are clearly (13) or mostly snowmelt dominated (11), with annual water yield increasing along the precipitation gradient from north to south. Information on watershed total precipitation may be inaccurate and most likely underestimated, as highlighted by the runoff coefficient values greater than 1 (Figure 4.4d). The DGA precipitation stations are located mainly in the lower part of the watersheds (Table 4.1), and a strong orographic effect has been documented in the north part of the study area (26-32°S) (Favier et al., 2009). The UDelv4 interpolations of P use ground stations, which do not include sites above 3100 m. This may restrict the ability of the gridded P product for capturing the strong orographic effect in this area. Most of the process model used in the area require an improvement of the precipitation gradient to improve the accuracy of the models (Falvey and Garreaud, 2007; Favier et al., 2009; Ragettli et al., 2013; Rojas, 2005). In contrast, statistical models require that data have a good correlation with the target flow, so the absolute magnitude of precipitation across the entire watershed is not required (Garen, 2013). This study develops models to predict water yield volume and peak flow using the data that are available rather than trying to fill in the gaps in missing precipitation data at high elevations.

4.5.1. Individual watershed models

Univariate models of WY (SCA, T, or P) have varying performance in different hydrologic regimes (Figure 4.7). Watersheds with SDC<0.6, with limited snowmelt contribution, are better represented by annual P, whereas watersheds with greater snowmelt contributions are better represented by SCA and T. This division reflects the nature of the streamflow regime

because low values of SDC area associated with rain dominance (Fritze et al., 2011), and consequently snow has less effect on flow. Higher SDC values are associated with snowmelt dominance (Fritze et al., 2011), in which case high SCA and low T relate to the amount of water stored in the snowpack. For PF, SCA only reliably predicts PF magnitude (r^2>0.4) in the highest SDC (SDC>0.75), whereas correlations between SCA and PF are more variable between SDC 0.6-0.75. This may be because elevations that are transitional between snowmelt and rainfall dominance often have peak flows from rainfall or from a mixture of rain and snowmelt (Kampf and Lefsky, 2016). Multiple regression models of WY and PF for individual watersheds performed better than univariate models but had varying performance. Several watersheds had r^2 values exceeding 0.8, while other models did not perform as well (r^2 < 0.4) (Figure 4.7b). These multiple regression models do not have any evident stratification by snowmelt dominance category.

The monthly cumulative models are those that would be most likely be useful for streamflow forecasting. For these models, performance for WY prediction increases until September (Figure 4.8; Table 4.5), indicating that potential streamflow forecast accuracy is greatest in September, with no strong need for additional climate information from the remainder of the water year. Two of the watershed models have poor predictions even in September (r^2< 0.6; watersheds 2 and 27, last column Table 4.5). Watershed 27 is located in a mostly snowmelt dominant regime, but it has a large natural lake (Laguna del Maule) (Figure 4.2). This lake represents 6% of the total area of the watershed, and possibly disconnects the direct relation between snowmelt processes and streamflow runoff. Watershed 2 does not have any particular physiographic or streamflow characteristics that account for the low performance of the model. The cumulative monthly PF models (Figure 4.8; Table 4.6) have a similar pattern to the WY

models, with model performance increasing until September. Again, two watersheds have r^2 values under 0.4 in September (Watershed 27, and 28). Watershed 27 is the one with the large lake that was poorly predicted for SY. Watershed 28 is the largest watershed analyzed (214,072 ha), and possibly the heterogeneous physiographic characteristics make it difficult to predict PF from watershed aggregated climate variables. For the monthly cumulative models, climate variables were averaged over all preceding months. Future work should explore alternate approaches for accumulating climate information over time to ensure that the model performance continues to improve throughout the water year. Additional work is also needed to test these models against WY and PF values not used for model development.

4.5.2. All watersheds models

The model for all watersheds together to predict WY was generally more accurate (higher r^2) in all period (0.89) than annual (0.80) time scale, and the lowest accuracy was for the SON season time scale (0.73) (Table 4.9). This variability in performance with the time scale of input variables arises because the average over all period hides the inter-annual variability and predicts just the climate normal response. The all period time scale helps to make a first estimate of flow in ungauged basins, but it is not helpful for predicting the variability between years. The monthly cumulative model can be applied in forecasting mode, and it attains similar accuracy to the annual prediction with the input variables accumulated until August (Table 4.11). The relative importance analysis shows that P (UDelv4) is the most important predictor during any month evaluated, but its relative importance declines while the water year advances (Figure 4.9a). SCA

increases in importance during the snowmelt season. These patterns are similar for PF predictions in all watershed models.

In some watersheds, individual watershed models perform well, whereas in others they do not (Tables 4.5 and 4.6; r^2=0.41-0.95). For those with poor performance, future testing could examine how well the all watersheds model predicts their flow. Additional work is also needed to test the all watersheds models in watersheds or years that were not used in model development. After further testing the all watersheds model could also be applied to ungauged basins, similar to the applications of regional regression equations in other parts of the world. For example, Capesious and Verlin (2009) developed regional regression applied by USGS equations for estimating of natural streamflow in Colorado, which also has a mixture of snowmelt and rainfall-dominated flow regimes. These regressions were developed within five hydrologic regions based on physiographic and climatic characteristics to cluster similar watersheds. Future studies could expand on the work here to define hydrologic regions in the central Andes Mountains and potential improve the performance of the regional regression equations. Future work could also evaluate model performance when including other variables such as land cover, additional streamflow variables, and more of the physiographic variables not included in the final multivariate models shown here (Brown et al., 2008; Detenbeck et al., 2005; Ffolliott et al., 1989).

4.6. CONCLUSION

The scarcity of hydro-climatic data in the Andes Mountains poses a significant challenge for both streamflow forecasting and hydrologic model application. This study develops statistical streamflow prediction models that rely on available data from ground stations, GIS products, and remotely sensed snow cover. When forecasting streamflow for a single watershed, snow cover is most useful in watersheds that are mostly or clearly snowmelt dominated. The possibility to used just SCA to forecast streamflow is limited to watersheds with SDC greater than 0.6 for WY and greater than 0.75 for PF. Individual watershed models that used combined input variables of accumulated monthly precipitation, temperature, and snow cover information can predict annual water yield with r^2 values ranging from 0.41-0.95 and monthly peak flow with r^2 values ranging from 0.37-0.94 in September.

When all watersheds are combined for a single regional predictive model, the most important predictors are watershed area, latitude, precipitation, and snow cover. Latitude correlates strongly with precipitation, so we developed multivariate models for predicting water yield and peak flow in all watersheds using only area, precipitation, and snow covered area. Of these variables, precipitation contributes the most to the multivariate regression, whereas the role of snow cover is only important in the spring snowmelt season. The monthly cumulative models for all watersheds predict WY with an r^2 of 0.80 in August or later and PF with an r^2 of 0.69 for August or later in the season. Models that unify the information from all watersheds help to estimate ungauged or poorly gauged watershed within the study area. DGA forecasts WY and PF for 13 watersheds in the latitude range studied, and our results can be used to expand the number of watersheds with streamflow forecasts.

CHAPTER 5: CONCLUSIONS

This study has documented the spatial and temporal variability of snow cover throughout the Andes Mountains from 9-36°S using the MODIS snow covered area product (Chapter 1). This has allowed more detailed mapping of mountain climate regions than was previously possible using only ground measurements and/or coarser resolution gridded climate products. The study identified 5 snow regions, stratified primarily by latitude and three snow zones (intermittent, seasonal and permanent) that stratify by latitude and elevation. The Andes Mountains cause a clear difference in snow elevation between West and East sides, related to the strong effect on atmospheric circulation of its high mountains. The results of snow mapping in Chapter 2 improve the understanding of seasonal dynamics of snow at a broad scale and illustrate where and when snow accumulates throughout the region. The snow persistence methodology takes advance of high spatiotemporal resolution from MODIS, and this methodology can be extended to other regions to examine patterns in snow as they relate to latitude, elevation, and dominant slope aspect at regional or global scales.

Understanding snow climatology helps in interpreting snowpack trends. The second portion of the dissertation (Chapter 3) used snow cover data to analyze the trend of snow cover between 9-36°S. This represents the first study to quantify snow cover trends regionally across the Andes. Results show that a large area (70,515 km^2) south of 29°S is affected by a significant loss of snow cover (2-5 fewer days of snow cover per year), and 62% of the area affected by this trend is on the east side of the Andes. The loss of snow cover relates to trends of increasing temperature and decreasing precipitation, but the relative importance of precipitation and temperature to snow cover trends changes across the elevation and latitude range of the affected

area. Precipitation has greater relative importance in lower elevations than high elevations and greater importance in southern than northern areas. These findings on how climate connects to snow cover variability can be used to develop regionally specific management plans for different parts of the Andes. Previous research on snow trends in this area had used only point data (Masiokas et al., 2006) that probably cannot capture the variability in snow trends throughout the region. The findings in this study highlight where snow is most sensitive to changes in precipitation and temperature, demonstrating the utility of satellite imagery in spatiotemporal studies of snow cover trend and climate connection. The spatially varying effects of temperature and precipitation on snow are an active area of research, even in more intensively monitored regions. For example Morán-Tejeda et al. (2013) found that temperature is more important for snow depth and duration at low elevation, whereas precipitation is more important at high elevation in Switzerland. Findings in this research demonstrate how the relative importance of these variables varies substantially across latitudes and climates, and patterns identified in one region are not necessarily transferable elsewhere.

If the snow loss trend continues, this has important consequences for water supply in the central Andes (30-36°S) due the strong snowmelt-dominance of rivers in this region. Because of the limited snow and climate monitoring in high elevation, the final portion of the dissertation (Chapter 4) examined whether snow cover information could help to predict water yield and peak flow. Results show that using precipitation, snow cover and area of the watershed, it is possible to predict water yield ($r^2 = 0.8$) and peak flow ($r^2 = 0.7$) using a monthly cumulative approach. The predictions can be applied in late winter (August) before the beginning of the growing season. The use of just snow cover as a univariate predictor of water yield is limited to mostly or clearly snow dominated watersheds (SDC>0.6).

The study area was limited between 9-36°S due the high frequency of clouds present in other important snow areas. In the tropical Andes (north of 9°S) warming has a major effect on glacier/ice (Lejeune et al., 2007), and increased understanding of snow patterns in this area will help to prepare for future climate scenarios. South of 36°S the Northern Patagonia Icefield and the Southern Patagonia Icefield represent the largest ice masses of the Southern Hemisphere and provide an important source of fresh water (Lopez et al., 2008), so similarly research on snow dynamics in these areas is also critical. Several cloud removal algorithms have been developed and tested to apply in the MODIS snow products (Hall et al., 2010), and the new collection 6 for MODIS snow products released in 2016 incorporated gap-filled cloud and restoration of band 6 from the Aqua satellite to provide an additional source of snow cover information in the region. Test algorithms to remove cloud cover and new sources of snow cover data for the regions can be developed to help extend the study areas south of 36°S and north of 9°S.

Other sources of snow data are available to complement the analyses in this dissertation. Chapter 3 delineated areas with decreasing snow persistence trends south of 29°S, and Landsat and AVHRR data could potentially be used to extend the time series of the snow cover trend analysis and increase the spatial resolution (Landsat). Previous studies in this region used Landsat for some specific watershed and glacier analyses (Cortés et al., 2014), and the present study can help to define future sites for more detailed local investigations. The large scale analysis developed in this chapter defined critical watersheds affected by decreasing snow persistence, and this information can be integrated with economic, social, and/or ecological metrics to prioritize new monitoring locations to track snowpack in the region. Such monitoring sites could help in connecting snow cover patterns to snow water equivalent (SWE) to improve our ability to predict water yield.

The snow cover patterns and trends can also be connected with other landscape changes like fire, drought, soil moisture, and vegetation change. Snow and temperature trends have been linked to an increase of wildfire frequency and areas burned in the western USA (Westerling et al., 2006), and these types of connections may also be present in the Andes. The increase in elevation of the snowline documented in Chapter 3 opens new opportunities for ecohydrological research because vegetation and land surface energy budget are both connected to snow processes. Earlier melting and later accumulation of snow lengthens the growing season but can also limit water availability. Integration of snow cover analysis presented in this study with other remote sensing sources such as NDVI or burned areas from MODIS can help connect snow patterns with vegetation dynamics (Trujillo et al., 2012).

Chapter 4 generated streamflow forecasting models for individual watershed where streamflow data are available and for all watersheds combined to cover watersheds without sufficient streamflow data. The range of coefficients of regression (0.37 – 0.95) for individual models suggest that the variables used to develop these models do not capture the local variation between watersheds. Additional information as vegetation, soils, geology, land cover, distance from ocean, and/or orographic barriers can be evaluated in the future to determine whether they help improve model performance. In the study area of Chapter 3 the Coastal Range (Cordillera de la Costa) is located west of the Andes Mountain and rises to elevations close to 3000m. This barrier can affect westerly air flow to the Andes and could be an important variable affecting precipitation and snow patterns as reported in previous study (Daly et al., 2008). Identify hydrologic regions in the central Andes Mountains and test regression equations for streamflow prediction using additional information can improve the possibility to predict water yield and peak flow.

Remote sensing offers new opportunities to improve our understanding of landscape processes in areas that are poorly monitored. This dissertation proves the feasibility of incorporating remotely sensed snow cover data into climate and hydrologic applications across a large latitudinal range in the Andes Mountains as a first step to incorporate this data source into future work on climate change and water resource planning for the region. The results of this work highlight a significant snow decline in watersheds that drain to high population areas in the region, where future water security depends on adaptation plans that account for loss of snow.

BIBLIOGRAPHY

Abonyi, J., Feil, B., 2007. Cluster Analysis for Data Mining and System Identificaction. Birkhäuser Verlag AG, Germany.

Adam, J.C., Hamlet, A.F., Lettenmaier, D.P., 2009. Implications of global climate change for snowmelt hydrology in the twenty-first century. Hydrological Processes 23, 962-972.

Aravena, J.-C., Luckman, B.H., 2009. Spatio-temporal rainfall patterns in Southern South America. International Journal of Climatology 29, 2106-2120.

Arnaud, Y., Muller, F., Vuille, M., Ribstein, P., 2001. El Niño-Southern Oscillation (ENSO) influence on a Sajama volcano glacier (Bolivia) from 1963 to 1998 as seen from Landsat data and aerial photography. Journal of Geophysical Research 106, 17773.

Arsenault, K.R., Houser, P.R., De Lannoy, G.J.M., 2014. Evaluation of the MODIS snow cover fraction product. Hydrological Processes 28, 980-998.

Bales, R.C., Dressler, K.A., Imam, B., Fassnacht, S.R., Lampkin, D., 2008. Fractional snow cover in the Colorado and Rio Grande basins, 1995-2002. Water Resources Research 44, n/a-n/a.

Barnett, T.P., Adam, J.C., Lettenmaier, D.P., 2005. Potential impacts of a warming climate on water availability in snow-dominated regions. Nature 438, 303-309.

Barry, R.G., 2008. Mountain Weather and Climate, Third ed, University of Colorado, Boulder, USA.

Barry, R.G., Seimon, A., 2000. Research for Mountain Area Development: Climatic Fluctuations in the Mountains of the Americas and Their Significance. Ambio 29, 364-370.

Bendjoudi, H., Hubert, P., 2002. Le coefficient de compacité de Gravelius: analyse critique d'un indice de forme des bassins versants. Hydrological Sciences Journal 47, 921-930.

Borsdorf, A., Stadel, C., 2015. The Andes, a Geographical Portrait. Springer, New York Dordrecht London, U.K.

Bradley, R.S., 2004. Projected temperature changes along the American cordillera and the planned GCOS network. Geophysical Research Letters 31.

Bradley, R.S., Vuille, M., Diaz, H.F., Vergara, W., 2006. Threats to Water Supplies in the Tropical Andes. Science 312, 1755-1756.

Brown, L., Thorne, R., Woo, M.-K., 2008. Using satellite imagery to validate snow distribution simulated by a hydrological model in large northern basins. Hydrological Processes 22, 2777-2787.

Brown, R.D., Mote, P.W., 2009. The Response of Northern Hemisphere Snow Cover to a Changing Climate. Journal of Climate 22, 2124-2145.

Capesious, J., Verlin, S., 2009. Regional Regression Equations for Estimation of Natural Streamflow Statistics in Colorado, in: USGS (Ed.), Reston, Virginia.

Carrasco, J., Osorio, R., Casassa, G., 2008. Secular trend of the equilibrium-line altitude on the western side of the southern Andes, derived from radiosonde and surface observations. Journal of Glaciology 54, 538-550.

Cartes, M., 2008. Investigacion de Nieves y Escorrentia de Deshielo en la Cuenca Alta del Rio Aconcagua. Aplicacion de Modelos de Simulacion Nival y de Pronostico de Volumenes de Deshielo, in: DGA (Ed.).

Casassa, G., 2014. Status of Cryispheric Observation in South America, Global Cyosphere Watch GCW.
Cornwell, E., Molotch, N.P., McPhee, J., 2015. Spatio-temporal variability of snow water equivalent in the extra-tropical Andes cordillera from a distributed energy balance modeling and remotely sensed snow cover. Hydrology and Earth System Sciences Discussions 12, 8927-8976.
Cortés, G., Girotto, M., Margulis, S.A., 2014. Analysis of sub-pixel snow and ice extent over the extratropical Andes using spectral unmixing of historical Landsat imagery. Remote Sensing of Environment 141, 64-78.
Cortés, G., Vargas, X., McPhee, J., 2011. Climatic sensitivity of streamflow timing in the extratropical western Andes Cordillera. Journal of Hydrology 405, 93-109.
Cortes, G.C., 2010. Evaluacion de un Modelo Hidrologico Semi Distribuido Para la Estimacion de la Escorrentia de Deshielo en el Rio Juncal, Departamento de iNgenieria Civil. Universidad de Chile, Santiago, Chile, p. 84.
Dahe, Q., Shiyin, L., Peiji, L., 2006. Snow Cover Distribution, Variability, and Response to Climate Change in Western China. Journal of Climate 19, 1820-1833.
Daly, C., Halbleib, M., Smith, J.I., Gibson, W.P., Doggett, M.K., Taylor, G.H., Curtis, J., Pasteris, P.P., 2008. Physiographically sensitive mapping of climatological temperature and precipitation across the conterminous United States. International Journal of Climatology 28, 2031-2064.
Dedieu, J.P., Lessard-Fontaine, A., Ravazzani, G., Cremonese, E., Shalpykova, G., Beniston, M., 2014. Shifting mountain snow patterns in a changing climate from remote sensing retrieval. Science of The Total Environment.
Detenbeck, N.E., Brady, V.J., Taylor, D.L., Snarski, V.M., Batterman, S.L., 2005. Relationship of stream flow regime in the western Lake Superior basin to watershed type characteristics. Journal of Hydrology 309, 258-276.
Dietz, A.J., Kuenzer, C., Gessner, U., Dech, S., 2012. Remote sensing of snow – a review of available methods. International Journal of Remote Sensing 33, 4094-4134.
Falvey, M., Garreaud, R., 2007. Wintertime Precipitation Episodes in Central Chile: Associated Meteorological Conditions and Orographic Influences. Journal of Hydrometeorology 8, 171-193.
Falvey, M., Garreaud, R.D., 2009. Regional cooling in a warming world: Recent temperature trends in the southeast Pacific and along the west coast of subtropical South America (1979–2006). Journal of Geophysical Research 114.
Fassnacht, S.R., Dressler, K.A., Hultstrand, D.M., Bales, R.C., Patterson, G., 2012. Temporal Inconsistencies in Coarse-Scale Snow Water Equivalent Patterns: Colorado River Basin Snow Telemetry-Topography Regression. Pirineos. Revista de Ecologia de Montana 167, 167-186.
Favier, V., Falvey, M., Rabatel, A., Praderio, E., López, D., 2009. Interpreting discrepancies between discharge and precipitation in high-altitude area of Chile's Norte Chico region (26-32°S). Water Resources Research 45, n/a-n/a.
Ffolliott, P., Gottfried, G., Baker, M., 1989. Water yield from forest Snowpack management: research finding in Arizona and New Mexico. Water Resources Management 25, 1999-2007.
Foster, J., Chang, A., Hall, D.K., Kelly, R.E.J., 2001. Seasonal snow extent and snow mass in South America using SSMI passive microwave data. Polar Geography 25, 41-53.

Foster, J.L., Hall, D.K., Kelly, R.E.J., Chiu, L., 2009. Seasonal snow extent and snow mass in South America using SMMR and SSM/I passive microwave data (1979–2006). Remote Sensing of Environment 113, 291-305.
Fritze, H., Stewart, I.T., Pebesma, E., 2011. Shifts in Western North American Snowmelt Runoff Regimes for the Recent Warm Decades. Journal of Hydrometeorology 12, 989-1006.
Gafurov, A., Bardossy, A., 2009. Cloud Removal Methodology from MODIS Snow Cover Product. Hydrological Earth Systemic Science 13, 1361-1373.
Gao, Y., Xie, H., Yao, T., Xue, C., 2010. Integrated assessment on multi-temporal and multi-sensor combinations for reducing cloud obscuration of MODIS snow cover products of the Pacific Northwest USA. Remote Sensing of Environment 114, 1662-1675.
Garen, D.C., 2013. Choosing and assimilating forcing data for hydrological prediction, in: Pomeroy, P., Whitfield, H., Spence, C. (Eds.), Putting Prediction in Ungauged Basins into Practice. Canadian Water Resources Association, Canada, pp. 89-100.
Garreaud, R., Vuille, M., Clement, A.C., 2003. The climate of the Altiplano: observed current conditions and mechanisms of past changes. Palaeogeography, Palaeoclimatology, Palaeoecology 194, 5-22.
Garreaud, R.D., 2009. The Andes climate and weather. Advances in Geosciences 22, 3-11.
Garreaud, R.D., Aceituno, P., 2007. Chaper 2. Atmospheric Circulation Over South America: Mean Features and Variability, in: Veblen, T.T., Young, K.R., Orme, A.R. (Eds.), The Physical Geography of South America. Oxford University Press, New York, New York. USA.
Garreaud, R.D., Vuille, M., Compagnucci, R., Marengo, J., 2009. Present-day South American climate. Palaeogeography, Palaeoclimatology, Palaeoecology 281, 180-195.
GCOS, 2003. Report of the GCOS Regional Workshop for South America on Improving Observing System for Climate.
Groemping, U., Matthias, L., 2013. Relative importance of regressors in linear models. R package version 2.2.
Grömping, U., 2006. Relative Importance for Linear Regression in R: The Package relaimpo. Journal of Statistical Software 17, 1 -27.
Gu, L., Ren, R., Zhang, S., 2011. Automatic Cloud Detection and Removal Algorithm for MODIS Remote Sensing Imagery. Journal of Software 6, 1289-1296.
Hall, D.K., Foster, J.L., DiGirolamo, N.E., Riggs, G.A., 2012. Snow cover, snowmelt timing and stream power in the Wind River Range, Wyoming. Geomorphology 137, 87-93.
Hall, D.K., Riggs, G.A., Foster, J.L., Kumar, S.V., 2010. Development and evaluation of a cloud-gap-filled MODIS daily snow-cover product. Remote Sensing of Environment 114, 496-503.
Hall, D.K., Riggs, G.A., Salomonson, V.V., DiGirolamo, N.E., Bayr, K.J., 2002. MODIS snow-cover products. Remote Sensing of Environment 83, 181-194.
Hanshaw, M.N., Bookhagen, B., 2014. Glacial areas, lake areas, and snow lines from 1975 to 2012: status of the Cordillera Vilcanota, including the Quelccaya Ice Cap, northern central Andes, Peru. The Cryosphere 8, 359-376.
Houston, J., Hartley, A.J., 2003. The central Andean west-slope rainshadow and its potential contribution to the origin of hyper-aridity in the Atacama Desert. International Journal of Climatology 23, 1453-1464.

Immerzeel, W.W., Droogers, P., de Jong, S.M., Bierkens, M.F.P., 2009. Large-scale monitoring of snow cover and runoff simulation in Himalayan river basins using remote sensing. Remote Sensing of Environment 113, 40-49.
Kampf, S.K., Lefsky, M.A., 2016. Transition of dominant peak flow source fromsnowmelt to rainfall along the Colorado Front Range: Historical patterns, trends, and lessons from the 2013 Colorado Front Range floods. Water Resources Research 52.
Kennedy, A.M., Garen, D.C., Koch, R.W., 2009. The association between climate teleconnection indices and Upper Klamath seasonal streamflow: Trans-Niño Index. Hydrological Processes 23, 973-984.
Kennedy, M., Kopp, S., 1994. Understanding Map Projections, USA.
Khaled, H.H., Ramachandra, A.R., 1998. A modified Mann-Kendall trend test for autocorrelated data. Journal of Hydrology 204, 182–196.
Kluver, D., Leathers, D., 2015. Regionalization of snowfall frequency and trends over the contiguous United States. International Journal of Climatology 35, 4348-4358.
Knowles, N., Cayan, D.R., 2004. Elevational Dependence of Projected Hydrologic Changes in the San Francisco Estuary and Watershed. Climatic Change 62, 319 - 336.
Knowles, N., Dettinger, M., Cayan, D.R., 2006. Trends in Snowfall versus Rainfall in the Western United States. Journal of Climate, 4545-4559.
Kottek, M., Grieser, J., Beck, C., Rudolf, B., Rubel, F., 2006. World Map of the Köppen-Geiger climate classification updated. Meteorologische Zeitschrift 15, 259-263.
Kwon, H.-H., Brown, C., Xu, K., Lall, U., 2009. Seasonal and annual maximum streamflow forecasting using climate information: application to the Three Gorges Dam in the Yangtze River basin, China. Hydrological Sciences 54, 582-595.
Le Quesne, C., Acuña, C., Boninsegna, J.A., Rivera, A., Barichivich, J., 2009. Long-term glacier variations in the Central Andes of Argentina and Chile, inferred from historical records and tree-ring reconstructed precipitation. Palaeogeography, Palaeoclimatology, Palaeoecology 281, 334-344.
Legates, D.R., Willmott, C.J., 1990. Mean seasonal and spatial variability in global surface air temperature. Theor. Appl. Climatology 41, 11-21.
Lejeune, Y., Bouilloud, L., Etchevers, P., Wagnon, P., Chevallier, P., Sicart, J.-E., Martin, E., Habets, F., 2007. Melting of Snow Cover in a Tropical Mountain Environment in Bolivia: Processes and Modeling. Journal of Hydrometeorology 8, 922-937.
Liniger, H., Weingartner, R., 1998. Mountains and freshwater supply. Unasylva, FAO 49, 39-46.
Liu, X., Cheng, Z., Yan, L., Yin, Z.-Y., 2009. Elevation dependency of recent and future minimum surface air temperature trends in the Tibetan Plateau and its surroundings. Global and Planetary Change 68, 164-174.
Llamedo, P., Hierro, R., de la Torre, A., Alexander, P., 2016. ENSO-related moisture and temperature anomalies over South America derived from GPS radio occultation profiles. International Journal of Climatology, n/a-n/a.
López-Moreno, J.I., Goyette, S., Beniston, M., 2009. Impact of climate change on snowpack in the Pyrenees: Horizontal spatial variability and vertical gradients. Journal of Hydrology 374, 384-396.
Lopez, P., Sirguey, P., Arnaud, Y., Pouyaud, B., Chevallier, P., 2008. Snow cover monitoring in the Northern Patagonia Icefield using MODIS satellite images (2000–2006). Global and Planetary Change 61, 103-116.

Maechler, M., Rousseeuw, P., Struyf, A., Hubert, M., Hornik, K., Studer, M., Roudier, P., 2015. Finding Group in Data, p. 79.
Martinec, J., Rango, A., Roberts, R., 2008. Snowmelt Runoff Model (SRM) User's Manual. New Mexico State University, Las Cruces, New Mexico, USA.
Masiokas, M., Villalba, R., Luckman, B., Le Quesne, C., Aravena, J.C., 2006. Snowpack variations in the Central Andes of Argentina and Chile, 1951-2005: Large-scale atmospheric influences and implications for water resources in the region. Journal of Climate 19, 6334-6352.
Masiokas, M.H., Rivera, A., Espizua, L.E., Villalba, R., Delgado, S., Aravena, J.C., 2009. Glacier fluctuations in extratropical South America during the past 1000years. Palaeogeography, Palaeoclimatology, Palaeoecology 281, 242-268.
Masiokas, M.H., Villalba, R., Christie, D.A., Betman, E., Luckman, B.H., Le Quesne, C., Prieto, M.R., Mauget, S., 2012. Snowpack variations since AD 1150 in the Andes of Chile and Argentina (30°–37°S) inferred from rainfall, tree-ring and documentary records. Journal of Geophysical Research 117.
Masiokas, M.H., Villalba, R., Luckman, B.H., Montaña, E., Betman, E., Christie, D., Le Quesne, C., Mauget, S., 2013. Recent and Historic Andean Snowpack and Streamflow Variations and Vulnerability to Water Shortages in Central-Western Argentina, Climate Vulnerability, pp. 213-227.
Matsuura, K., Willmott, C., 2015. Terrestrial Air Temperature: 1900-2014 Gridded Monthly Time Series, http://climate.geog.udel.edu/~climate/html_pages/Global2014/README.GlobalTsT2014.html.
McLeod, A.I., 2011. Kendall-package: Kendall correlation and trend tests. R package version 2.2.
Mendoza, P., 2010. Pronostico de Caudales de Crecida Mediante un Modelo Hidrologico Distribuido y la Asimilacion de Datos Observados, Departamento de Ingenieria Civil. Universidad de Chile, Santiago, Chile, p. 228.
Mendoza, P.A., Rajagopalan, B., Clark, M.P., Cortés, G., McPhee, J., 2014. A robust multimodel framework for ensemble seasonal hydroclimatic forecasts. Water Resources Research 50, 6030-6052.
Meza, F.J., 2013. Recent trends and ENSO influence on droughts in Northern Chile: An application of the Standardized Precipitation Evapotranspiration Index. Weather and Climate Extremes 1, 51-58.
Molotch, N.P., Margulis, S.A., 2008. Estimating the distribution of snow water equivalent using remotely sensed snow cover data and a spatially distributed snowmelt model: A multi-resolution, multi-sensor comparison. Advances in Water Resources 31, 1503-1514.
Molotch, N.P., Meromy, L., 2014. Physiographic and climatic controls on snow cover persistence in the Sierra Nevada Mountains. Hydrological Processes 28, 4573-4586.
Moore, C., Kampf, S., Stone, B., Richer, E., 2015. A GIS-based method for defining snow zones: Aplication to the Western United States. Geocarto International 3, 62-81.
Morales, M.S., Christie, D.A., Villalba, R., Argollo, J., Pacajes, J., Silva, J.S., Alvarez, C.A., Llancabure, J.C., Soliz Gamboa, C.C., 2012. Precipitation changes in the South American Altiplano since 1300 AD reconstructed by tree-rings. Climate of the Past 8, 653-666.

Morán-Tejeda, E., López-Moreno, J.I., Beniston, M., 2013. The changing roles of temperature and precipitation on snowpack variability in Switzerland as a function of altitude. Geophysical Research Letters 40, 2131-2136.
Norusis, M., 2012. IBM SPSS Statistics 19 Statistical Procedures Companion. Addison Wesley, Upper Saddle River, NJ. USA.
Oyler, J.W., Dobrowski, S.Z., Ballantyne, A.P., Klene, A.E., Running, S.W., 2015. Artificial amplification of warming trends across the mountains of the western United States. Geophysical Research Letters 42, 153-161.
Pagano, T., Erxleben, J., Perkins, T., 2005. Operational Simulation Modeling at the NRCS National Water and ClimateCenter, Western Snow Conference, Great Falls, Montana, pp. 87-100.
Pagano, T., Garen, D.C., 2006. Integration of climate information and forecasts into western US water supply forecasts, in: Garbrecht, J., Piechota, T. (Eds.), Climate Variations, Climate Change, and Water Resources Engineering, pp. 86-103.
Painter, T.H., Rittger, K., McKenzie, C., Slaughter, P., Davis, R.E., Dozier, J., 2009. Retrieval of subpixel snow covered area, grain size, and albedo from MODIS. Remote Sensing of Environment 113, 868-879.
Parajka, J., Bloschl, G., 2008. Spatio-temporal combination of MODIS images - potential for snow cover mapping. Water Resources Research 44, 1-13.
Parajka, J., Blöschl, G., 2008. The value of MODIS snow cover data in validating and calibrating conceptual hydrologic models. Journal of Hydrology 358, 240-258.
Peduzzi, P., Herold, C., Silverio, W., 2010. Assessing high altitude glacier thickness, volume and area changes using field, GIS and remote sensing techniques: the case of Nevado Coropuna (Peru). The Cryosphere 4, 313-323.
Pellicciotti, F., Ragettli, S., Carenzo, M., McPhee, J., 2013. Changes of glaciers in the Andes of Chile and priorities for future work. The Science of the total environment.
Pepin, N., Bradley, R.S., Diaz, H., Baraer, M., Caceres, E., Forsythe, N., Fowler, H., Greenwood, G., Hashmi, M., Liu, X., Miller, J.R., Ning, L., Ohmura, A., Palazzi, E., Rangwala, I., Schoner, W., Severskiy, I., Shahgedonova, M., Wang, M., Williamsn, S., Yang, D., 2015. Elevation-dependent warming in mountain regions of the world. Nature Climate Change 5, 424-430.
Prieto, R., Herrera, R., Dousel, P., 2001. Interannual oscillations and trend of snow occurrence in the Andes region since 1885. Australian Meteorogical Magazine 50.
Quintana, J.M., 2012a. Changes in the Rainfall Regime Along the Extratropical West Coast of South America (Chile): 30-43 S. Atmosfera 25, 1-22.
Quintana, J.M., 2012b. Changes in the rainfall regime along the extratropical west coast of South America (Chile): 30-43°C. Atmosfera 25, 1-22.
Rabatel, A., Bermejo, A., Loarte, E., Soruco, A., Gomez, J., Leonardini, G., Vincent, C., Sicart, J.E., 2012. Can the snowline be used as an indicator of the equilibrium line and mass balance for glaciers in the outer tropics? Journal of Glaciology 58, 1027-1036.
Rabatel, A., Francou, B., Soruco, A., Gomez, J., Cáceres, B., Ceballos, J.L., Basantes, R., Vuille, M., Sicart, J.E., Huggel, C., Scheel, M., Lejeune, Y., Arnaud, Y., Collet, M., Condom, T., Consoli, G., Favier, V., Jomelli, V., Galarraga, R., Ginot, P., Maisincho, L., Mendoza, J., Ménégoz, M., Ramirez, E., Ribstein, P., Suarez, W., Villacis, M., Wagnon, P., 2013. Current state of glaciers in the tropical Andes: a multi-century perspective on glacier evolution and climate change. The Cryosphere 7, 81-102.

Ragettli, S., Cortés, G., McPhee, J., Pellicciotti, F., 2013. An evaluation of approaches for modelling hydrological processes in high-elevation, glacierized Andean watersheds. Hydrological Processes, n/a-n/a.
Raleigh, M.S., Rittger, K., Moore, C.E., Henn, B., Lutz, J.A., Lundquist, J.D., 2013. Ground-based testing of MODIS fractional snow cover in subalpine meadows and forests of the Sierra Nevada. Remote Sensing of Environment 128, 44-57.
Rango, A., 2009. Spaceborne remote sensing for snow hydrology applications. Hydrological Sciences Journal 41, 477-494.
Rango, A., Salomonson, V.V., Foster, J., 1977. Seasonal Streamflow Estimation in the Himalayan Region Employing Meteorological Satellite Snow Cover Observations. Water Resources Research 13, 109-112.
RCoreTeam, 2013. R: A language and environment for statistical computing, Vienna, Austria.
Richer, E., Kampf, S., Fassnacht, S., Moore, C., 2013. Spatiotemporal index for analyzing controls on snow climatology: application in the Colorado Front Range. Physical Geography 34, 85-107.
Riggs, G.A., Hall, D.K., Salomonson, V.V., 2006. MODIS snow products user guide to Collection 5.
Rittger, K., Painter, T.H., Dozier, J., 2013. Assessment of methods for mapping snow cover from MODIS. Advances in Water Resources 51, 367-380.
Rivera, A., Cassassa, G., Acuna, C., Lange, H., 2000. Variaciones recientes de glaciares en Chile. Investigacio Geografica 34, 29-60.
Rojas, M., 2005. Multiply Nested Regional Climate Simulation for Southern South America: Sensitivity to Model Resolution. Monthly Weather Review 134, 2208-2223.
Saavedra, F.A., Kampf, S.K., Fassnacht, S.R., Sibold, J.S., 2016. A Snow Climatology of the Andes Mountains from MODIS Snow Cover Data. International Journal of Climatology.
Salomonson, V.V., Appel, I., 2004. Estimating fractional snow cover from MODIS using the normalized difference snow index. Remote Sensing of Environment 89, 351-360.
Salzmann, N., Huggel, C., Rohrer, M., Silverio, W., Mark, B.G., Burns, P., Portocarrero, C., 2013. Glacier changes and climate trends derived from multiple sources in the data scarce Cordillera Vilcanota region, southern Peruvian Andes. The Cryosphere 7, 103-118.
Santos, J.L., 2006. The Impact of El Nino-Sothern Ossilation Events on South America. Advances in Geosciences 6, 221-225.
Scherer, D., Hall, D.K., Hochschild, V., König, M., Winther, J.-G., Duguay, C.R., Pivot, F., Mätzler, C., Rau, F., Seidel, K., Solberg, R., Walker, A.E., 2005. Remote sensing of snow cover. 163, 7-38.
Sen, P.K., 1968. Estimates of the Regression Coefficient Based on Kendall's Tau. Journal of the American Statistical Association 63, 1379-1389.
Squeo, F.A., Holmgren, M., Jiménez, M., Albán, L., Reyes, J., Gutiérrez, J.R., 2007. Tree establishment along an ENSO experimental gradient in the Atacama desert. Journal of Vegetation Science 18, 195-202.
Steele, C., Hall, D.K., Bleiweiss, M., 2010. Sensitivity of the Snowmelt Runoff Model to Underestimates of Remotely Sensed Snow Covered Area. IEEE, 2382-2385.
Stewart, I.T., 2009. Changes in snowpack and snowmelt runoff for key mountain regions. Hydrological Processes 23, 78-94.
Stewart, I.T., Cayan, D.R., Dettinger, M., 2005. Change Toward Earlier Streamflow Timing Across North America. Journal of Climate 18, 1136-1155.

Stroeve, J.C., Box, J.E., Haran, T., 2006. Evaluation of the MODIS (MOD10A1) daily snow albedo product over the Greenland ice sheet. Remote Sensing of Environment 105, 155-171.
Sturm, M., 2013. North Slope Snow Remote Sensing, Remote Sensing-Derived Monitoring Product for the Arctic North Slope Science Initiative Workshop, Fairbanks, Alaska. USA.
Tekeli, A.E., Akyürek, Z., Arda Şorman, A., Şensoy, A., Ünal Şorman, A., 2005. Using MODIS snow cover maps in modeling snowmelt runoff process in the eastern part of Turkey. Remote Sensing of Environment 97, 216-230.
Theil, H., 1950. A rank-invariant method of linear and polynomial regression analysis. Mathematic 53, 386–392.
Trujillo, E., Molotch, N.P., Goulden, M.L., Kelly, A.E., Bales, R.C., 2012. Elevation-dependent influence of snow accumulation on forest greening. Nature Geosci 5, 705-709.
Valdés-Pineda, R., Pizarro, R., Valdés, J.B., Carrasco, J.F., García-Chevesich, P., Olivares, C., 2015a. Spatio-temporal trends of precipitation, its aggressiveness and concentration, along the Pacific coast of South America (36°–49°S). Hydrological Sciences Journal, null-null.
Valdés-Pineda, R., Valdés, J.B., Diaz, H.F., Pizarro-Tapia, R., 2015b. Analysis of spatio-temporal changes in annual and seasonal precipitation variability in South America-Chile and related ocean-atmosphere circulation patterns. International Journal of Climatology, n/a-n/a.
Vergara, W., Deeb, A., Valencia, A., Zarzar, A., Grunwaldt, A., Haeussling, S., 2007. Economic Impacts of Rapid Glacier Retreat in the Andes. EOS, Transactions Amarican Geophysical Union 88, 261-268.
Vicuña, S., Garreaud, R.D., McPhee, J., 2010. Climate change impacts on the hydrology of a snowmelt driven basin in semiarid Chile. Climatic Change 105, 469-488.
Vuille, M., Ammann, C., 1997. Regional Snowfall Patterns in the High, Arid Andes. Climatic Change 36, 413-423.
Vuille, M., Bradley, R.S., 2000. Mean annual temperature trends and their vertical structure in the tropical Andes. Geophysical Research Letters 27, 3885-3888.
Wagnon, P., Lafaysse, M., Lejeune, Y., Maisincho, L., Rojas, M., Chazarin, J.P., 2009. Understanding and modeling the physical processes that govern the melting of snow cover in a tropical mountain environment in Ecuador. Journal of Geophysical Research 114, D19113.
Wang, X., Xie, H., Liang, T., 2008. Evaluation of MODIS snow cover and cloud mask and its application in Northern Xinjiang, China. Remote Sensing of Environment 112, 1497-1513.
Wang, Z., Schaaf, C.B., Chopping, M.J., Strahler, A.H., Wang, J., Román, M.O., Rocha, A.V., Woodcock, C.E., Shuai, Y., 2012. Evaluation of Moderate-resolution Imaging Spectroradiometer (MODIS) snow albedo product (MCD43A) over tundra. Remote Sensing of Environment 117, 264-280.
Westerling, A.L., Hidalgo, H.G., Cayan, D.R., Swetnam, T.W., 2006. Warming and earlier spring increase western U.S. forest wildfire activity. Science 313, 940-943.
Williams, R., Ferringo, J., 1998. Satellite Image Atlas of Glaciers of the World, South America, in: USGS (Ed.), Washington, USA.
Willmott, C.J., Robeson, S.M., 1995. Climatologically aided interpolation (CAI) of terrestrial air temperature. International Journal of Climatology 15, 221-229.

Wolter, K., Timlin, M.S., 1998. Measuring the strength of ENSO events: How does 1997/98 rank? Weather 53, 315-324.
Zamboni, L., Kucharski, F., Mechoso, C.R., 2011. Seasonal variations of the links between the interannual variability of South America and the South Pacific. Climate Dynamics 38, 2115-2129.